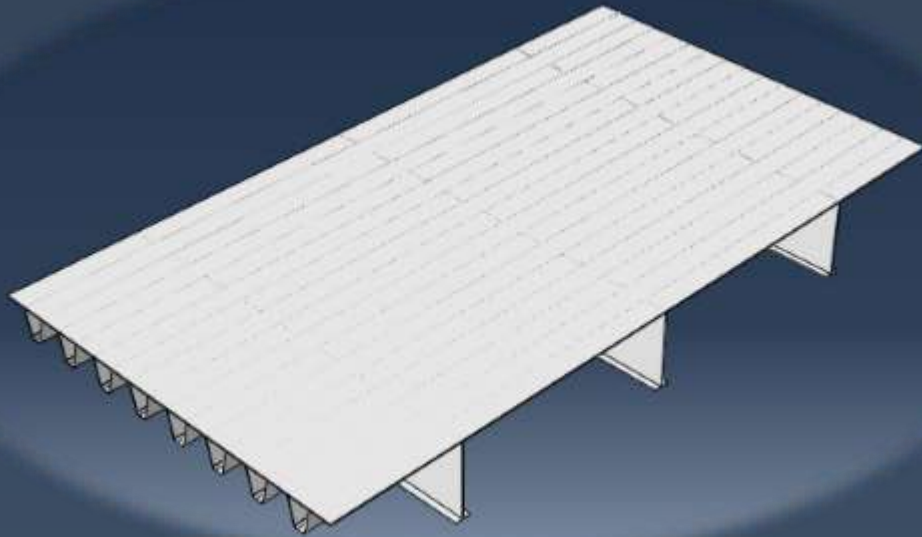


Measurements and Monitoring the Behaviour of Crossbeam in Orthotropic Bridge Deck with 3D Digital Image Correlation

Reiner Parlindungan Simarmata (4521501)



Measurements and Monitoring the Behaviour of Crossbeam in Orthotropic Bridge Deck with 3D Digital Image Correlation

By

Reiner Parlindungan Simarmata
(4521501)

in partial fulfilment of the requirements for the degree of

Master of Science

in Civil Engineering

at the Delft University of Technology,

to be defended publicly on Tuesday, 19th December 2017 at 10:00 AM.

Supervisor:	Dr. Marko Pavlovic,	TU Delft, Steel & Composite
Thesis committee:	Prof. dr. M. Veljkovic,	TU Delft, Steel & Composite
	Dr. M. H. Kolstein,	TU Delft, Steel & Composite
	Dr. Henk den Besten,	TU Delft, Ship & Offshore Structures

An electronic version of this thesis is available at <http://repository.tudelft.nl/>.

Preface and Acknowledgement

This thesis has been written as the partial fulfilment of the degree of my Master of Science in Civil engineering, majoring in structural engineering with steel structure specialisation at Delft University of Technology, Delft, Netherlands.

I would like to thank my entire graduation committee for their assistance through my research. For Milan Veljkovic, Henk Kolstein, and Henk den Besten for their guidance and wisdom which had helped me during my thesis period. Special thanks to Marko Pavlovic who had put trust and assisted me from the beginning of the project. I also thank Weijian Wu and Kevin Mouthaan for their willingness to help me during the experimental period.

Thank you to the Indonesian Endowment Fund for Education (Lembaga Pengelola Dana Pendidikan) for the scholarship provided throughout my study at TU Delft. Without them, I would not have the chance to pursue my study here. I would also like to thank my Professors from Institute Teknologi Bandung; Prof.Ir. R. Bambang Boediono ME,Ph.D., Ir. Made Suarjana M.Sc.,Ph.D., and Ir. R. Muslinang Moestopo MSEM,Ph.D. that had given me recommendation to continue my study at TU Delft.

I would like to extend my sincerest gratitude to my beloved family, my father Barce Mercedes Simarmata, my mother Happy Herowaty Santoso, both of my brothers (David Febrian Simarmata & Joey Somuntul Simarmata) and also my sister Destiny Simarmata, for their endless support and encouragement throughout my master study period here in TU Delft. Without them I would not be here, at this point of my life. To my friend here in TU Delft and Indonesia, thank you for keeping the faith in me. I would also like to thank my small family in the Netherlands, Oma Lucy, Opa Louwen, Tante Yanti, Om Peter, and Christel for providing shelter and comfort during my study at TU Delft. Finally, special gratitude to my dearest friend Ghina Kamila who inspired and supported me during the good and hard times.

Reiner Parlindungan Simarmata

Delft, December 2017

Abstract

Digital Image Correlation is a cheap and easy to use measurement method that has been proved to characterise any solid material parameters up to plastic deformation range. The digital image correlation measurement system is based on the tracking of a collective number of pixels from the surface of the reference image to the deformed image. This summation of pixels is called subset. To achieve a reliable measurement in DIC, each of the subsets must contain sufficient speckle pixels. Therefore, there is a firm distinctive intensity pattern contained in a particular subset relative to other subsets. However, with the current DIC method, the user must rely on the intuition and experience for determining these number of speckle pixels. To investigate this problem, a study of measurement and monitoring the behaviour of crossbeam in Orthotropic Bridge due to in-plane quasi-static load is conducted. The reliability of DIC method on measuring strain and deformation in an elastic zone of a steel material is also examined and compared to the other measurement technique such as strain gauge and LVDT. Also, a finite element model is developed to estimate the strain and out-of-plane deformation at the certain location of the crossbeam.

The study focuses on the specific location at the crossbeam with 'haibach' shape cope hole, where the strain concentration is expected to be significantly high. The applied quasi-static load is set until 250 kN, with strain gauges and LVDT are installed at the same side of the crossbeam (free edge side), and DIC is installed at the exact opposite side (inner side). Parallel with the test on the Orthotropic Deck Bridge specimen, several benchmarking test is also conducted. These tests are used to examine the problems encountered during the initial experiment.

The study shows that owing to the quasi-static in-plane load, the crossbeam encounter an out-of-plane behaviour. Therefore, to achieve an accurate measurement, a 3-D DIC measurement system is obliged to use. Strain observed into two different directions: x and y-direction, gives different results in term of accuracy. Due to the low strain limit of DIC system, the result in x-direction can be considered as unreliable. For strain measurement in y-direction, some of the results exceeding the low limit strain of the equipment, give a close match result with the strain gauges, within the acceptable amount of deviation. For out-of-plane deformation, all the measurement show a good agreement between the DIC and LVDT technique. The average speckle pattern size that is used in this research is 0.2 mm, and an average area of 38 pixels² for a particular speckle pattern. One of the benchmark study shows that under the same condition with same expected level of displacement, an average speckle pattern area between 36 and 45 pixels² leads to reliable 3D measurement. The finite element model that has been developed in this study also gives close strain estimation for both x and y-direction, compared to the measurement data (DIC and strain gauges).

Table of Content

Preface and Acknowledgement.....	5
Abstract.....	7
Table of Content	9
List of Figures	11
List of Tables	13
1 INTRODUCTION.....	15
1.1. Background and Motivation	15
1.2. Main Objectives and Research Questions.....	16
1.3. Research Methodology	17
1.4. Limitations	18
1.5. Structure of the Thesis	18
2 INTRODUCTION TO DIGITAL IMAGE CORRELATION AND ORTHOTROPIC BRIDGE DECK.....	19
2.1. Digital Image Correlation	19
2.1.1. Classification of Digital Image Correlation (DIC)	19
2.1.2. Principle Work of Digital Image Correlation.....	20
2.1.3. Measuring Displacement & Strain.....	21
2.1.4. Speckle Pattern Principals	23
2.1.5. Calibration Procedure.....	25
2.2. Orthotropic Bridge Deck.....	26
2.2.1. Structural Component of Orthotropic Bridge Deck.....	26
2.2.2. The Behaviour Mechanism of the Orthotropic Deck Steel Bridge	28
2.2.3. Conventional cope hole & 'haibach' cope hole shape	29
2.2.4. In-lane Loading Mechanism and The Effects on the Crossbeam	30
3 OVERVIEW OF THE FULL-SCALE EXPERIMENT ON ORTHOTROPIC STEEL DECK.....	32
3.1. Specimen Layout	32
3.2. In-plane Loading Schemes and Values.....	33
3.3. Specification & Locations of the Measurement System.....	34
3.3.1. Strain Gauges	34
3.3.2. Linear Variable Differential Transformer (LVDT).....	35
3.3.3. Digital Image Correlation.....	35
4 DATA ACQUISITION & TESTING RESULTS ON FULL-SCALE ORTHOTROPIC STEEL DECK EXPERIMENT	39
4.1. Data acquisition and Result of the First Test (Region Interest B and Region Behind B)	39
4.2. Data acquisition and Result on Second Test (Region Interest A and Region Behind A)	44
5 COMPARISON & ANALYSIS OF THE 3D DIC MEASUREMENT RESULTS TO OTHER MEASUREMENTS.....	49
5.1. Strain Gauges Results Compared to The DIC Measurement Result	49

5.2.	LVDT Results Compare with DIC Measurement for Out-of-plane Deformation.....	51
5.3.	DIC Measurement at Location A compare to Location B	53
5.4.	Number of Pixels for the Captured Image	55
6	VALIDATION WITH FINITE ELEMENT METHOD	56
6.1.	ABAQUS FEA.....	56
6.2.	Strategy of Finite Element Modelling.....	56
6.3.	Process of Modelling	56
6.3.1.	Cross Section Detailing & Physical Properties Assignment	56
6.3.2.	Application of Loading and Boundary Condition.....	58
6.3.3.	Assignment of element size and meshing properties.	59
6.4.	Validation of Finite Element Model With Measurement Results.....	60
6.4.1.	Validation of FEM with Strain Gauges & LVDT Measurement at Free Edge Side .	60
6.4.2.	Validation of FEM with DIC Measurement.....	63
6.5.	Sensitivity Analysis on Mesh Refinement.....	65
6.6.	Conclusion on Finite Element Method	67
7	DISCUSSION OF RESULTS AND ANSWERS TO RESEARCH QUESTIONS	68
8	CONCLUSION & RECOMMENDATION	70
	REFERENCES	71
	ANNEX A – 2D BENCHMARK TESTING.....	72
	ANNEX B – 2D & 3D BENCHMARK TESTING UNDER THE ORTHOTROPIC BRIDGE DECK.....	88

List of Figures

Figure 1. Cross-section of the crossbeam	16
Figure 2. Diagram of research methodology	17
Figure 3. Classification of DIC measurement	19
Figure 4. Schematic figures of reference and deformed subset for 2D [4]	19
Figure 5. Schematic figures of reference and deformed subset for 3D [5]	20
Figure 6. Monocular vision of 2D DIC measurement [5]	20
Figure 7. Binocular vision of 3D DIC measurement system [5]	21
Figure 8. Tracking point for undeformed and deformed image [5]	21
Figure 9. Subset or facet definition for DIC measurement [5]	22
Figure 10. Deformation of subset shape [5]	22
Figure 11. The examples of poor and good pattern (red means poor & green means good) [7]	23
Figure 12. An example of problem with speckle pattern size [7]	24
Figure 13. Image acquisition of calibration target [5]	25
Figure 14. Millau Viaduct Bridge (Nicolas Janberg, 2017)	26
Figure 15. Cross Section of Millau Viaduct [6]	26
Figure 16. Main structural component of typical orthotropic steel bridge [2]	26
Figure 17. Variation of open stiffener (left to right: flat, angle, bulb stiffener) [1].....	27
Figure 18. Variation of closed stiffeners (Left to right: Trapezoidal shape, U-shape, V-shape) [1]	27
Figure 19. Principal stress distribution around cope hole and fit continuous weld due to in- plane load [2]	29
Figure 20. Stress distribution along the edges of conventional cope hole (left image) and 'haibach' shape cope hole (right image) [2]	30
Figure 21. Full-scale test for continuous stiffener on crossbeam [9]	30
Figure 22. "Vierendeel-system" in crossbeam of orthotropic steel deck [1]	31
Figure 23. In-plane closed stiffener to crossbeam connection behaviour [2].....	31
Figure 24. Cross Section of the orthotropic steel deck [10]	32
Figure 25. Detail of the closed stiffener (unit in mm) [10]	32
Figure 26. Location of the Static Load	33
Figure 27. Location of the Strain Gauges on both side (Left and Right).....	34
Figure 28. Location of the LVDT relative to strain gauge	35
Figure 29. Location of the LVDT from side view	35
Figure 30. The 3D DIC system Q-400	35
Figure 31. Location of the DIC equipment from top view of the bridge	36
Figure 32. Location of the camera for left and right measurement.....	37
Figure 33. Location of DIC measurement	37
Figure 34. Calibration plate for the particular test.....	38
Figure 35. Applied speckle pattern using airbrush device (zoom 100% from the actual image)	38
Figure 36. Location of the Strain Gauges for first measurement	39
Figure 37. Images From Left and Right Camera for Step 0 (-2kN).....	39

Figure 38. Location for Strain and Displacement DIC Measurement	40
Figure 39. Global Reference z axis sign for measurement system	41
Figure 40. Out-of-plane deformation plot over the step	42
Figure 41. Strain in Y direction plot over the step	42
Figure 42. Strain in X direction plot over the step	43
Figure 43. Spatial plot strain in Y direction over the line	43
Figure 44. Location of the Strain Gauges for second measurement	44
Figure 45. Images From Left and Right Camera for Step 0 (-2kN)	44
Figure 46. Location for strain and displacement DIC measurement	45
Figure 47. Out-of-plane deformation plot over the step	46
Figure 48. Strain in Y direction plot over the step	47
Figure 49. Strain in X direction plot over the step	47
Figure 50. Spatial plot strain in Y direction over the line	48
Figure 51. DIC & strain gauges plot for strain in Y direction for location A	49
Figure 52. DIC & strain gauge plot for strain in Y direction for location B	50
Figure 53. Out-of-plane deformation measurement at location A	52
Figure 54. Out-of-plane deformation measurement at location B	52
Figure 55. DIC strain measurement	53
Figure 56. DIC out-of-plane measurement	54
Figure 57. Left - Middle - Right (Full scale Image - 100% zoom - Cropping 2.2 mm x 1.7 mm)	55
Figure 58. Strategy of finite element method	56
Figure 59. Technical drawing of the specimen	57
Figure 60. 3D view finite element model	57
Figure 61. Side view of finite element model	57
Figure 62. Boundary condition of the crossbeam	58
Figure 63. Cross section mesh (left image: 5 mm, right image: 10 mm)	59
Figure 64. 1x1x1 integration point scheme in hexahedral elements [11]	59
Figure 65. 3D view mesh element	59
Figure 66. Location of the strain gauges from free edge side	60
Figure 67. Strain distribution ϵ_{xx} from the free edge side	60
Figure 68. Strain distribution ϵ_{yy} from the free edge side	61
Figure 69. Out-of-plane distribution at the crossbeam I	62
Figure 70. Location of the DIC measurement	63
Figure 71. Strain-yy distribution along the 25 mm horizontal line path	65
Figure 72. Location of the mesh study	65
Figure 73. DIC result for strain yy distribution along the 25 mm horizontal line path	66

List of Tables

Table 1. Orthotropic steel deck deformation mechanism [8]	29
Table 2. Detail of strain gauges.....	34
Table 3. Technical data of the system Q-400	36
Table 4. Detail of field of view, focal length, and working distance of the camera	37
Table 5. Location of the DIC measurement relative to strain gauges	37
Table 6. Results from each of measurement system for the first test	40
Table 7. Results from each of measurement system for the second test.....	45
Table 8. Strain Gauges and DIC Results with Error Calculation	49
Table 9. Out-of-plane deformation measurement for DIC & LVDT.....	51
Table 10. Comparison DIC measurement location A & location B	53
Table 11. Comparison left side cope hole with right side cope hole from the free edge side	54
Table 12. Physical Properties of the material	58
Table 13. Detail of the strain gauge on the crossbeam I	60
Table 14. Strain measurement results from strain gauges and FEM for in-plane quasi-static loading.....	61
Table 15. Out-of-plane deformation results from FEM and LVDT for in-plane quasi-static loading.....	62
Table 16. Strain Measurement Results from FEM & DIC.....	64
Table 17. Out-of-plane deformation Results from DIC & FEM... Error! Bookmark not defined.	
Table 18. Deviation of DIC measurement relative to other measurement technique for strain and out-of-plane deformation.....	68

1 INTRODUCTION

1.1. Background and Motivation

Strain and displacements are essential parameters when it comes to engineering project such as solid mechanics experiment. However, sometimes it is challenging to measure these parameters, especially when the level of the strain and displacements are relatively very small. Also, to choose an adequate measurement technique, many considerations need to be taken into accounts, such as accuracy, simplicity, and cost efficiency. Digital Image Correlation (DIC), is a measuring technique that may provide all the answers. The popularity of this measurement technique has been increased and widely used nowadays in many aspects of engineering area. It is simple to use, relatively cheap compared to other measurement technique (for example speckle interferometry), and capable of measuring such a very small strain and displacements (micro and nano-scale) with accurate results.

Digital Image Correlation (DIC) uses an optical method that works by comparing digital photographs of a specimen at different phases of deformations. By tracking the subpixels of the images, DIC can measure surface displacement and produce a 2D and 3D field of strain and deformation. This technique relies on the contrasting pattern of the specimen surface. Recently, many software has been developed to acquire the sub-pixels of captured images, and then execute the algorithm for deformation and strain measurement. It means, even a simple commercial digital camera can achieve such an accurate measurement with high-resolution results.

Measuring strain and deformation in an elastic zone of steel material might be challenging for any measurement techniques. The level of strain could vary from a few to hundreds of micro-strain. A perfect example of this case is the behaviour of crossbeam connected to the continuous closed stiffener, due to the quasi-static load in the orthotropic bridge deck. The series of quasi-static loads are limited in certain nominal value. Thus the deformation and strain propagation on the steel bridge material remain in elastic phase. Several tests on this case have been conducted in the past with another measurement techniques, for instance, strain measurements using strain gauges, and deformation measurements using linear variable differential transformer (LVDT). For strain gauges itself, the results are quite reliable for the level of strain in elastic zone steel material. However, it is laborious to install the strain gauges. With the DIC technique, this kind of problem can be overcome, since DIC equipment is relatively cheaper and easier to use compared to the strain gauges technique. The results can be achieved as accurate as LVDT and strain gauges regarding displacement and strain field.

1.2. Main Objectives and Research Questions

The main purpose of this research is to monitor and measure the behaviour of the crossbeam connected to the continuously closed stiffener, due to the in-plane and out-of-plane quasi-static load exerted on the deck. The research will focus on the crossbeam with 'haibach' shape cope hole in the orthotropic bridge deck, specifically in the area where strain concentration is expected to be significantly high. Figure 1 below depicts the cross-section of the crossbeam.

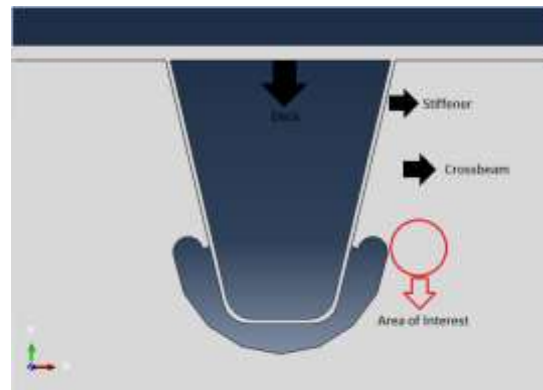


Figure 1. Cross-section of the crossbeam

Two different methods are applied in this research: a numerical approach by finite element modelling, and experiment on full-scale model approach. For numerical approach, ABAQUS software will be used to analyse the model. For the experiment, 3D Digital Image Correlation (DIC) will be the main tool to measure the behaviour of the crossbeam.

The objective of this study can be derived from these following research questions:

1. Is it reliable to use Digital Image Correlation (DIC) system to measure the behaviour of the crossbeam with 'haibach' cope hole due to the in-plane quasi-static loading?

This research questions can be sub-divided into:

- a. What is the best method to apply Digital Image Correlation System in Orthotropic Bridge Deck in order to measure the behaviour of the crossbeam?
 - b. What is the optimum number of pixels for one particular dot of speckle pattern and field of view of the measurement to get the proper results, given by the circumstances of the experiment and limitation of the equipment specifications?
2. What is the reliability of the Finite Element Modelling that has been developed in this research, to estimate the behaviour of the crossbeam with the 'haibach' cope hole?

1.3. Research Methodology

The research questions which mentioned above will be answered through these following phases:

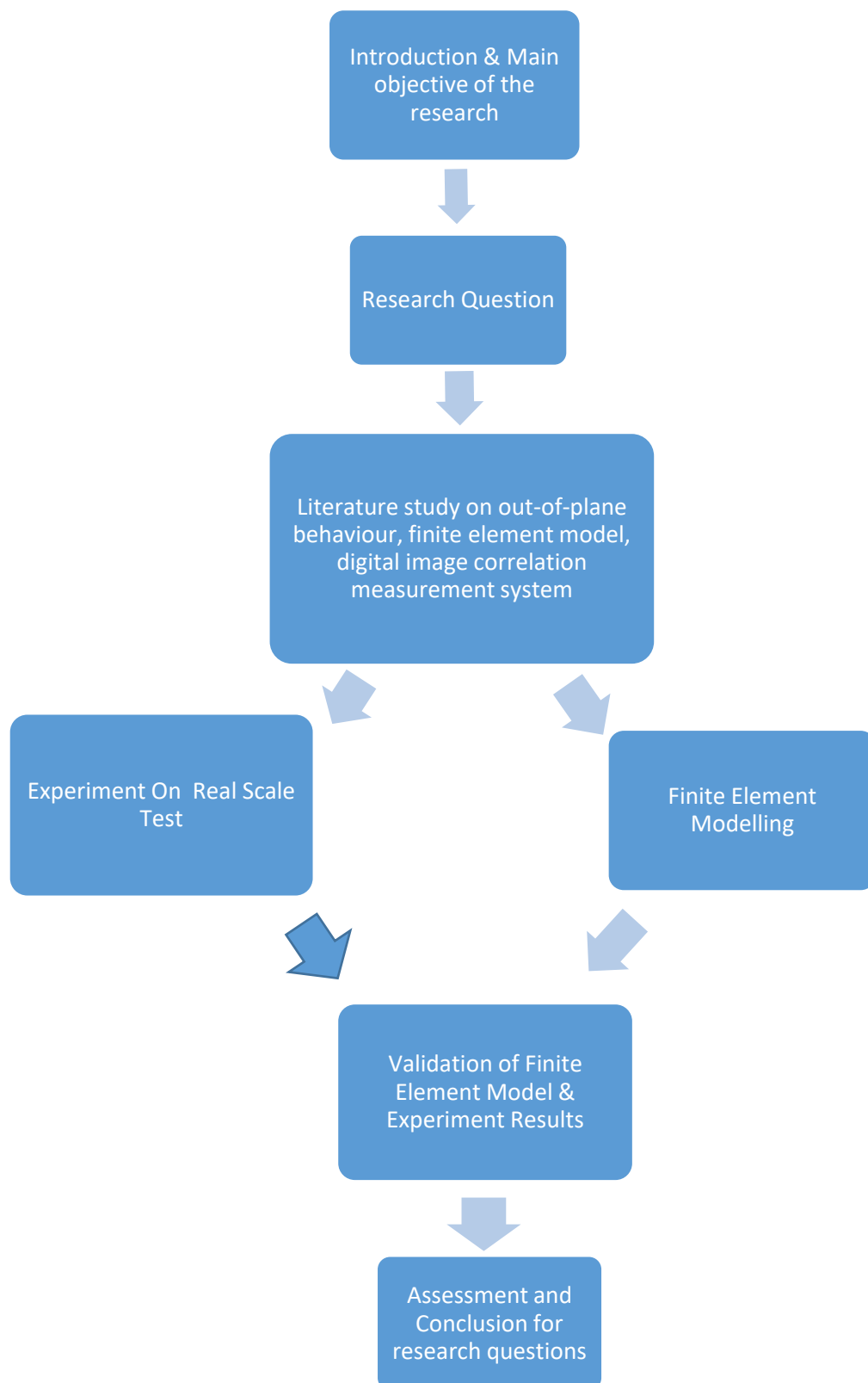


Figure 2. Diagram of research methodology

1.4. Limitations

This thesis study is limited to the data evaluation of strain and out-of-plane deformation due to the specific set of load position from experiment and finite element model. Another location of measurements is not the scope of this thesis work.

1.5. Structure of the Thesis

The thesis report will be composed of background theory which is relevant to the research, experimental tests results, finite element modelling results, and the analysis and conclusion for the study.

- Chapter 1 gives the general overview of the research. Background, objectives and also the methodology of thesis works are provided.
- Chapter 2 introduces the theoretical background of Digital Image Correlation measurement system and also an introduction to the orthotropic bridge deck.
- Chapter 3 gives the introduction to the geometry of new layout orthotropic bridge deck, load positions, boundary conditions. In this chapter, the setting layout of 3D digital image correlation on the bridge will also be presented
- Chapter 4 describes the comprehensive processes, data acquisition and results of the experiment using the Digital Image Correlation, other measurement techniques data (strain gauges and LVDT).
- Chapter 5 provides the analysis and comparison of the acquired data from Digital Image Correlation to other measurement techniques.
- Chapter 6 provides the validation of data obtained from the measurement technique with Finite Element Model approach.
- Chapter 7 addresses the discussion and analysis results regarding the problem statement and research questions
- Chapter 8 states the conclusion as well as the recommendation for further research

2 INTRODUCTION TO DIGITAL IMAGE CORRELATION AND ORTHOTROPIC BRIDGE DECK

2.1. Digital Image Correlation

Digital Image Correlation is simple to use, relatively cheap compared to other measurements, and accurate enough to measure such a very small deformation and strain distribution. Due to the fast development in high resolution of imaging sensors and also computer technology, the application of this measurement method has broadened in wide aspects of engineering.

2.1.1. Classification of Digital Image Correlation (DIC)

Regarding measurements, the DIC can be classified into two types of measurements:

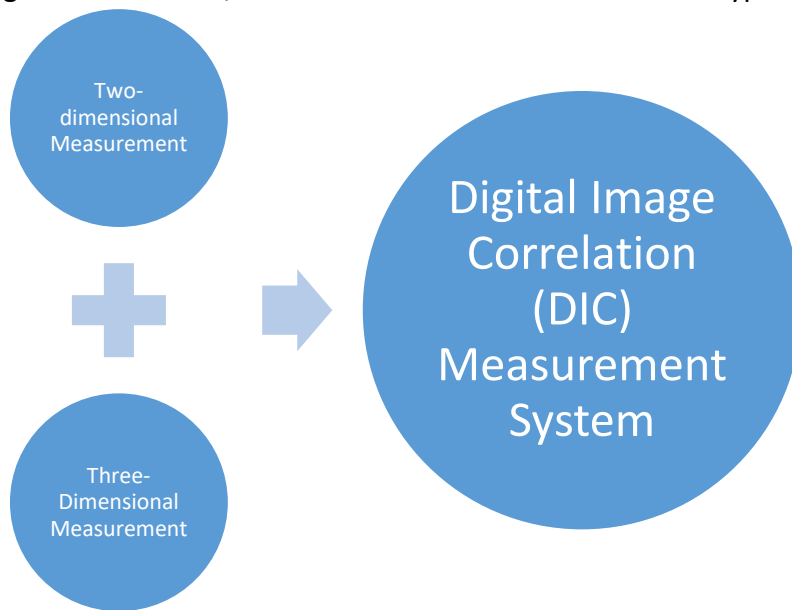


Figure 3. Classification of DIC measurement

The classification of the measurements is based on the motion and deformation of the specimen in global coordinates. For two-dimensional measurement, it is assumed that the specimen will only move and deform in two axes only (planar specimen). Figure 4 below depicts the fundamental works of 2D measurements.

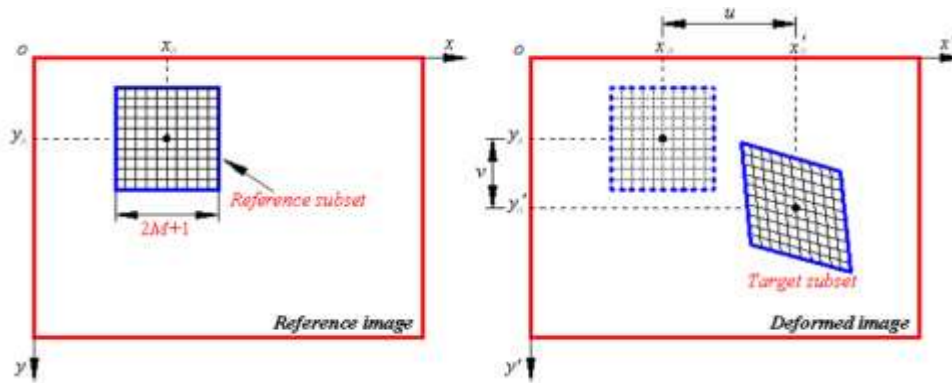


Figure 4. Schematic figures of reference and deformed subset for 2D [4]

For the three-dimensional system, the measurement is based on the motion and deformed in 3 axes (x, y, and z-axis). Unlike 2D measurements, in 3D measurement, the out-of-plane deformation is measured. Figure 5 below shows the principle works of 3D measurement.

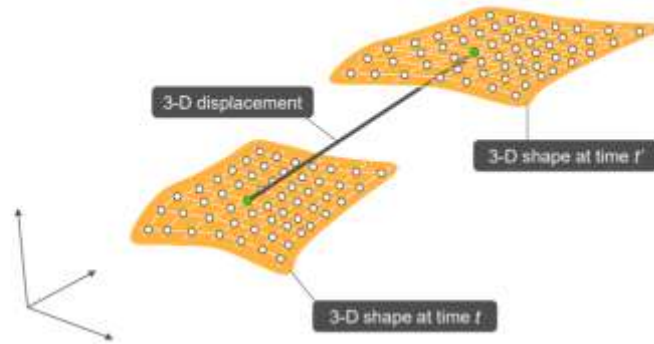


Figure 5. Schematic figures of reference and deformed subset for 3D [5]

2.1.2. Principle Work of Digital Image Correlation

It is mentioned in the previous section, that the measurement is classified in two-dimensional and three-dimensional. The process of monitoring and capturing an image of 2D DIC measurement system is based on monocular vision. For this measurement, the object is assumed to be a planar plane, parallel to the measuring system and at a constant distance from the sensor during data acquisition. An object that expands twice from its original shape in isotropic direction will yield the same image that is moved to half of its original position relative to the visual sensor. Figure 6 depicts what the visual looks like for 2D measurement.

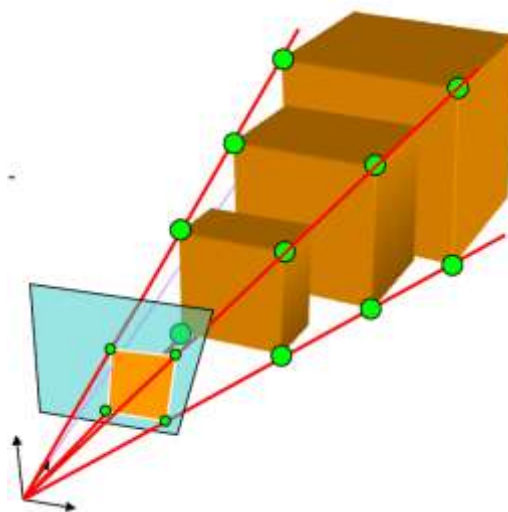


Figure 6. Monocular vision of 2D DIC measurement [5]

For 3D measurement, binocular vision is used instead of the monocular vision. It has two imaging sensors. Therefore the system can perceive three-dimensional images of its surroundings. The terms of this definition are called stereo-triangulation. Unlike the 2D system, 3D DIC system can resolve the scale of the objects. Figure 7 below illustrates the way binocular vision works.

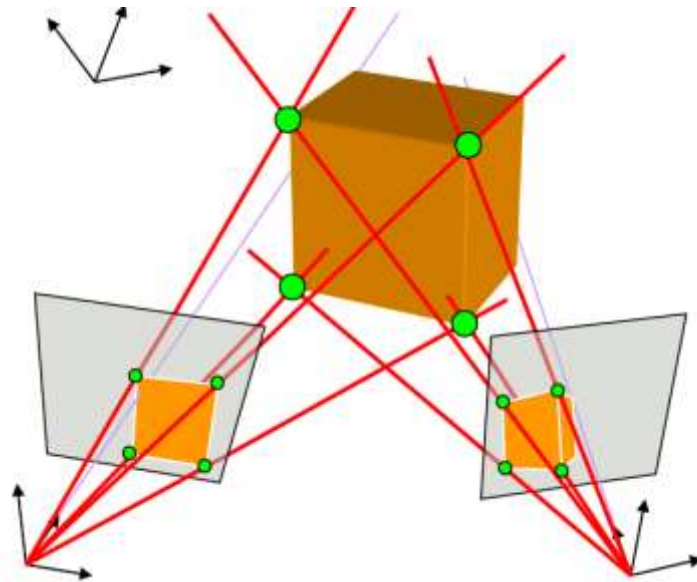


Figure 7. Binocular vision of 3D DIC measurement system [5]

2.1.3. Measuring Displacement & Strain

The fundamental way of DIC in measuring displacement is by tracking a point and its signature between un-deformed and deformed image, as it is shown in figure 8 below.

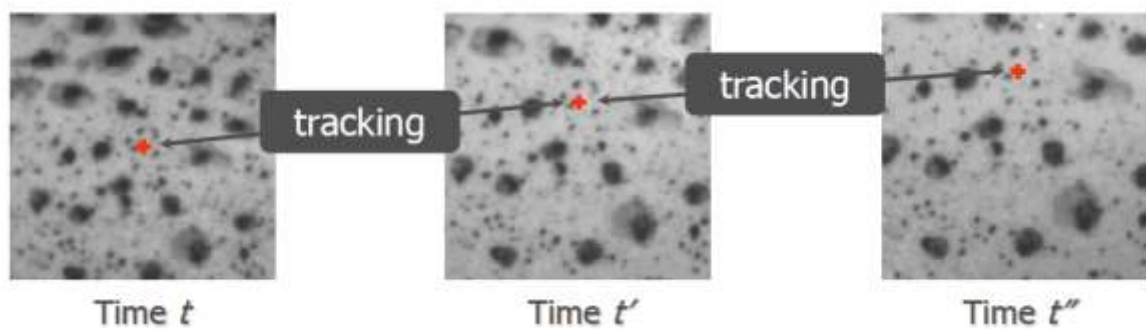


Figure 8. Tracking point for undeformed and deformed image [5]

In practice, the particular value is not a unique signature of the point, but it uses neighbouring pixels. A summation of a certain value of pixels is called **subset** or **facet**, as it is shown in figure 9 below.

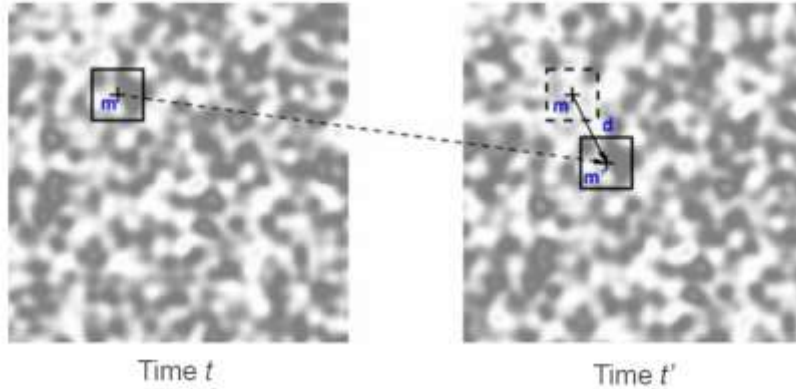


Figure 9. Subset or facet definition for DIC measurement [5]

To measure the displacement, the algorithm formula for correlation is using:

$$\sum_{x,y}(G_t(x_t, y_t) - G(x, y))^2 \dots \text{eq(1)}$$

$$G_t(x_t, y_t) \text{ equals to } g_0 + g_1G(x_t, y_t) \dots \text{eq(2)}$$

Where $G(x, y)$ is the grey value reference coordinate inside the subset or facet function, and:

$$x_1 = a_0 + a_1x + a_2y + a_3xy$$

$$y_1 = a_4 + a_5x + a_6y + a_7xy$$

The measurements do not depend on one unique signature point or grey value. Instead, it depends on the collection of the pixels which is called subset or facet. In practice, this subset will deform and has a changed shape as shown in figure 10. In this figure, it can be seen that the initial shape of the subset is square. However, at the deformed stage, the shape is more likely to be non-square. This displacement transformation is modelled in DIC measurement, and it is called subset shape function.

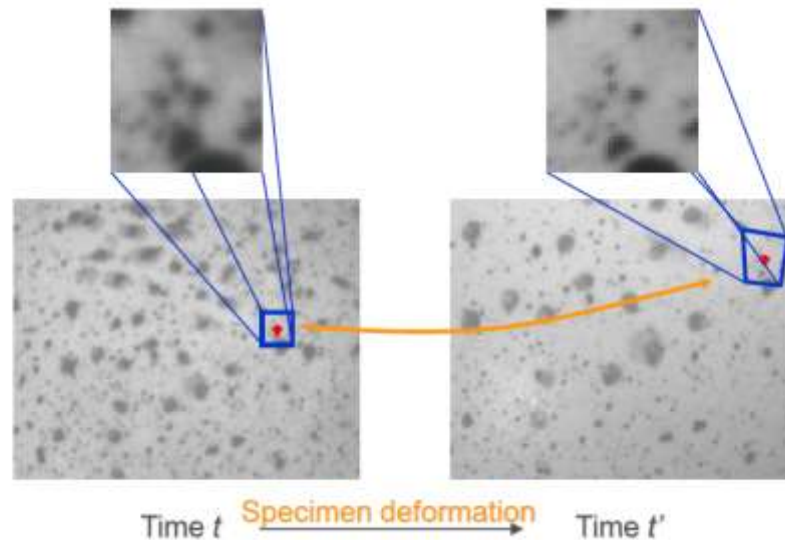


Figure 10. Deformation of subset shape [5]

For 3D measurement, once the object contour is known, the 3D deformation of the object surface can be determined by correlating the reference images to the deformed images. With known displacement vectors of each particular surface point and reference contour, the strain measurement can be computed. There are two options to compute the strain; first is by the direct differentiation of the displacements for adjacent surface points; secondly is by the analysis of the distortion of each local facets. The strain computed in 3D measurements is only defined in the tangential plane of the surface.

2.1.4. Speckle Pattern Principals

One of the crucial factors in Digital Image Correlation measurements is the quality of the pattern. Good quality of the pattern leads to a better accuracy of the measurements. There is no absolute guidance about how the pattern should be applied, yet there are several boundaries and general ways to achieve such good pattern.

Pattern Requirements

To achieve optimum correlation, the pattern must fulfil this condition:

- Random pattern (not only show one orientation)
- Non-repetitive pattern
- Isotropic
- High contrast pattern

Figure 11 below depicts the example of good and poor pattern

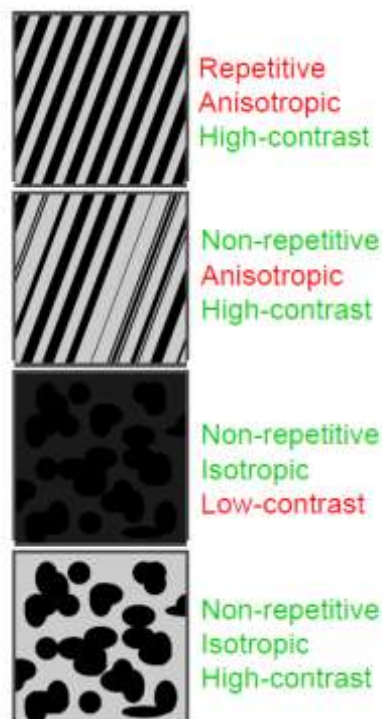


Figure 11. The examples of poor and good pattern (red means poor & green means good) [\[7\]](#)

Applied Speckle Pattern Colour

Most of the DIC measurement software only captures the contrasting field of the pattern. Thus, when it comes to the application of speckle pattern, the white speckles on the black field can work as well as black speckle on a white field.

Pattern Scale

The size of the speckle pattern depends on the test requirement. It is also related to the expected magnitude of deformation and strain. That will be investigated more in this research, related to the case study. There is also some theoretical background about how to obtain an optimum speckle pattern size. In Digital Image Correlation measurement, a subset of the image is tracked from the reference image to the deformed image. The subset is moved until the pattern in the deformed image matches the reference image. If the pattern is too large, one particular dot pattern may overlap the subset area, which resulted in an error of measurement. It can be solved by increasing the subset size. However, the spatial resolution is reduced as a consequence. Figure 12 below shows the example:

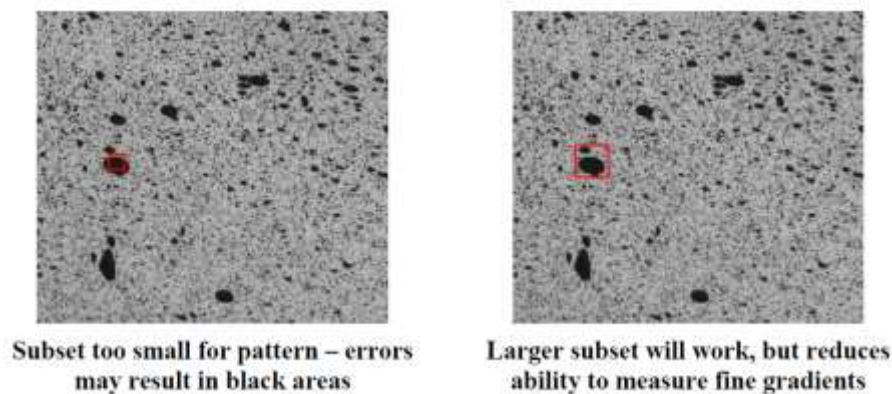


Figure 12. An example of problem with speckle pattern size [\[7\]](#)

Methods of Applying Pattern

There are several methods to apply the speckle pattern required for effective measurements.

- Spray Paint
This technique is the most common method used for applying the speckle pattern. One of the advantages of using this method is that the object or specimen is not chemically affected by the paint. This technique fits best with metal and ceramic specimen. Matte paints are better than satin and gloss paints because it can avoid specular reflections.
- Toner
This method suits for a very small specimen. The very fine pattern can be achieved with tone powder.
- Printing
Printing the speckle pattern could also be an effective way to achieve good measurement. The pattern can be generated and printed on paper or vinyl.

2.1.5. Calibration Procedure

In Digital Image Correlation, calibration is extremely fundamental for the accuracy of the results, particularly for 3D measurements. There are several reasons behind this. First of all, the target or specimen may have arbitrary or unidentified shape, so it needs to be specified. Second, the scale of the specimen is important to be known. The calibration procedure can be defined as a shape measurement of the target as well. Before the data acquisition, there are several parameters that are obliged to be obtained:

- Intrinsic parameters of the cameras. They are; focal length of the lenses, principle point of the lenses, radial distortions, and tangential distortions.
- Extrinsic parameters. For 3D measurements, it is important to know the translation vector and rotation matrix of the camera orientations for the triangulation.

To achieve effective calibration, several image acquisition from the calibration target is necessary. The figure 13 below shows calibration process of the target. One image must not be identical with another image, as seen in the image below, thus the calibration target is rotated one relative to another.

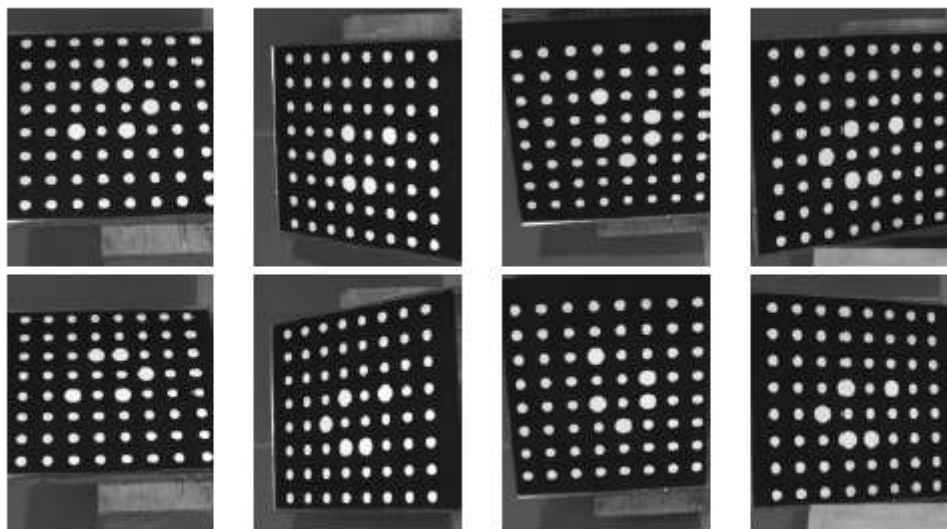


Figure 13. Image acquisition of calibration target [\[5\]](#)

2.2. Orthotropic Bridge Deck

Nowadays, Orthotropic Bridge Deck (OBD) are widely used in the world. The application of this type of deck is increasing, especially for long-span bridges and movable bridges. *Millau Viaduct* is the example of a cable-stayed bridge with the largest orthotropic steel deck as it is shown in figure 5 and 6 below.



Figure 14. Millau Viaduct Bridge (Nicolas Janberg, 2017)

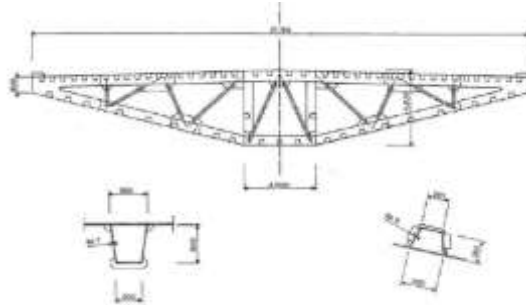


Figure 15. Cross Section of Millau Viaduct [6]

Many professionals tend to adopt this method rather than conventional deck mainly because of the cost-effective benefit. It permits a relatively shallow deck that leads to a reduction of other components usage, such as cable, towers, piers. The process of constructions is also relatively easy compared to the other types of deck. The orthotropic deck itself is comprised of steel deck which is stiffened in both longitudinal & transversal direction. If the deck stiffness in these directions is different, thus it is called 'Orthotropic'.

2.2.1. Structural Component of Orthotropic Bridge Deck

Orthotropic bridge deck consists of several elements of the structure. The figure 2 below shows the typical section of the orthotropic bridge deck.

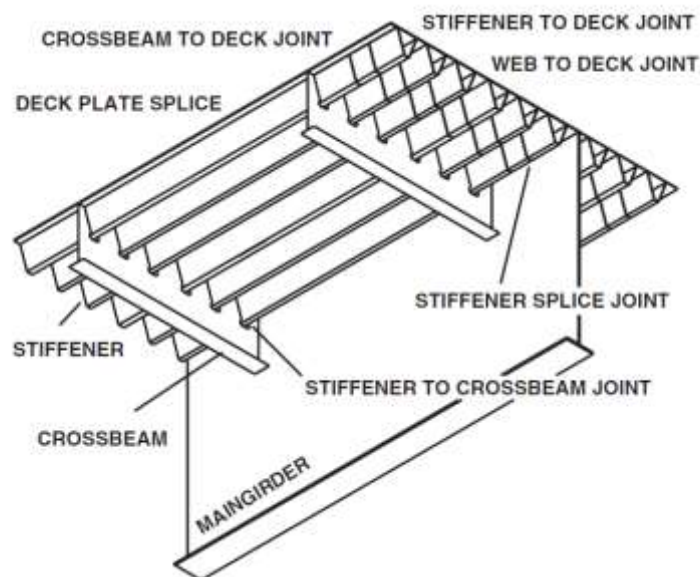


Figure 16. Main structural component of typical orthotropic steel bridge [2]

Deck Plate

This particular structural component is made by a relatively thin steel plate. The conventional deck plate design consists of 10 mm to 12 mm thickness. However, due to the recent fatigue problem, newly designed of deck plate is introduced, with thickness varied between 15 mm to 22 mm. In this research, the deck plate with thickness 20 mm will be used. The deck plate acts as a top flange for the whole structural behaviour, directly receive the traffic loads, which is generated by the axle of the vehicle, and then transfer the loads into the other components such as longitudinal stiffeners, crossbeams, and the main girder.

Stiffeners

The other components of the orthotropic bridge deck are the stiffeners. There are two type of stiffeners, closed and open stiffeners. The figure shows the typical open stiffener: flat, angle and bulb stiffener. While for the closed stiffener, the most commonly used are trapezoidal shape, U-shape, and V-shape as it is shown in the figure 17 and 18.

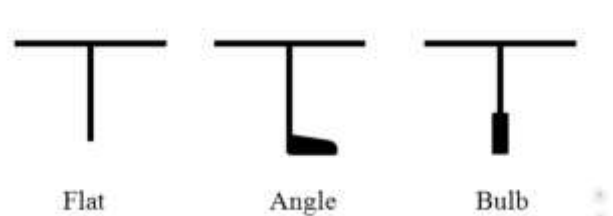


Figure 17. Variation of open stiffener (left to right: flat, angle, bulb stiffener) [1]

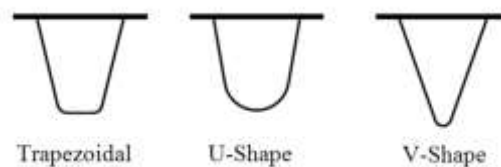


Figure 18. Variation of closed stiffeners (Left to right: Trapezoidal shape, U-shape, V-shape) [1]

There are always cost & benefit for using each type of stiffeners. For open stiffeners, the advantages are a reduction regarding production, inspections, and maintenance. The flexibility in the shape and dimension and also it is easy to construct this element with another part of the bridge (US Department of Transportation, 2012). However, there is some drawback regarding structural performance for using open stiffeners. The lack of torsional and flexural stiffness, which can lead to non-uniformly distributed load. This phenomenon requires more stiffeners and reduce of crossbeam spacing, therefore higher amount of material is necessary to be used. Also, the number of welding part is higher compared to the same deck with closed stiffeners. The open stiffener is also proven inefficient for taking bending stresses. These are the reasons, why open stiffeners are no longer used in steel bridges (De Jong, 2006).

On the other hand, closed stiffener provides a better structural performance compare to the open stiffeners for orthotropic bridge steel deck. The closed stiffeners provide the elastic stability to the deck and also increase the bending capacity, due to high flexural

and torsional rigidity (Janss, 1986). Therefore, the spacing between the stiffeners as well as crossbeam can be increased. By increasing the spacing, the amount of material used for this type of deck can be reduced. Due to the shape of closed stiffeners, the structure can develop larger static strength and stiffness compared to the open stiffeners. This advantages also lead to the simplicity regarding erection and construction of the bridge. However, besides the benefits, there are also some shortcoming of using closed stiffeners. First, it is more difficult to produce and to assemble the stiffeners with other parts of structures. Secondly, welding quality specifically in fatigue prone area between the deck and stiffeners can yield be a serious problem. The major problem of the orthotropic deck bridge with closed stiffeners is the fatigue damage in the intersection between the deck plate with the closed stiffeners, and the conjunction between crossbeam and closed stiffeners.

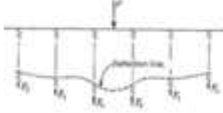
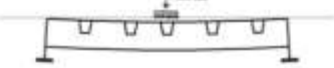
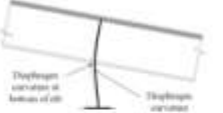
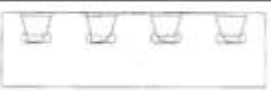
Crossbeam

In orthotropic deck steel bridge, the main crossbeam function is to transfer the load from the deck plate to the main girder. The dimension of the crossbeam is designed by the allowed deflection and construction requirement (AISC, 1962). The shape of crossbeam is based on inverted T-section, where the top of the crossbeam is welded to the deck plate. In general, crossbeam provides the torsional rigidity and the load carrying capacity (AISC,1962).

2.2.2. The Behaviour Mechanism of the Orthotropic Deck Steel Bridge

In the conventional method, the analysis of the bridge is based on the assumption where the complete structural system consists of multiple independent sub-elements such as a deck, stiffeners, and primary structures. In this assumption, each of elements is acting independently and transfer the loads to another element without considering the interactions between sub-elements. Nowadays, a simplified method has been proposed and used to analyse the structural behaviour due to the traffic loads. This method is comprised of decomposing the Orthotropic Bridge Steel Deck structure into series of pseudo sub-system which is more easily to be analysed individually. In this system, the stresses in the panel can be computed by series of the simple mechanistic system. After the stresses are calculated, the principle of linear superposition can be used to combine these stresses. The classification of the pseudo sub-system is depicted in the table 1 below:

Table 1. Orthotropic steel deck deformation mechanism [8]

System	Action	Figure	Result
1	Local Deck Plate Deformation		Transverse flexural stress in deck and rib plates and RD
2	Panel Deformation		Transverse deck stress from rib differential displacements
3	Rib Longitudinal Flexure		Longitudinal flexure and shear in rib acting as a continuous beam on flexible FB supports
4	Floorbeam In-plane Flexure		Flexure and shear in FB acting as beam spanning between rigid girders
5	Floorbeam Distortion		Out-of-plane flexure of FB web at rib due to rib rotation
6	Rib Distortion		Local flexure of rib wall due to FB cut-out
7	Global		Axial, flexural, and shear stresses from supporting girder deformations

2.2.3. Conventional cope hole & 'haibach' cope hole shape

It is well known that the design with long continuous stiffener through the cut-out in crossbeam provide a better fatigue strength in the intersection rather than the discontinuous stiffener welded between crossbeam. However, such a fit connection between the stiffeners and the crossbeam is difficult to control due to the manual cutting. The alternative for this matter is to put a cope hole at the bottom edges of the longitudinal stiffener. Not only it is simple to fabricate, but the area which is necessary to be welded is then reduced. Nevertheless, either a close fit continuous stiffener design and cope hole shape designed still produce relatively high stress concentration due to the load. Figure 19 below depicts the area which has high-stress concentration value due to the in-plane load.

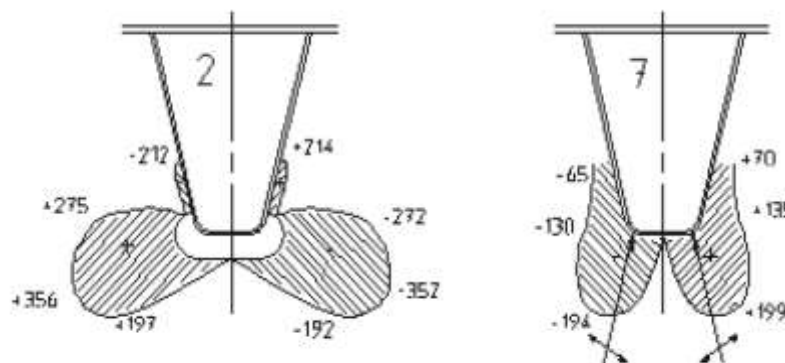


Figure 19. Principal stress distribution around cope hole and fit continuous weld due to in-plane load [2]

The high-stress concentration at the bottom of the conjunction between stiffeners and crossbeam can lead to crack initiation, which later can propagate into the larger crack area. By creating a cope hole in this region, there will be no weld at the high-stress concentration area, which means the crack can be avoided for the particular area.

Although there are some improvements, the crossbeam with conventional cope hole still has a problem with the intersection of the cope hole and the crossbeam. As it can be seen from the figure below, the stresses at the conjunction of conventional cope hole (left images), cover a larger area compared to the new design 'haibach' cope hole shape. By introducing the new concept 'haibach' shape cope hole, the stresses at the intersection between the weld, crossbeam, and the stiffeners can be reduced.

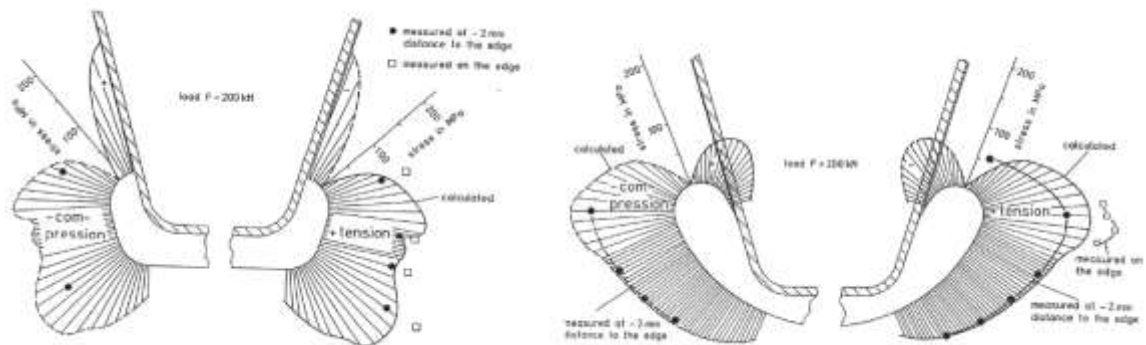


Figure 20. Stress distribution along the edges of conventional cope hole (left image) and 'haibach' shape cope hole (right image) [2]

2.2.4. In-lane Loading Mechanism and The Effects on the Crossbeam

Full-scale tests on the crossbeam with cut-outs can represent the reality of the crossbeam behaviour due to the traffic load. Figure 21 below shows one of the examples of the full scale test by Kolstein, 1995.

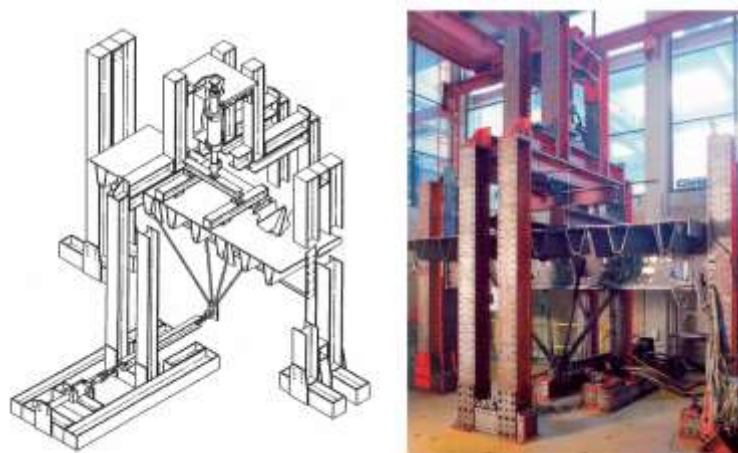


Figure 21. Full-scale test for continuous stiffener on crossbeam [9]

The crossbeam with the cut-out which acts in-plane can be defined as a "Vierendeel Girder" (characterised by vertical members between the top and bottom chords and it is a statically indeterminate structure), it is shown by the figure 22. In this system, the general shear forces are taken by secondary bending and shear in the remaining vertical and horizontal elements.

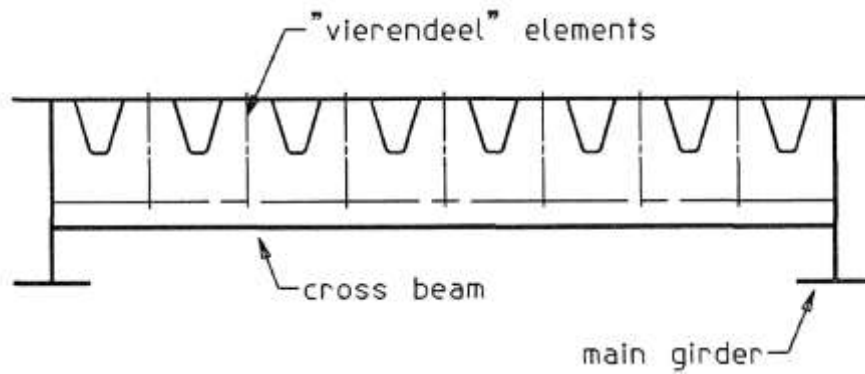


Figure 22. "Vierendeel-system" in crossbeam of orthotropic steel deck [1]

Figure 23 below depicts the behaviour of the crossbeam and the deformed shape due to the in-plane load, with b4 is known as deeper conventional crossbeam with floating deck structures. The in-plane shear and bending yield horizontal displacement of the deck plate, imposing deformation in the closed stiffeners.

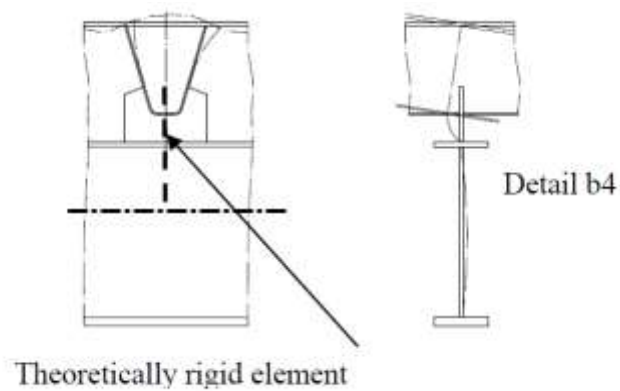


Figure 23. In-plane closed stiffener to crossbeam connection behaviour [2]

3 OVERVIEW OF THE FULL-SCALE EXPERIMENT ON ORTHOTROPIC STEEL DECK

3.1. Specimen Layout

The research study will take place on full-scale experiment of Orthotropic Steel Deck. Figure 24 below depicts the cross-section of the whole orthotropic deck.

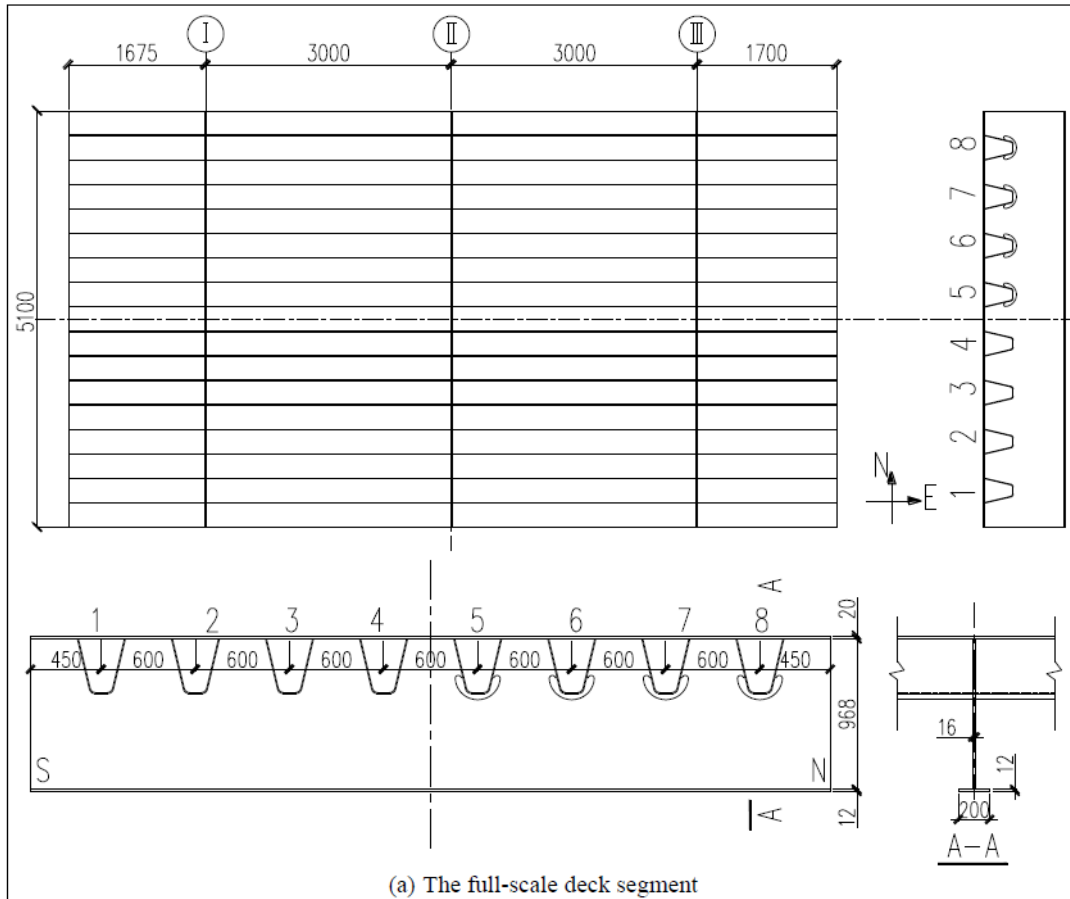


Figure 24. Cross Section of the orthotropic steel deck [10]

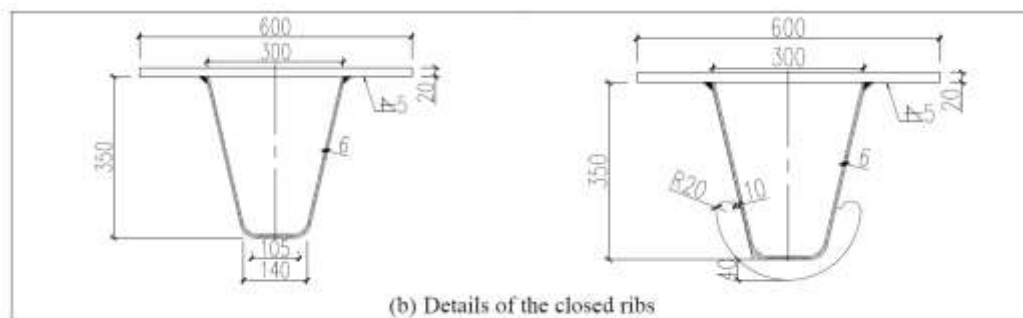


Figure 25. Detail of the closed stiffener (unit in mm) [10]

As it can be seen from the figure 24 and 25 above, the deck consist of 8 closed stiffeners, which is classified into 4 type fully welded trapezoidal stiffeners, and 4 type stiffeners with Haibach cope hole shape. The structural steels S355J2 and S355J2C are used to fabricate the steel plates and the stiffeners. In this research, the study will only focus on crossbeam number 1.

3.2. In-plane Loading Schemes and Values

A series of in-plane quasi-static loading is applied at the location number 10, which is depicted in the figure 26 below.

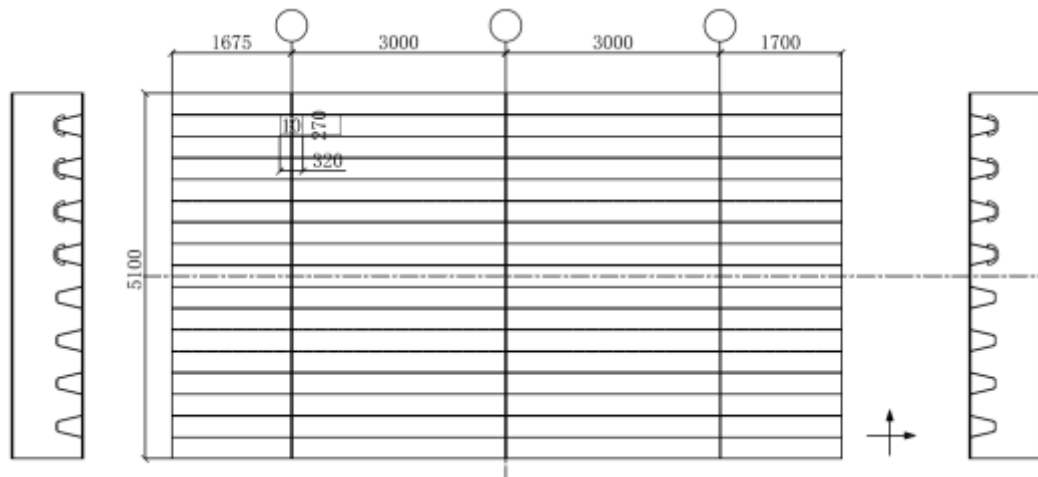


Figure 26. Location of the Static Load

The in-plane quasi-static load is given using hydraulic jack with three layers of rubber plates. The loading is 270 mm x 320 mm, which is the same type C wheel in EN1991-3:2003 Table 4.8. The static loads are performed at the low level to avoid plastic deformation of the steel specimen. The maximum load which is given is 250 kN with the increment of load 25 kN.

3.3. Specification & Locations of the Measurement System

In this research, three measurements system will be utilized. Strain gauges will be used to monitor the strain distribution for a specific location. Linear Variable Differential Transformers (LVDT) will be performed to monitor the out-of-plane deformation of the crossbeam due to the static in-plane load. Digital Image Correlation (DIC) will be employed to monitor both strain distribution and out-of-plane deformation.

3.3.1. Strain Gauges

The strain gauges system is positioned at the location where the most critical strain occurs. The figure below depicts the location of the strain gauges from the free edge of the crossbeam 1. Three strain gauges are installed in each position (left and right of the cope hole) in x, y, and 45-degree direction. It is positioned 15 mm from the edge of the cope hole. The detail of the strain gauges is also described in the table below.

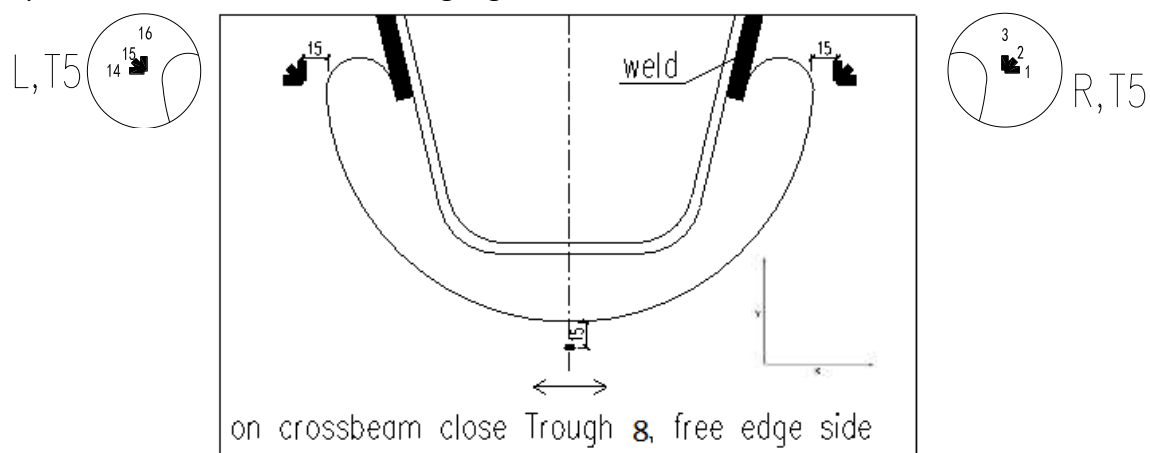


Figure 27. Location of the Strain Gauges on both side (Left and Right)

Table 2. Detail of strain gauges

Position of the Strain Gauges Relative from Outer Side of Crossbeam	Parameter	Code Name
Left	ϵ_{xx}^{left}	Rk014
Left	ϵ_{45}^{left}	Rk015
Left	ϵ_{yy}^{left}	Rk016
Right	ϵ_{xx}^{right}	Rk001
Right	ϵ_{45}^{right}	Rk002
Right	ϵ_{yy}^{right}	Rk003

In this research, the monitoring and measurement will mainly focus on results from x and y-axis only.

3.3.2. Linear Variable Differential Transformer (LVDT)

The load which is applied to the orthotropic steel deck is classified as in-plane static loading. This research will investigate whether the given loading will cause an out-of-plane deformation at certain locations. Two measurement system will be used to monitor the deformation at the different side of the crossbeam. One of the measurement systems is LVDT, and the other is DIC, which will be elaborated below. The LVDT will be installed at the free edge side of the crossbeam, 15 mm below the installation of the strain gauges, as it is depicted in the figure 28 and 29 below.



Figure 29. Location of the LVDT from side view



Figure 28. Location of the LVDT relative to strain gauge

3.3.3. Digital Image Correlation

For this research, the correlation system Q-400 3D measurement system is going to be used. The cameras within the correlation system Q-400 are set to resolution 5 megapixels, with no more than two shots per second can be taken (Dantec Dynamics, Digital Image Correlation System (Q-400), www.dantecdynamics.com). The table 3 below illustrates the technical specification of the system Q-400.

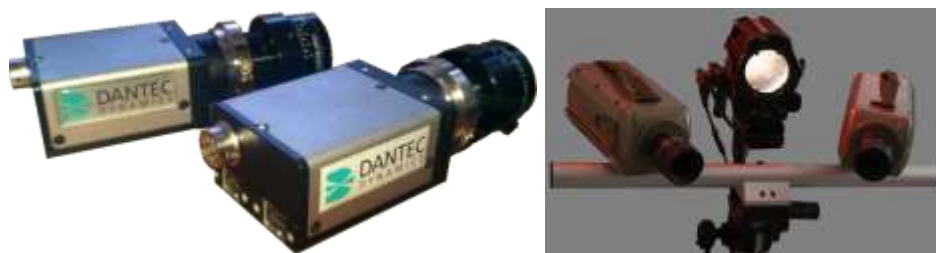


Figure 30. The 3D DIC system Q-400

Table 3. Technical data of the system Q-400

Analysed Surface	20 x 15 mm ² to mm ²
Results of the measurement	3D Displacement and strains
Calibration boards	105 x 148 mm ² to 420 x 594 mm ²
Measurement range	up to hundreds percent of deformation
Measurement sensitivity	Displacements up to 1/100000 of visual field based on measurement conditions (e.g., up to 1 μm within visual field of 100 mm)
Strain sensitivity lower limit	10 μstrain - 100 μstrain depending on the quality of the acquisition (setup, pattern)
Electronic control	Notebook; Windows 7, Vista or XP Professional; implemented analogue device for receiving and recording input-output data; 16-bit resolution; 8 independent freely adjustable analogue channels for data collection; ± 0.05V up to ±10V synchronised for camera launch; 2 channels of analogue output, software Istra 4D
Application	Measurements of displacements and strain on objects of various materials

The DIC system is located on the exact opposite side of other component measurements system (LVDT and strain gauges). It is installed at the inner side of the crossbeam (figure 31 below).

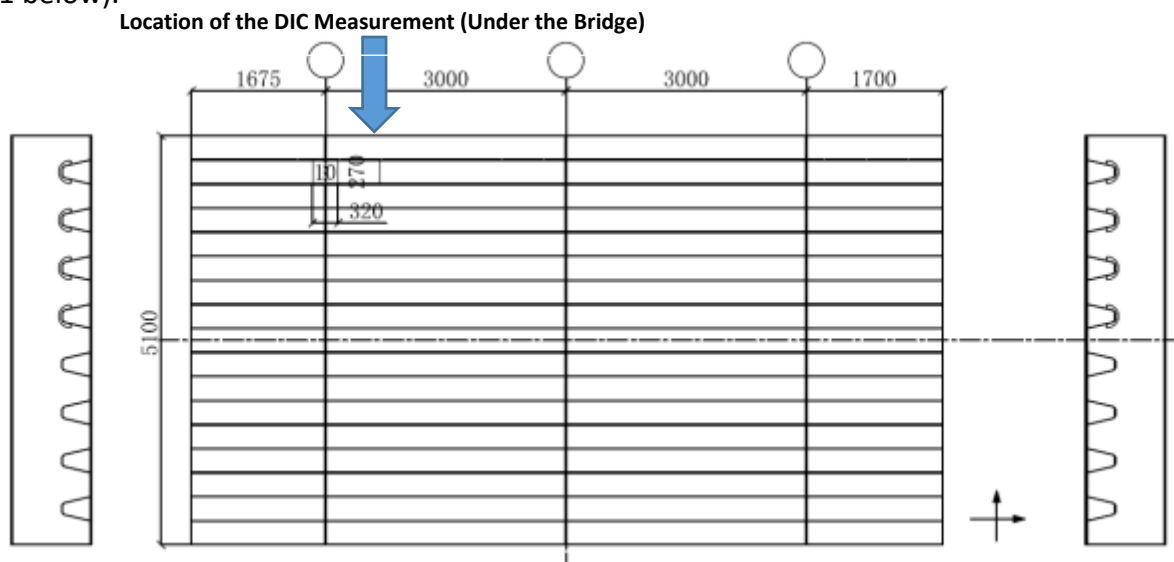


Figure 31. Location of the DIC equipment from top view of the bridge



Figure 32. Location of the camera for left and right measurement



Figure 33. Location of DIC measurement

Table 4. Detail of field of view, focal length, and working distance of the camera

	Position A	Position B
Field of View (mm)	75	75
Focal Length (mm)	75	75
Working Distance (mm)	740	740

There are two different locations of the measurement; “A” and “B”. Where location A is right behind the strain gauges code name Rk001, Rk002, and Rk003. Location B is exactly behind the strain gauges code name Rk014, Rk015, Rk016.

Table 5. Location of the DIC measurement relative to strain gauges

Position of Strain Gauge From Outer Side	Parameter	Code Name	Location of DIC Behind the Strain Gauges
Left	ϵ_{xx}^{left}	Rk014	B
Left	ϵ_{45}^{left}	Rk015	
Left	ϵ_{yy}^{left}	Rk016	
Right	ϵ_{xx}^{right}	Rk001	A
Right	ϵ_{45}^{right}	Rk002	
Right	ϵ_{yy}^{right}	Rk003	

It is also important to be acknowledged that in this particular test 5 mm calibration plates are used. The Q-400 LIMESS DIC measurement system software only provides default scale of 1mm calibration plate. It means the deformation results from DIC reading has to be multiplied by 5. The calibration plate is depicted in figure 34 below.

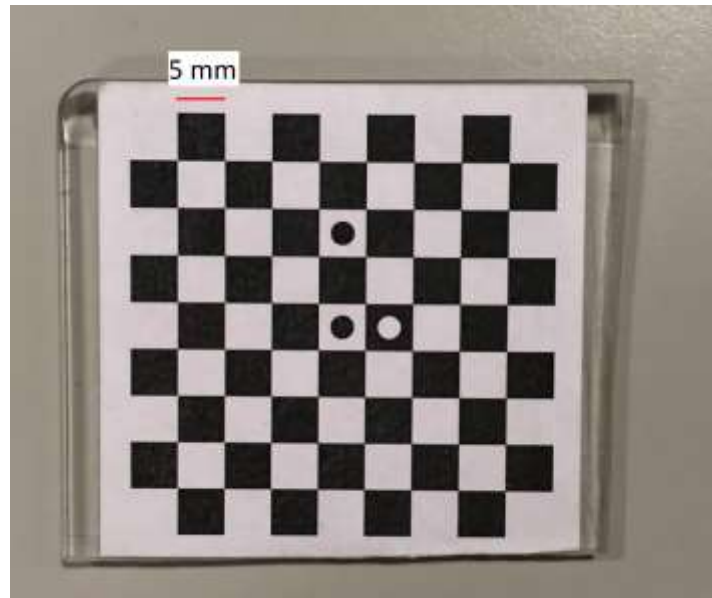


Figure 34. Calibration plate for the particular test

The pattern is made by airbrush device. Figure 35 below shows the appearance of the speckle pattern on the crossbeam for both location A and B. The estimation of the dot size is around 0.02 mm – 0.5 mm with the average size of the dot 0.21 mm.

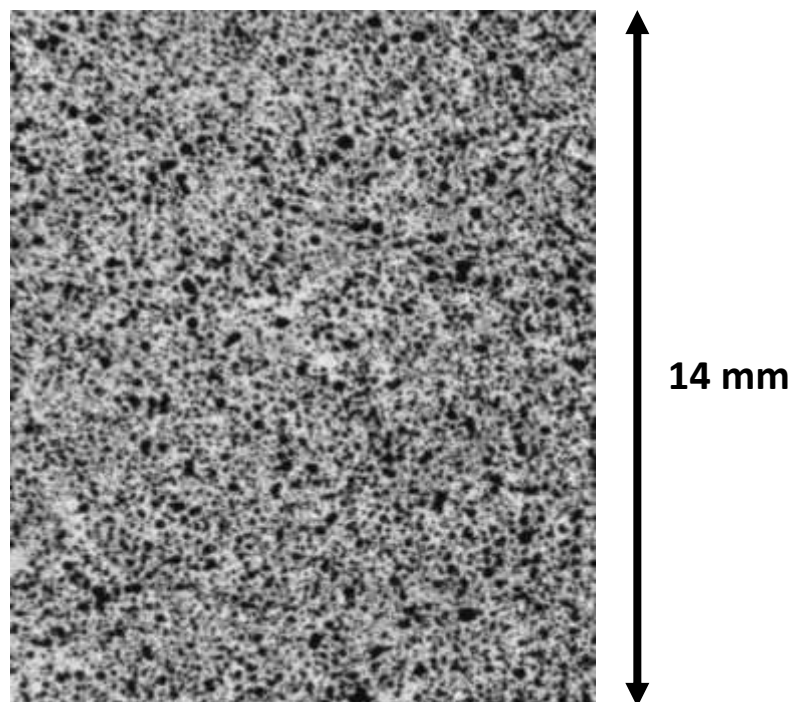


Figure 35. Applied speckle pattern using airbrush device (zoom 100% from the actual image)

4 DATA ACQUISITION & TESTING RESULTS ON FULL-SCALE ORTHOTROPIC STEEL DECK EXPERIMENT

4.1. Data acquisition and Result of the First Test (Region Interest B and Region Behind B)

The first test was conducted in the region of interest B (see figure 33 for location). It is located on the right side of the 'haibach' cope hole (seen from the inner side of crossbeam 1). The other measurement system which is located on the opposite side is also reported in this summary. Figure 36 below shows the location of the strain gauges for the first test.

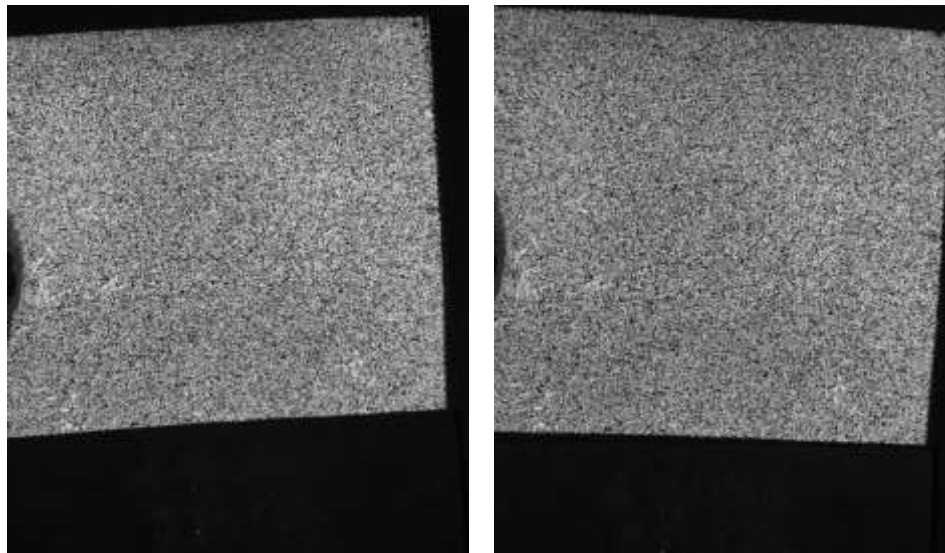
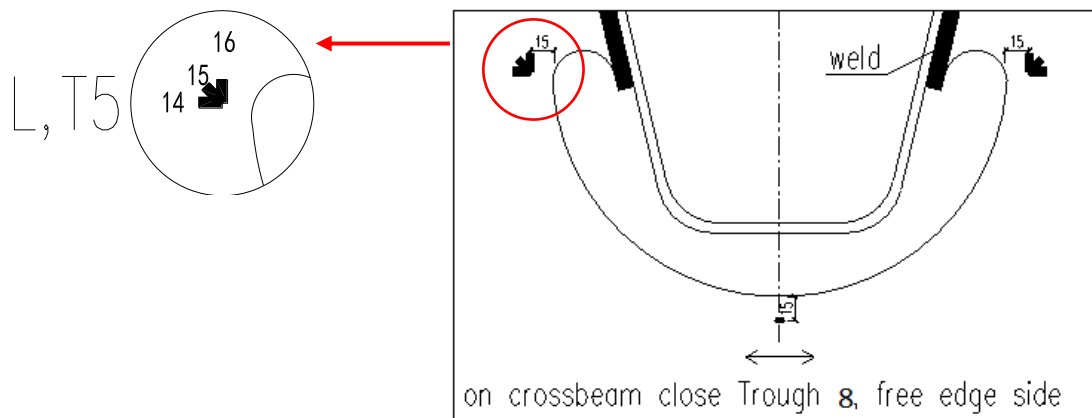


Figure 37. Images From Left and Right Camera for Step 0 (-2kN)

As it is already stated in the previous section, the position for strain monitoring is at 15 mm next to the 'haibach' cope hole. For the out-of-plane deformation, the location is located 15 below the strain monitoring location. Figure 38 below shows the chosen location for out-of-plane deformation and strain measurement.

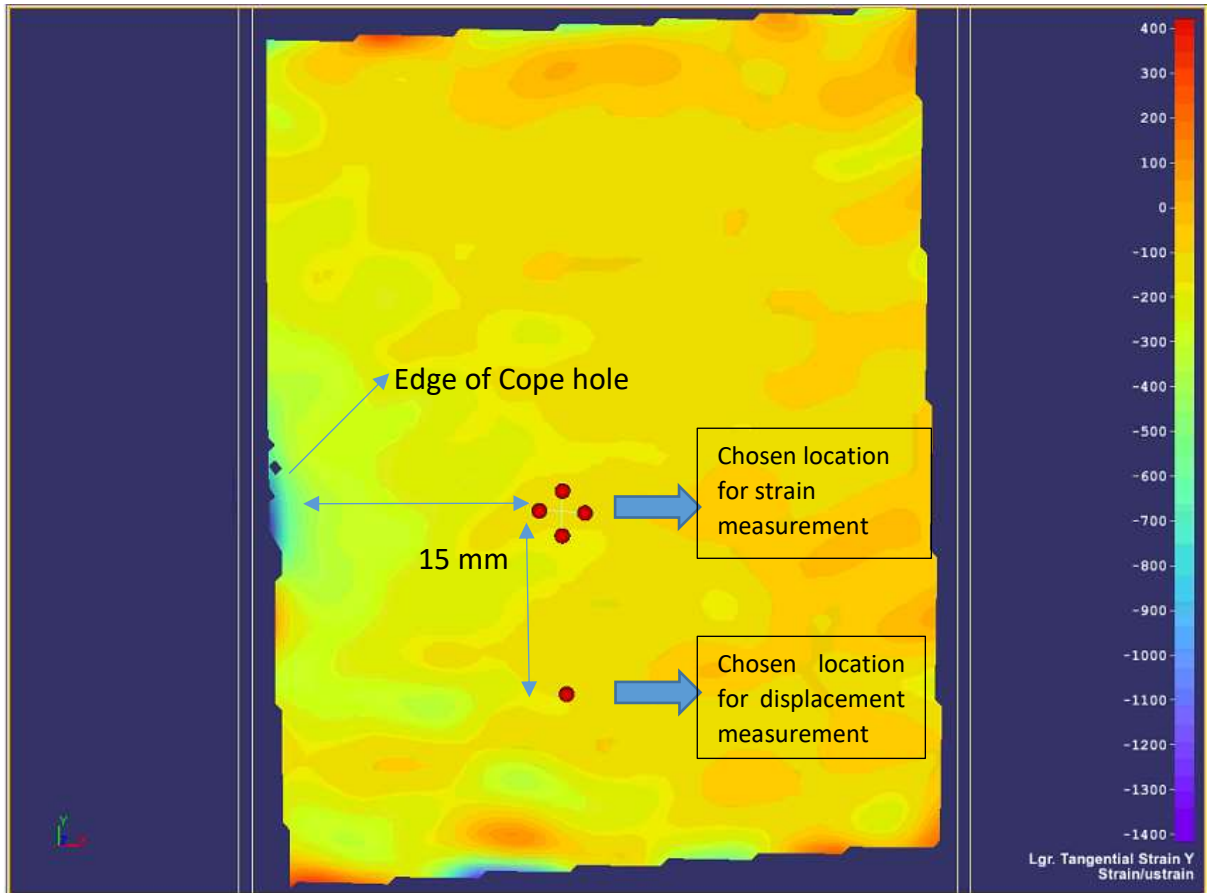


Figure 38. Location for Strain and Displacement DIC Measurement

Table 6 below shows the results from strain gauges, LVDT, and DIC Measurement system.

Table 6. Results from each of measurement system for the first test

Step	Load Value (kN)	Strain Measurement (μ strain)				Out-of-plane Deformation	
		Strain Gauges		DIC (Location B)		LVDT (mm)	DIC (mm)
		Rk014	Rk016	ϵ_{xx}^{right}	ϵ_{yy}^{right}		
0	-2	0	0	0	0	0.0000	0.0000
1	-25	-0.23	-29.38	-10	-40	0.0766	0.0751
2	-50	-2.87	-70.13	-35	-50	0.0764	0.0794
3	-75	-5.17	-112.24	-30	-20	0.0501	0.0565
4	-100	-8.71	-153.68	-35	-100	0.0193	0.0263
5	-125	-12.22	-194.78	-85	-140	-0.0181	-0.0094
6	-150	-15.56	-235.23	-50	-160	-0.0518	-0.0402
7	-175	-19.65	-277.67	-75	-200	-0.0691	-0.0551
8	-200	-23.30	-320.50	-125	-250	-0.0806	-0.0667
9	-225	-26.92	-364.40	-100	-300	-0.0913	-0.0742
10	-250	-30.42	-408.98	-118	-330	-0.0990	-0.0761

Both strain measurement results from DIC and strain gauges give the negative value of strain for every step. The negative sign means compression phenomena is occurred on the specimen during the test, for both x and y-direction. The minimum value of strain in y-direction occurs on the last step of loading (-250 kN), with 409.9 μ strain for strain gauges, and 330 μ strain for DIC measurement. In x-direction, the minimum value occurs on the last step of loading (-250 kN) with 30 μ strain, while for DIC it occurs in step 8 (-200 kN) with -125 μ strain.

For out-of-plane deformation, the direction of the motion was switching from negative to positive sign during the test. It indicates that the crossbeam is bending through positive and negative z-direction during the execution. The reference z-axis for both measurement system (DIC and LVDT) is shown in the figure 39 below. The minimum deformation occurs in the last step of loading (-250 kN) with -0.099 for LVDT and -0.0761 for DIC. The maximum value occurs in the first step of loading (-25 kN) for LVDT with 0.0766 mm while for DIC it is occurred in the second step of loading (-50 kN) with 0.0794 mm.

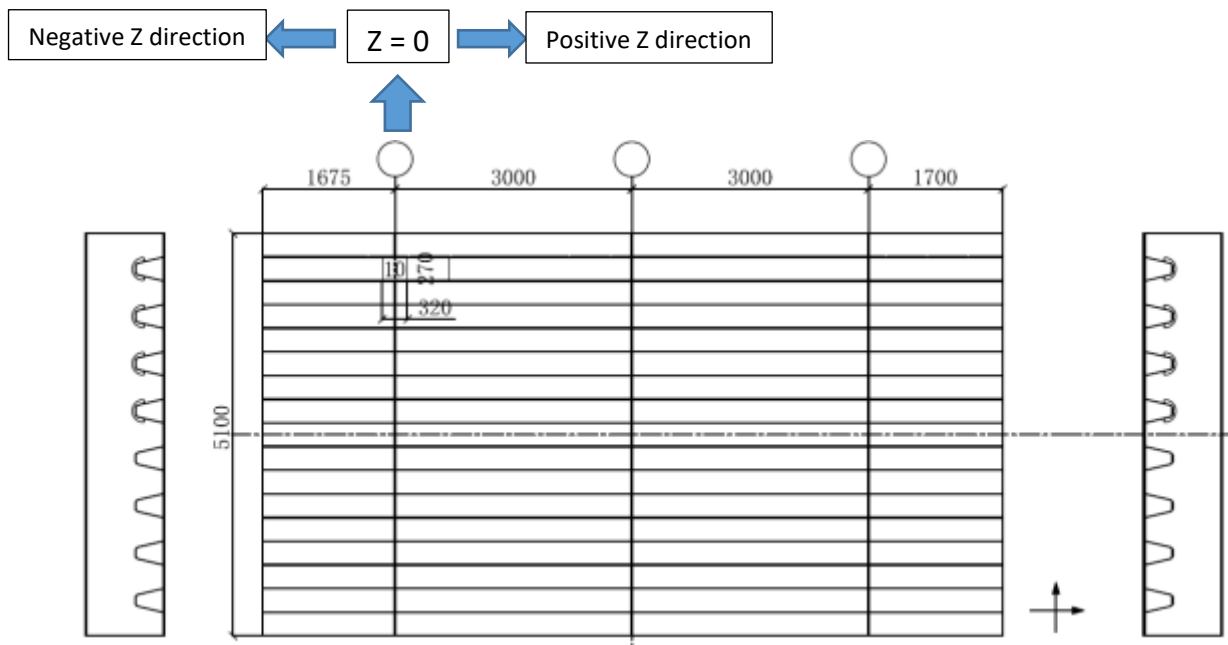


Figure 39. Global Reference z axis sign for measurement system

Figure 40 below shows the out-of-plane deformation of the crossbeam measurement by the 3D DIC for every step. The following figures describe the strain distribution measurement in x and y-direction for every step of the loading.

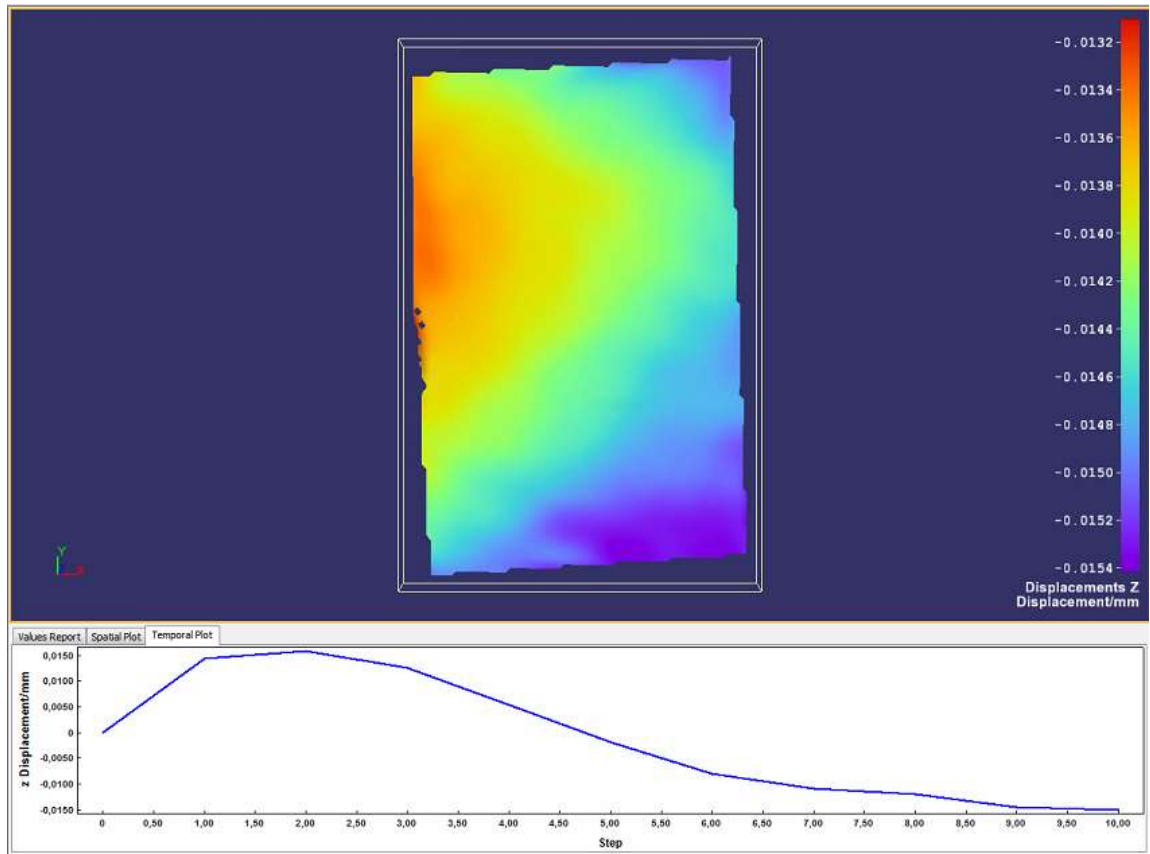


Figure 40. Out-of-plane deformation plot over the step

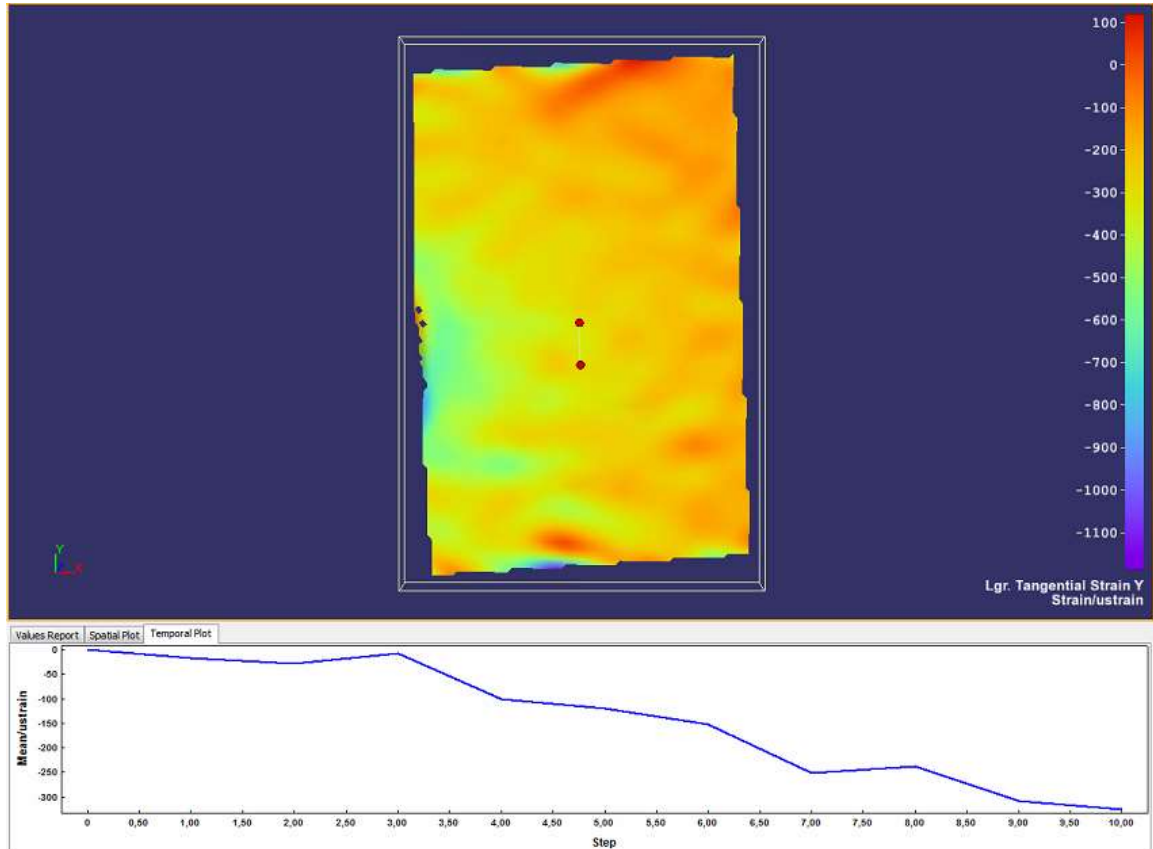


Figure 41. Strain in Y direction plot over the step

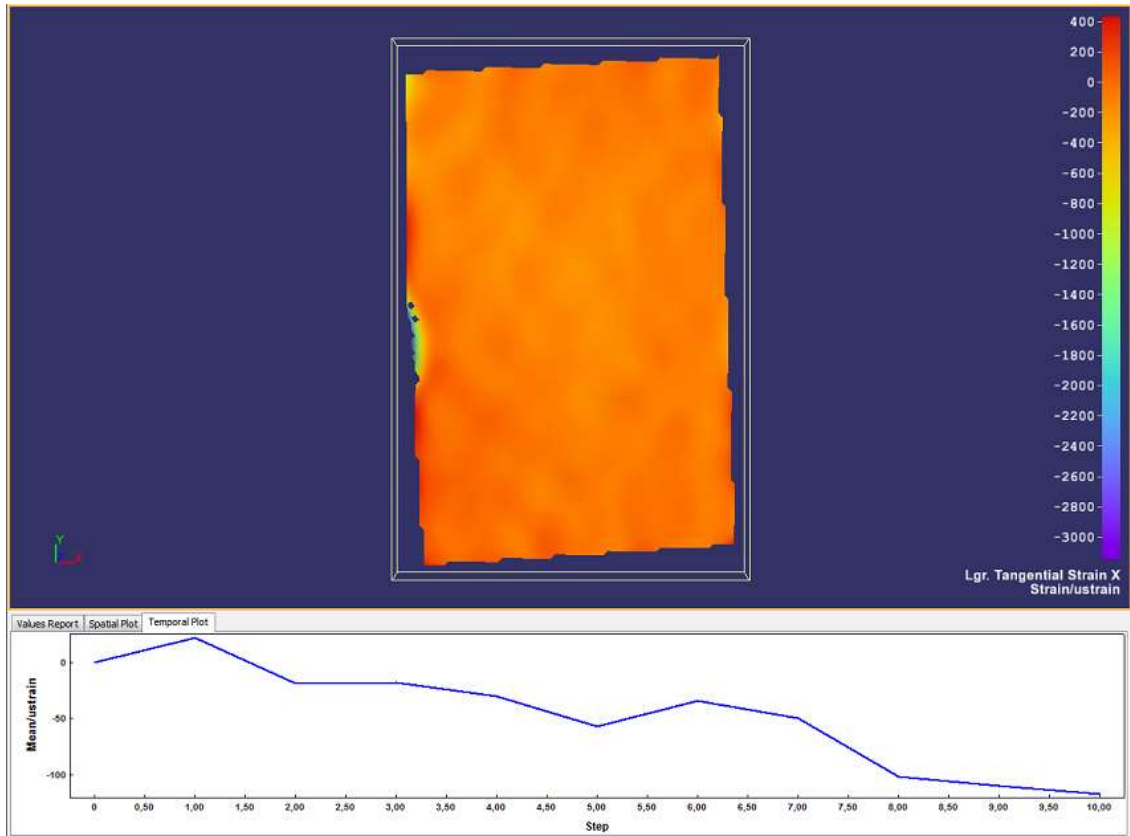


Figure 42. Strain in X direction plot over the step

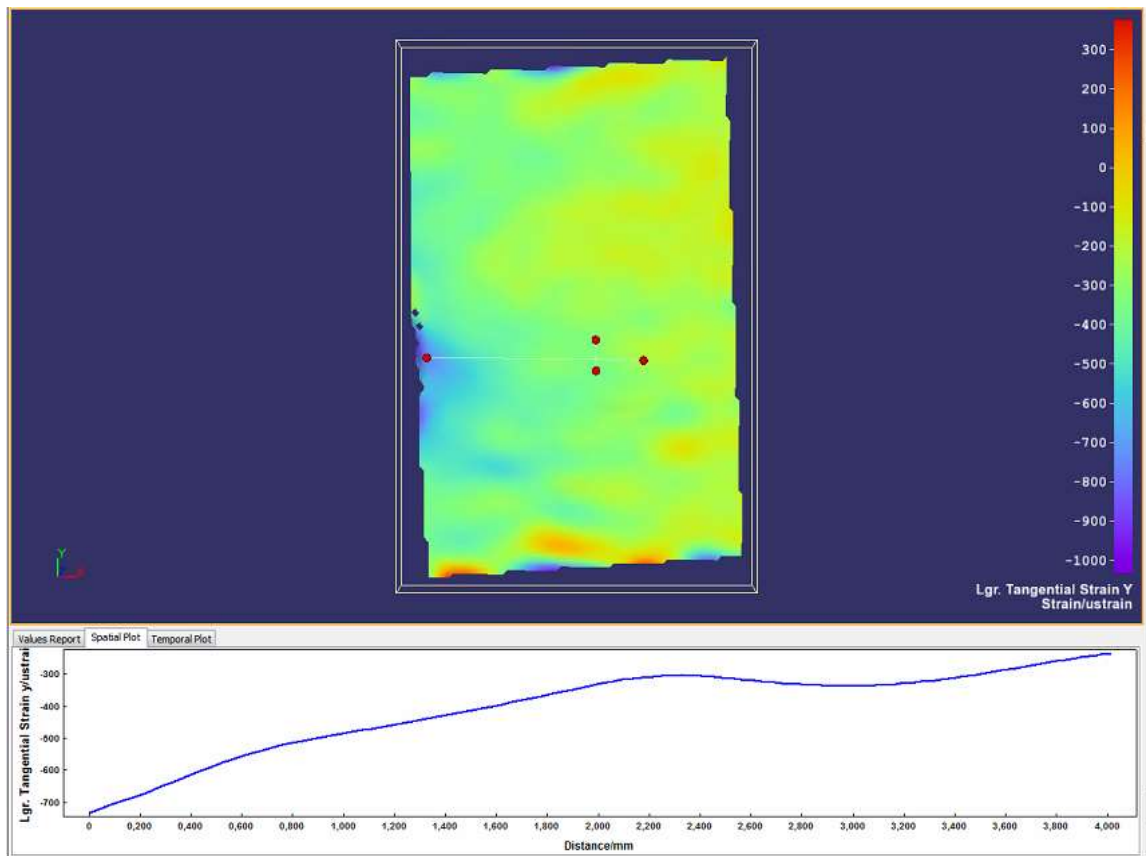


Figure 43. Spatial plot strain in Y direction over the line

Figure 43 above illustrates the spatial plot for strain in the Y direction. It can be observed that the strain concentration in y-axis along the reference line can also be captured in this image. The strain value gradually increases from the very edge of cope hole through the line. From the minimum value around $-700 \mu\text{strain}$ until the position where the strain gauges are installed at the opposite side, with $-330 \mu\text{strain}$.

4.2. Data acquisition and Result on Second Test (Region Interest A and Region Behind A)

The second test was conducted in the region of interest A (see figure 33 for the location). It is located on the left side of the 'haibach' cope hole (seen from the inner side of crossbeam 1). The other measurement system located on the opposite side is also reported in this summary. Figure 44 below shows the location of the strain gauges for the first test.

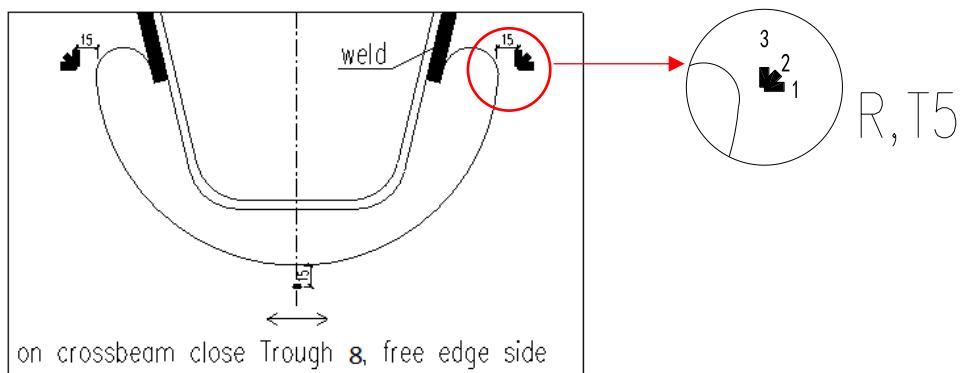


Figure 44. Location of the Strain Gauges for second measurement

The figure shows the images that are taken from the cameras for initial step (-2kN).

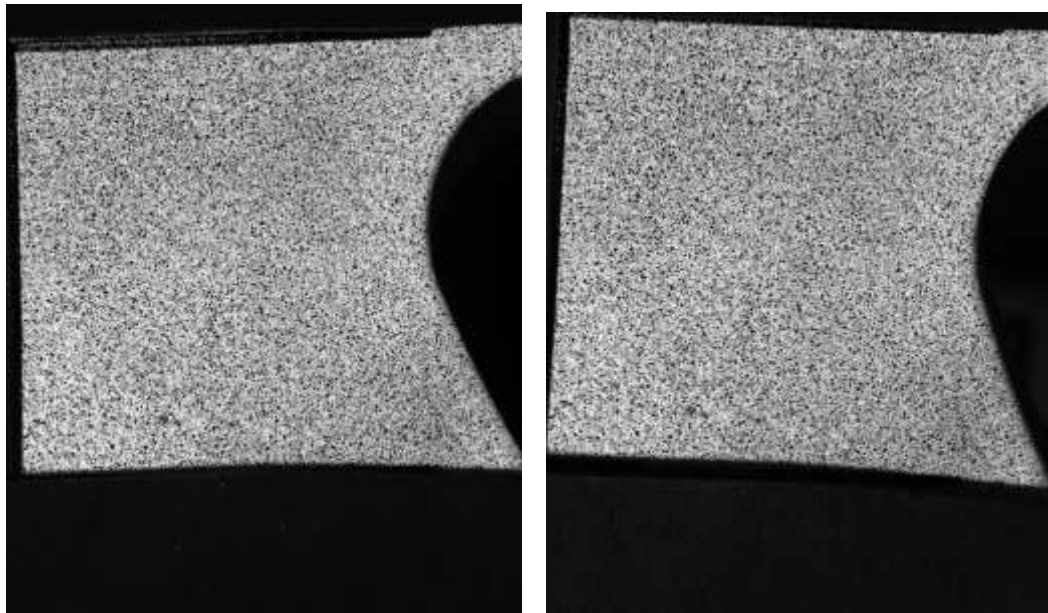


Figure 45. Images From Left and Right Camera for Step 0 (-2kN)

It is also shown in the figure 46 below the chosen location for strain and displacement measurement using DIC.

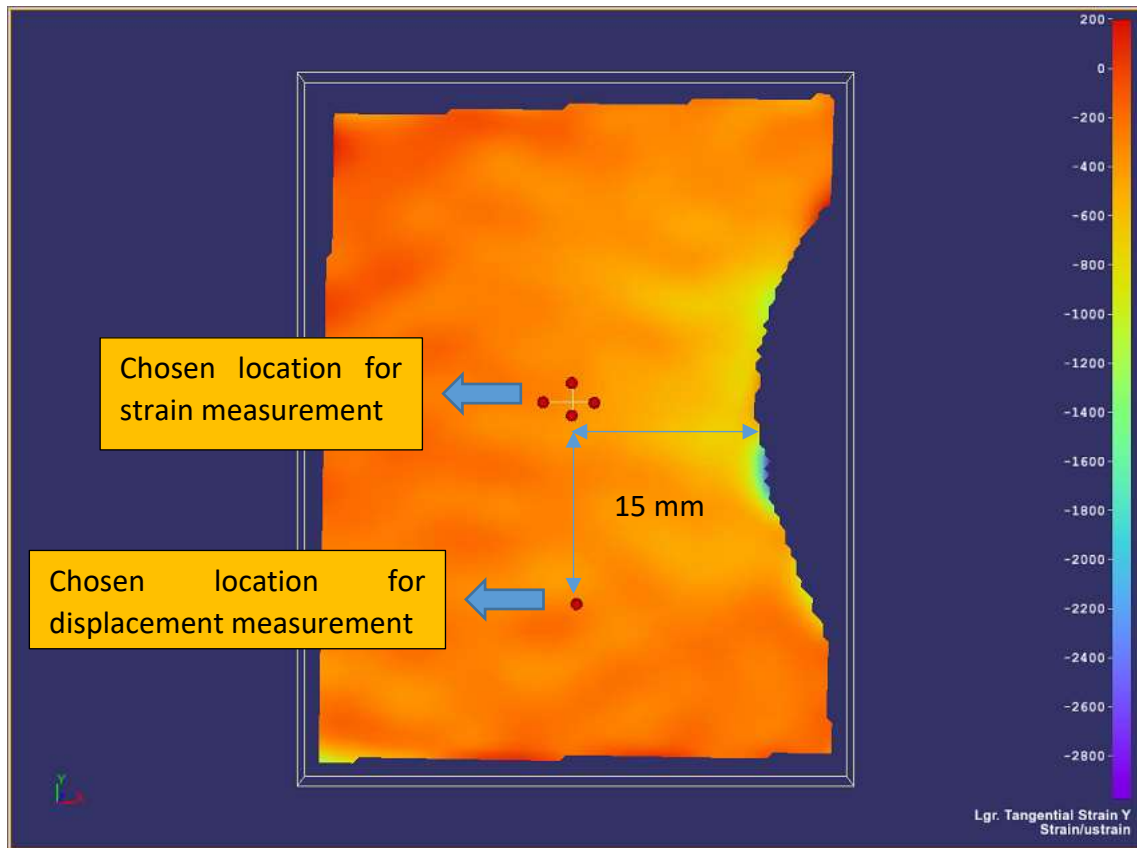


Figure 46. Location for strain and displacement DIC measurement

Table 7 below shows the results from strain gauges, LVDT, and DIC Measurement system.

Table 7. Results from each of measurement system for the second test

Step	Load Value (kN)	Strain Measurement(μ strain)				Out-of-plane Deformation	
		Strain Gauges		DIC (Location A)		LVDT	DIC
		Rk001	Rk003	x	y		
0	-2	0	0	0	0	0.000	0.000
1	-25	-3.10	-38.00	-40	-40	0.085	0.071
2	-50	-6.01	-77.31	-115	-80	0.080	0.069
3	-75	-9.29	-117.36	-50	-40	0.051	0.063
4	-100	-12.86	-153.44	-100	-120	0.015	0.009
5	-125	-16.82	-186.89	-20	-130	-0.025	-0.025
6	-150	-21.25	-220.18	-20	-170	-0.061	-0.063
7	-175	-25.42	-254.12	-30	-200	-0.080	-0.079
8	-200	-29.58	-288.22	-40	-220	-0.093	-0.096
9	-225	-33.59	-322.51	-110	-250	-0.105	-0.101
10	-250	-37.66	-356.80	-110	-340	-0.117	-0.103

For strain results, as it is mentioned before in table 4 explanation, the negative sign shows that the specimen experience compression in x and y-axis. The minimum value for the strain in y-direction occurs in the last step of loading (-250 kN) for both strain gauges and DIC with -356.8 μ strain and -340 μ strain respectively. For x-direction, the minimum value for strain gauge occurs in the last step of loading (-250 kN) with -37.66 μ strain while for DIC it occurs in the second step of loading (-50 kN) with -115 μ strain.

For the out-of-plane deformation measurement, the same phenomena occur similar to the previous test, where the crossbeam 1 bends through positive and negative z-direction during the test. The reference direction of the z-axis is shown in figure 39 above. The maximum value for displacement occurs in the first step of loading (-25 kN) for both measurement LVDT and DIC with 0.085 mm and 0.071 mm respectively. For the minimum value of displacement, it occurs in the last step of loading (-250 kN) with -0.117 mm and -0.103 mm respectively for LVDT and DIC.

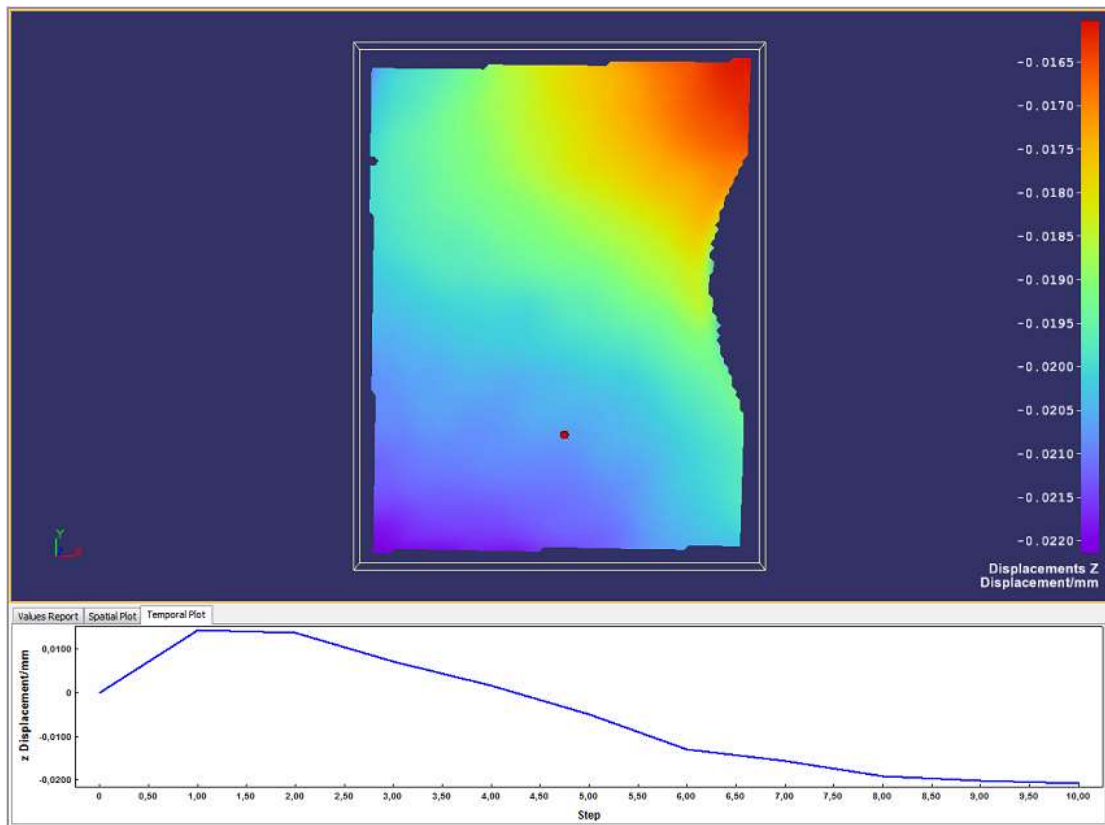


Figure 47. Out-of-plane deformation plot over the step

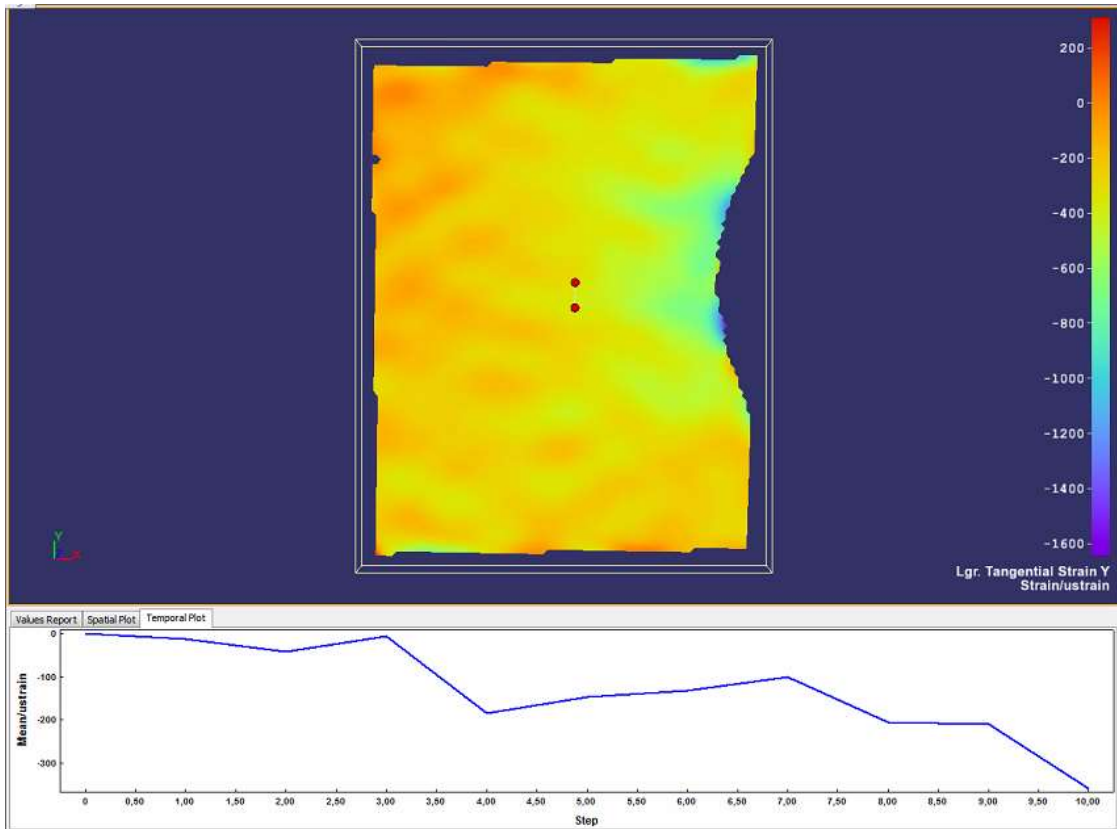


Figure 48. Strain in Y direction plot over the step

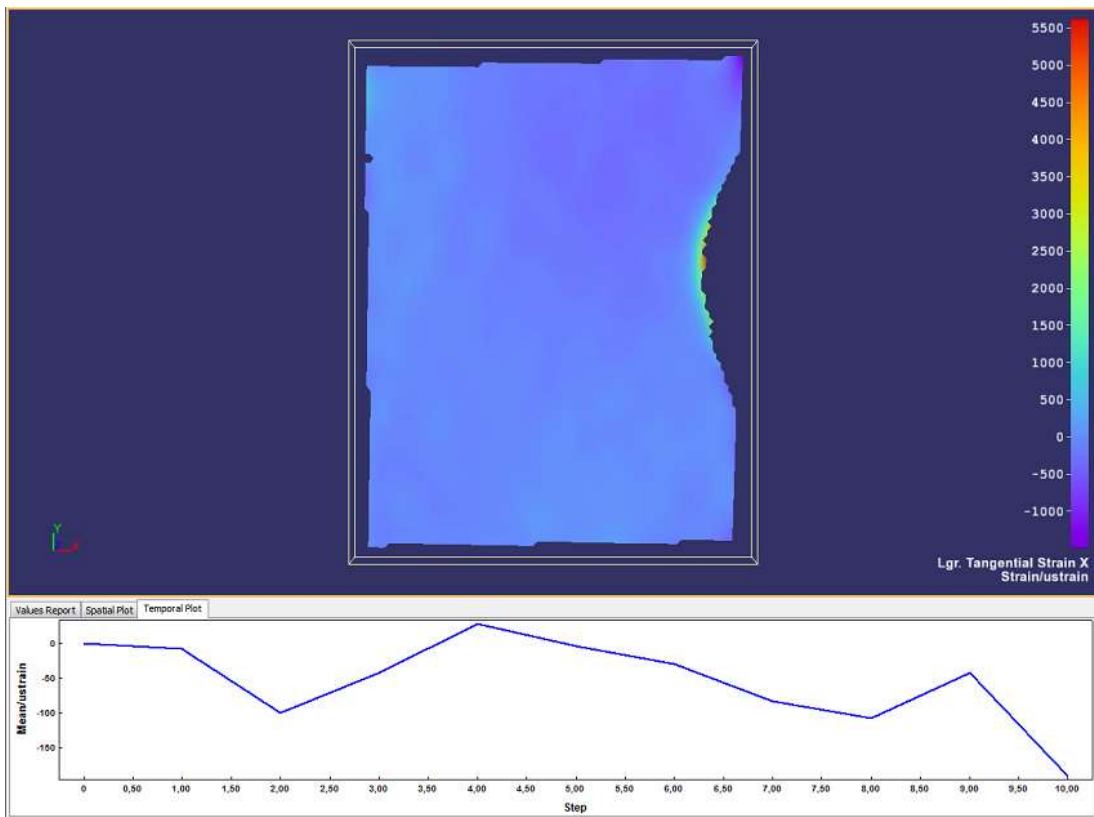


Figure 49. Strain in X direction plot over the step

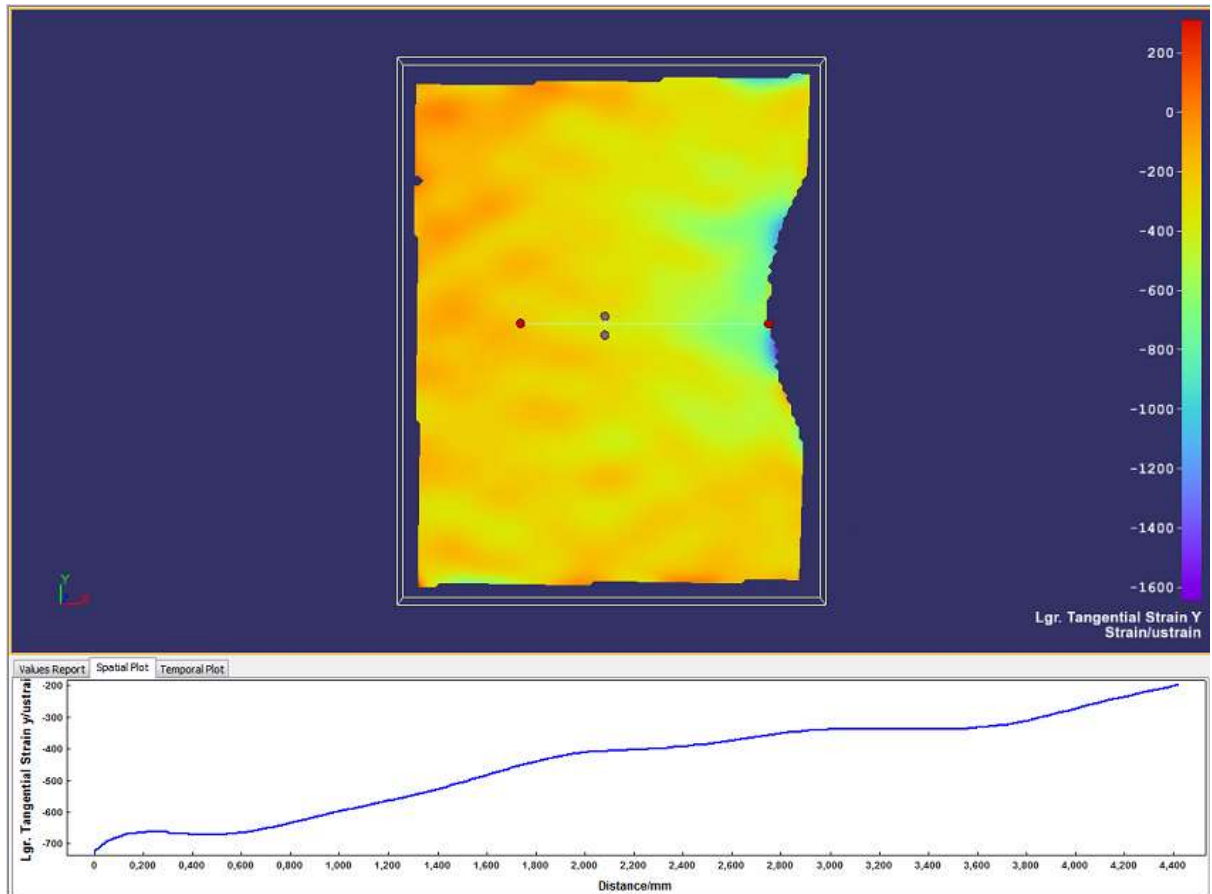


Figure 50. Spatial plot strain in Y direction over the line

Figure 23 shows the strain distribution over the region of interest. It can be seen the strain concentrated near the edge of cope hole. The strain gradually increases from the edge of cope hole until the location where the strain gauges are installed at the backside. The minimum value is at the edge with around -700 microstrain while at the chosen measurement area, the value is -340 microstrain.

5 COMPARISON & ANALYSIS OF THE 3D DIC MEASUREMENT RESULTS TO OTHER MEASUREMENTS

5.1. Strain Gauges Results Compared to The DIC Measurement Result

Table 8 below summarises the results of both of the test in the crossbeam with the calculation of deviation relative to the strain gauges value.

Table 8. Strain Gauges and DIC Results with Error Calculation

Step	Load Value (kN)	Strain Gauges (μ strain)				DIC Measurement (μ strain)				Deviation Strain			
		Rk001	Rk003	Rk014	Rk016	Location A		Location B		Location A		Location B	
						x	y	x	y	x	y	x	y
0	-2	0	0	0	0	0	0	0	0	0	0	0	0
1	-25	-3.10	-38.00	-0.23	-29.38	-40	-40	-10	-40	1191%	5%	4238%	36%
2	-50	-6.01	-77.31	-2.87	-70.13	-115	-80	-35	-50	1814%	3%	1122%	-29%
3	-75	-9.29	-117.36	-5.17	-112.24	-50	-40	-30	-20	438%	-66%	480%	-82%
4	-100	-12.86	-153.44	-8.71	-153.68	-100	-120	-35	-100	677%	-22%	302%	-35%
5	-125	-16.82	-186.89	-12.22	-194.78	-20	-130	-85	-140	19%	-30%	595%	-28%
6	-150	-21.25	-220.18	-15.56	-235.23	-20	-170	-50	-160	-6%	-23%	221%	-32%
7	-175	-25.42	-254.12	-19.65	-277.67	-30	-200	-75	-200	18%	-21%	282%	-28%
8	-200	-29.58	-288.22	-23.30	-320.50	-40	-220	-125	-250	35%	-24%	437%	-22%
9	-225	-33.59	-322.51	-26.92	-364.40	-110	-250	-100	-300	227%	-22%	271%	-18%
10	-250	-37.66	-356.80	-30.42	-408.98	-110	-340	-118	-330	192%	-5%	288%	-19%

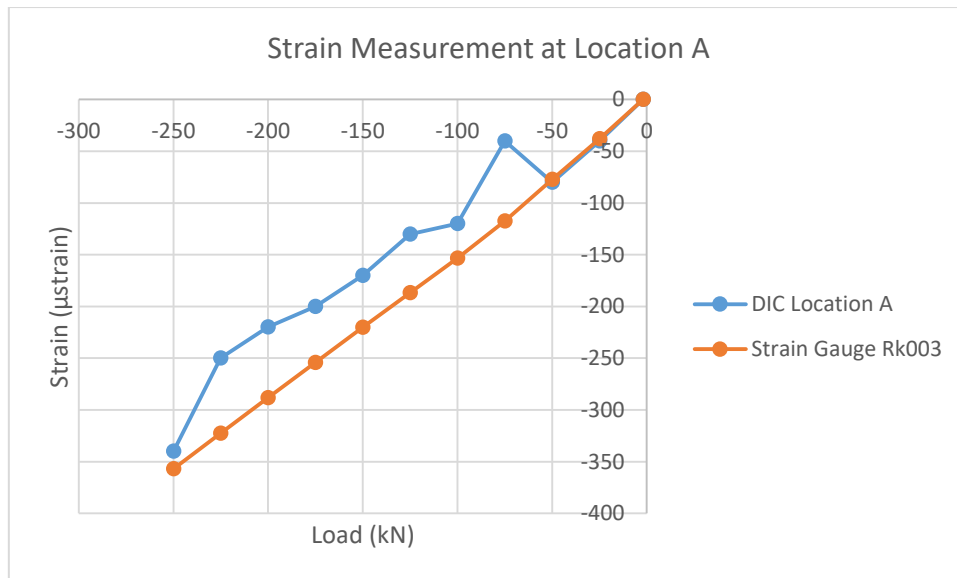


Figure 51. DIC & strain gauges plot for strain in Y direction for location A

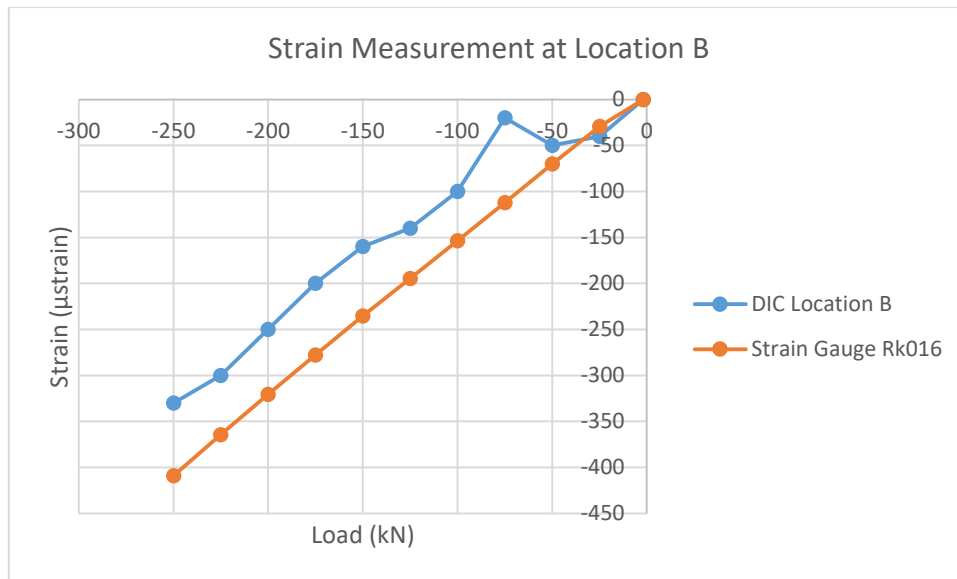


Figure 52. DIC & strain gauge plot for strain in Y direction for location B

The information for the low strain limit camera is known as between 10 µstrain – 100 µstrain. This information is provided by the company who produces the Q400 LIMESS DIC System. But the low strain limit can be changed apart from the default number, depending on many factors, such as quality of pattern and lighting condition. In *ANNEX B section 3D benchmark testing without internal forces present*, provide the study on this matter. Therefore, a benchmark testing without internal forces present was done exactly before the actual test is conducted. The DIC measurement shows value that oscillates from ± 10 µstrain until ± 150 µstrain. Therefore, it is expected that this measurement result will range from the nominal value of $-150 \mu\text{strain} < \text{strain measurement} < 150 \mu\text{strain}$.

From the table 8, it can be seen that all the value for strain measurement in x-direction has a nominal value $> -150 \mu\text{strain}$. Thus the error of measurement relative to strain gauges is incredibly high, that is greater than 100%. The strain measurement in the x-direction from strain gauges itself gives value at the very minimum number $-37.66 \mu\text{strain}$. So in this report, it can be considered that all the strain measurement in the x-direction are not reliable.

For strain in the y-direction, with the same assumption and given information, all the measurement falls within this category, $-150 \mu\text{strain} < \text{strain measurement} < 150 \mu\text{strain}$, can be neglected. This argument can be strengthened by observing the strain in y-direction deviation at step 3 (-75 kN). The deviation for the A and B location is 66% and 82% respectively. Thus, according to the DIC measurement results, the results can be considered as reliable measurement starting from step 4 (-100 kN). If the average error value is taken for strain measurement in location A and B relative to strain gauges, the results will be 21% deviation for measurement in Location A, and 26% deviation for measurement in Location B, for every 25 kN load step. The deviation of DIC measurement for the last step of loading relative to the strain gauges are 5% for location A and 19% for location B.

Due to the in-plane loading, the strain distribution at both sides of the crossbeam is assumed to have the same range value and distribution of strain. The difference between the strain gauges results and DIC can be explained by multiple reasons.

- First, due to the initial imperfection on the crossbeam. The imperfection can be formed globally (the crossbeam already bent) or local dimples on the surface. These phenomena can result in different data measured on both sides.
- Another explanation is owing to the quality of the images that taken by the DIC. Due to the inhospitality of the environment, as well as limitation of camera specification and lighting system, it is hard to achieve a good quality image. It can lead to inaccurate results.
- The error in strain gauges reading might be one of the explanations. The temperature of the environment can give additional strain to the strain gauges measurement.

Based on reasons above, the deviation of results from DIC to strain gauges in Y direction for the last step of the loading can be considered as acceptable (5% and 19%). In other words, the 3D strain measurement for strain in this region of value $< -150 \mu\text{strain}$ and $> 150 \mu\text{strain}$ in orthotropic bridge deck can be considered as reliable.

5.2. LVDT Results Compare with DIC Measurement for Out-of-plane Deformation

Table 7 below shows the comparison between the LVDT measurements with DIC measurement along with the deviation calculation relative to LVDT measurement.

Table 9. Out-of-plane deformation measurement for DIC & LVDT

Step	Load Value (kN)	DIC Measurement		LVDT Measurement		Deviation	
		Location A	Location B	Location A	Location B	Location A	Location B
0	-2	0.000	0.000	0.000	0.000	0%	0%
1	-25	0.071	0.075	0.085	0.077	16%	2%
2	-50	0.069	0.079	0.080	0.076	14%	-4%
3	-75	0.063	0.057	0.051	0.050	-25%	-13%
4	-100	0.009	0.026	0.015	0.019	40%	-36%
5	-125	-0.025	-0.009	-0.025	-0.018	1%	8%
6	-150	-0.063	-0.040	-0.061	-0.052	-3%	22%
7	-175	-0.079	-0.055	-0.080	-0.069	1%	20%
8	-200	-0.096	-0.067	-0.093	-0.081	-4%	17%
9	-225	-0.101	-0.074	-0.105	-0.091	4%	19%
10	-250	-0.103	-0.076	-0.117	-0.099	12%	23%

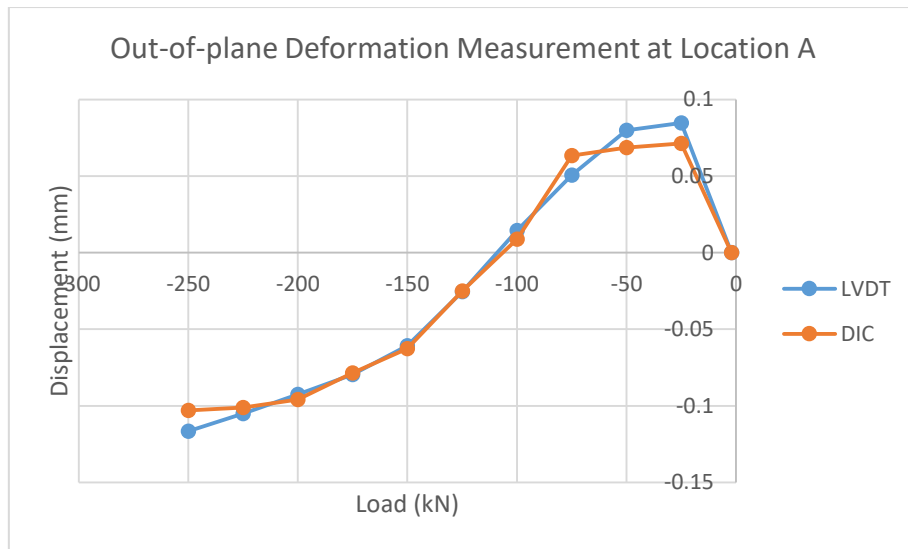


Figure 53. Out-of-plane deformation measurement at location A

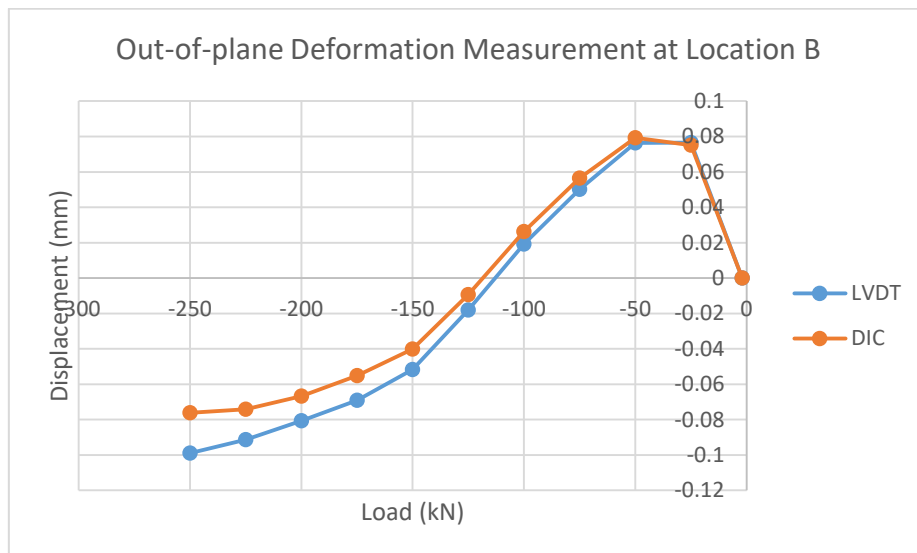


Figure 54. Out-of-plane deformation measurement at location B

In general, both DIC and LVDT show the same trend, with an average of DIC deviation relative to LVDT, is 12% for location A and 20% for Location B. Several reasons that can explain the discrepancies is already stated in the section 5.1. Nevertheless, with given level of deviation, the deviation can be categorised in an acceptable level. Therefore, 3D DIC measurement for Out-of-plane deformation with this level of motion at orthotropic bridge deck can be considered as reliable.

One important conclusion from the out-of-plane deformation measurement, both LVDT and DIC gives out-of-plane deformation around 0.1 mm at the maximum load for the in-plane static loading. From **ANNEX B Section 2D Strain Benchmark Test**, the study shows that for 2D measurement with 0.1 mm out-of-plane and 50 mm field of view, false strain $\pm 200 \mu\text{strain}$ could occur. It proves the chosen 3D DIC strain measurement method as the correct and proper measurement method for the particular research instead of using 2D strain measurement.

5.3. DIC Measurement at Location A compare to Location B

The previous section has been comparing the measurement in one side of measurement location to the opposite side which is exactly behind the chosen location. In this section, the results from the same side of crossbeam yet different location will be compared. In other words, the results from the left of cope hole will be compared with the results from the right side of cope hole.

Table 10. Comparison DIC measurement location A & location B

Step	Loading Value (kN)	Strain Y (microstrain)		Displacement (mm)		Deviation Relative to A	
		Location A	Location B	Location A	Location B	Strain	Displacement
0	-2	0	0	0	0	0%	0%
1	-25	-40	-40	0.07125	0.07505	0%	5%
2	-50	-80	-50	0.0685	0.07935	-38%	16%
3	-75	-40	-20	0.06345	0.0565	-50%	-11%
4	-100	-120	-100	0.00875	0.02625	-17%	30%
5	-125	-130	-140	-0.02505	-0.00935	8%	-63%
6	-150	-170	-160	-0.06265	-0.04015	-6%	-36%
7	-175	-200	-200	-0.0785	-0.0551	0%	-30%
8	-200	-220	-250	-0.0959	-0.0667	14%	-30%
9	-225	-250	-300	-0.1011	-0.0742	20%	-27%
10	-250	-340	-330	-0.10305	-0.0761	-3%	-26%

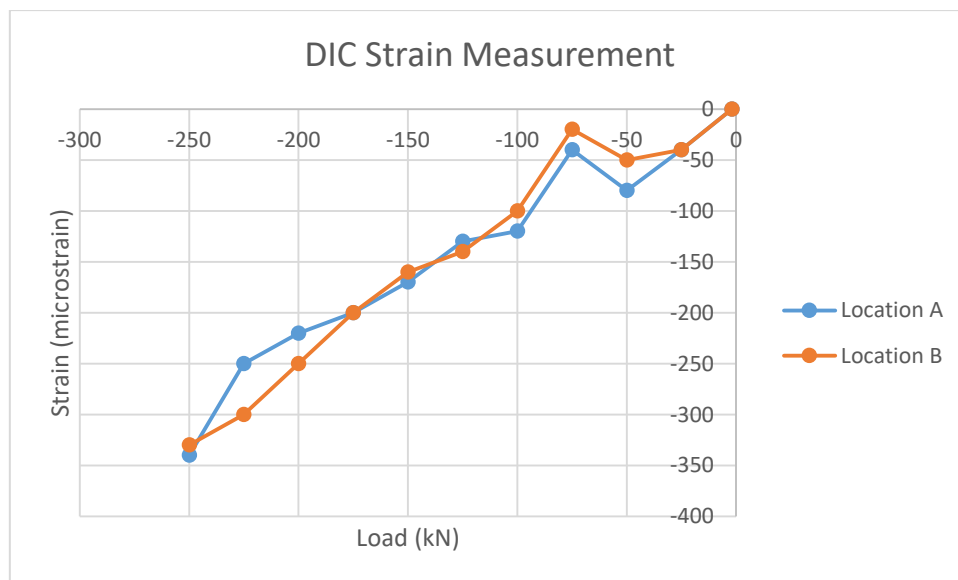


Figure 55. DIC strain measurement

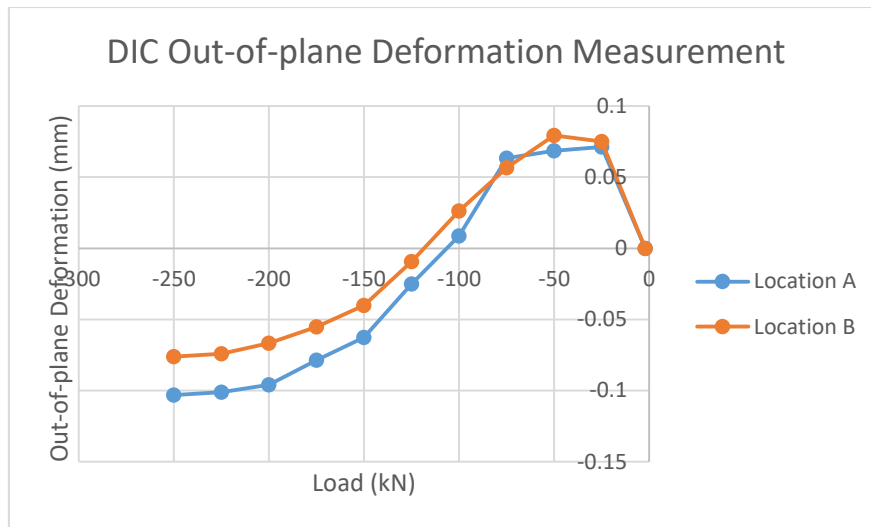


Figure 56. DIC out-of-plane measurement

It can be seen from table and figure above, the difference between measurement in location A and B is relatively significant. The strain deviation relative to one another gives an average value 15% while the displacement gives 24%. Meanwhile, on the opposite side of the crossbeam, strain gauges and LVDT results are tabulated in table 11 below. DIC measurement gives an average 9% strain deviation in comparison with strain gauges, and 15% deviation of displacement for LVDT. The discrepancies between these measurement data can be explained by this particular reason: Different boundary condition and stiffness of the particular observed area. Area B is located on the side where it has a free edge, while A area is fixed on the other side, so it is stiffer. Since both strain gauge and LVDT are installed in B area, it is possible that the strain and displacement at the left side of the cope hole or location B have higher value relative to the right side or location A.

Table 11. Comparison left side cope hole with right side cope hole from the free edge side

Step	Loading Value (kN)	Strain Y (microstrain)		Displacement (mm)		Deviation Relative to A	
		Rk016	Rk003	Location A	Location B	Strain	Displacement
0	-2	0	0	0.000	0.000	0%	0%
1	-25	-29.38	-38.00	-0.085	-0.077	29%	-10%
2	-50	-70.13	-77.31	-0.080	-0.076	10%	-4%
3	-75	-112.24	-117.36	-0.051	-0.050	5%	-1%
4	-100	-153.68	-153.44	-0.015	-0.019	0%	30%
5	-125	-194.78	-186.89	0.025	0.018	-4%	-29%
6	-150	-235.23	-220.18	0.061	0.052	-6%	-15%
7	-175	-277.67	-254.12	0.080	0.069	-8%	-13%
8	-200	-320.50	-288.22	0.093	0.081	-10%	-13%
9	-225	-364.40	-322.51	0.105	0.091	-11%	-13%
10	-250	-408.98	-356.80	0.117	0.099	-13%	-15%

5.4. Number of Pixels for the Captured Image

Digital Image Correlation measurement system is highly dependent on the quality of the captured image. High-quality images will result in a high accuracy of the measurement result. In this research, two main challenges need to be addressed and overcome. First is the location of the crossbeam which is directly under the deck causing a lack of natural lighting system. Second main problem is the level of observed strain which is very small regarding the order of magnitude. With these two main concerns, the benchmark study has been conducted before the actual test on the bridge. The complete process of the benchmark test can be seen in the Annex B. It was inferred from the benchmark study is to use 75 mm field of view. In the previous section, it is concluded that the measurement using Digital Image Correlation for the given level Out-of-plane deformation and strain in y-direction gives adequate results. Therefore, in this section, the terms of the good quality image will be examined more thoroughly. The number of pixels for one particular dot or the size of the dots will be the parameter of the analysis for this section.

As it can be seen from the figure below, a particular location is chosen to represent the dots size and the number of pixels inside one dot. The image below is taken with the right camera for the side of the cope hole location B.

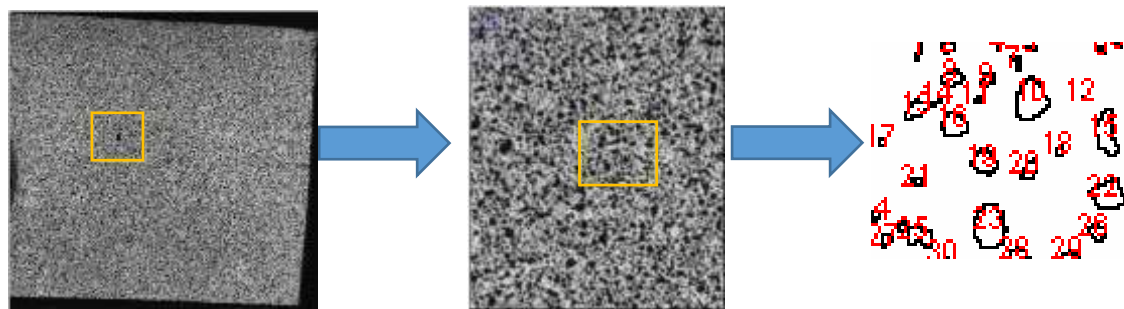


Figure 57. Left - Middle - Right (Full scale Image - 100% zoom - Cropping 2.2 mm x 1.7 mm)

The speckle pattern in the cope hole is comprised of a different size of black dots. The right image is taken for 79 pixels x 66 pixels or 2.2 mm x 1.7 mm area. The biggest dot in that particular is number 23 with the area of the dot around 116 pixels², while the smallest dot (number 12) has one pixels². Using the software of Image J, the average size of the dots of the whole area and number of the calculated dot can also be computed as 38 pixels².

It is known that with this speckle pattern size, the level of deviation for Out-of-plane deformation measurement and strain in y-direction measurement is less than 20%, which can be considered as reliable.

In this research, it is safe to assume that for the 3D DIC measurement on the particular location of crossbeam in the orthotropic steel deck, given by the level of expected displacement and light condition, one black dot with average 38 pixels² area gives a sufficient pattern thus leads to accurate results of the measurements.

6 VALIDATION WITH FINITE ELEMENT METHOD

6.1. ABAQUS FEA

Finite element modelling is important in this research to analyse and evaluate the strain and stress distribution of the monitoring area. ABAQUS finite element analysis software is used for numerical modelling the specimen in this study.

6.2. Strategy of Finite Element Modelling

To obtain the optimum results from finite element method analysis, a comprehensive and detail process of modelling needs to be performed. The figure below describes the process of modelling the specimen using the software.

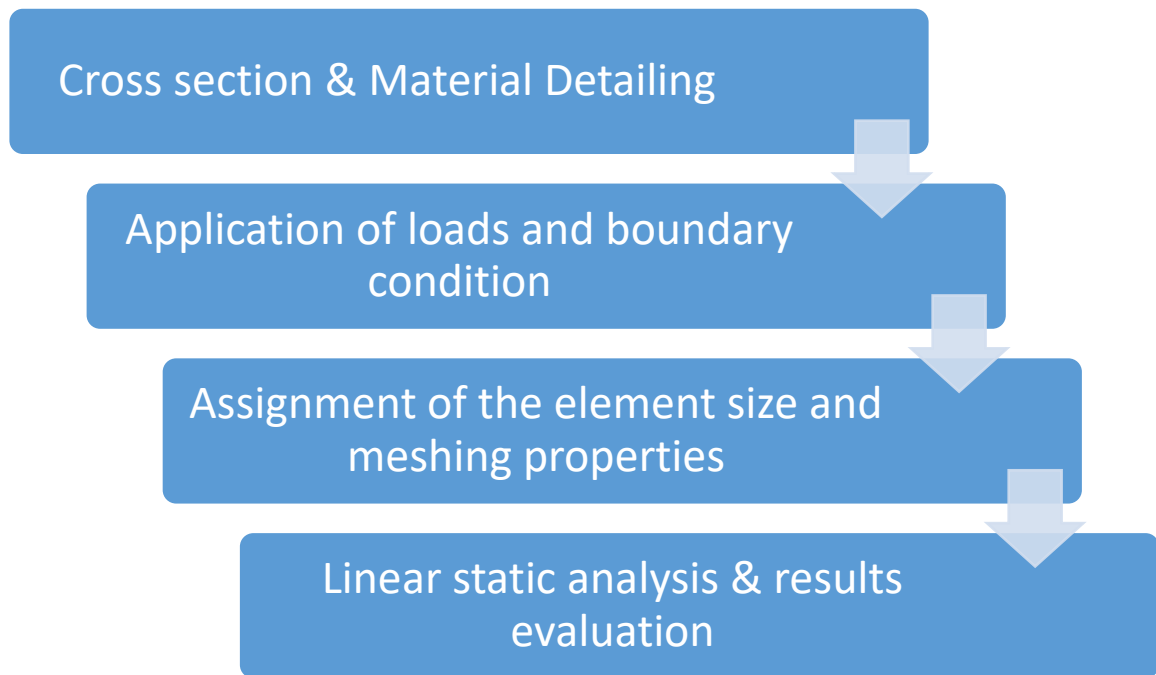


Figure 58. Strategy of finite element method

6.3. Process of Modelling

6.3.1. Cross Section Detailing & Physical Properties Assignment

The detail of the cross-section follows the real ideal shape of the specimen without imperfection. Considering the complexity of details, huge dimension of the specimen, computational efficiency and expected output, it is decided to use only 2 stiffeners and 2 crossbeams instead of a full scale of the model. Figure 59 below depicts the full cross-section of the finite element model of the orthotropic steel deck specimen.

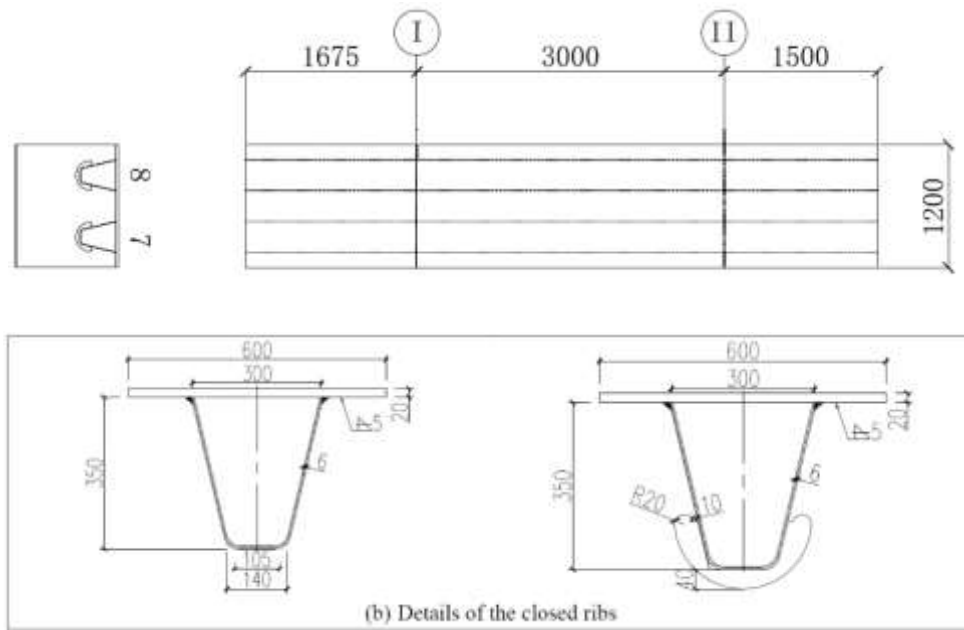


Figure 59. Technical drawing of the specimen

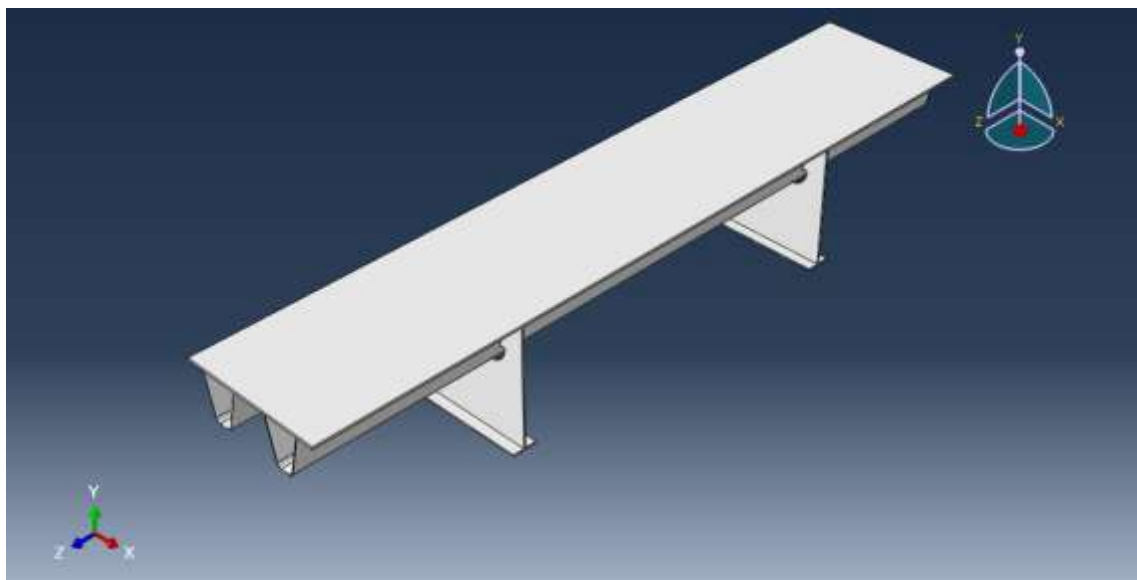


Figure 60. 3D view finite element model

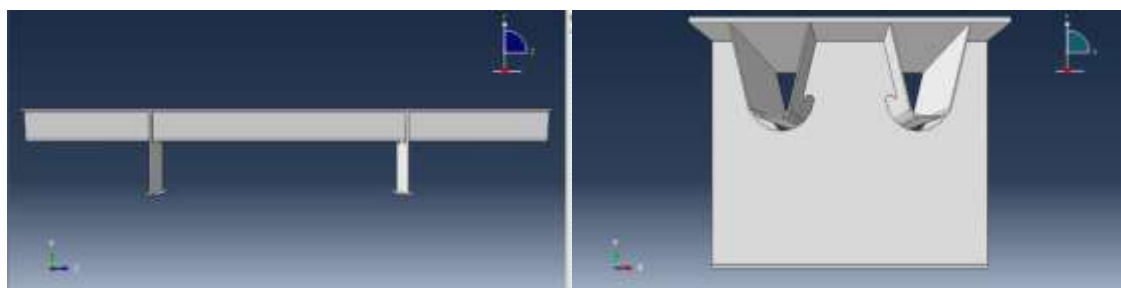


Figure 61. Side view of finite element model

Material that is used for modelling the specimen follow the specification of the real object:

Table 12. Physical Properties of the material

Properties	Value	Unit
Material	Steel	
Fyield	355	$\frac{N}{mm^2}$
Density	7850	$\frac{kg}{m^3}$
Poisson Ratio	0.3	
Modulus Elasticity	210000	$\frac{N}{mm^2}$

6.3.2. Application of Loading and Boundary Condition

It is defined that the applied maximum load is 250 kN, with an area of loading 270 x 320 mm². The position of the loading follows the description in real scale test. For boundary condition, both of the bottom flanges of the crossbeam is fixed in y-direction.

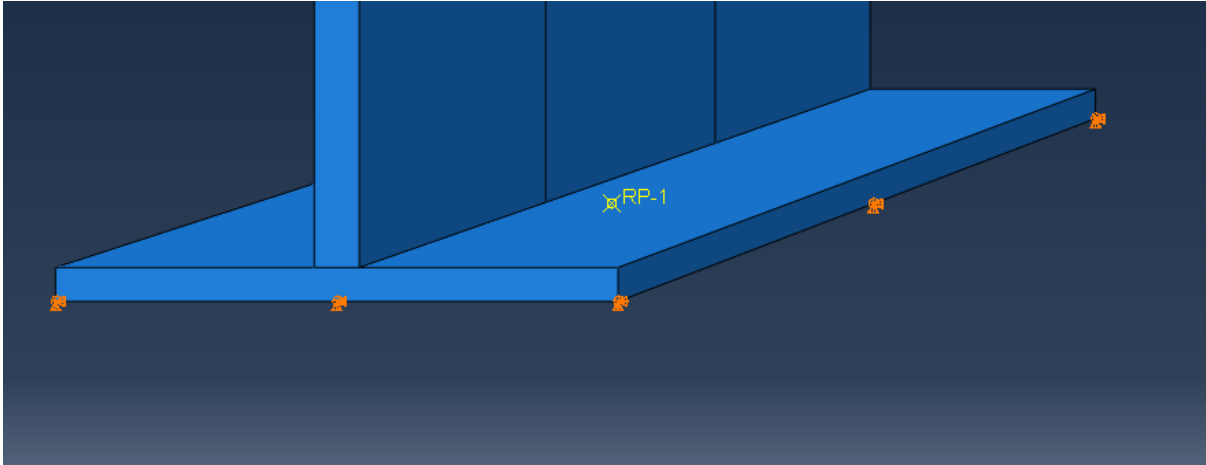


Figure 62. Boundary condition of the crossbeam

6.3.3. Assignment of element size and meshing properties.

Finite element modelling used in this research is composed of solid elements using an 8-node linear brick C3D8R with reduced integration.

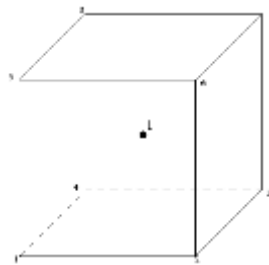


Figure 64. 1x1x1 integration point scheme in hexahedral elements [11]

In this research, the interest region of measurement is located next to the edge of the cope hole, on the crossbeam I. It is essential to model a finer mesh size in this region to get the optimum results. The other region that is located far from the measurement system is modelled using coarser mesh size. The deck plate closed stiffener, and crossbeam is modelled as coarse mesh, with the uniform 10 mm mesh size. While in the region of interest, the mesh size is chosen as 5 mm.

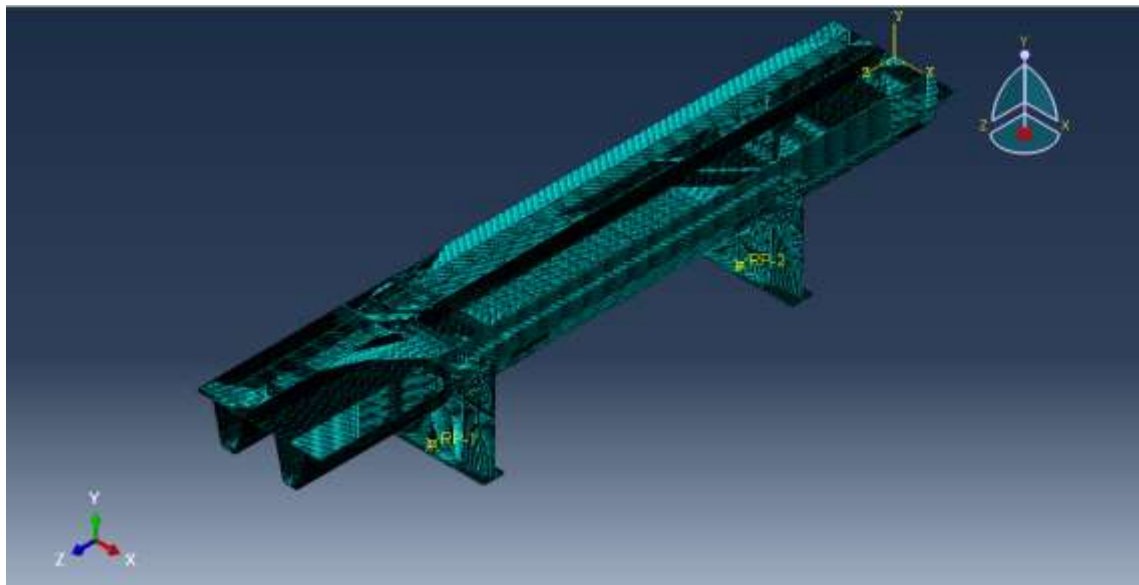


Figure 65. 3D view mesh element

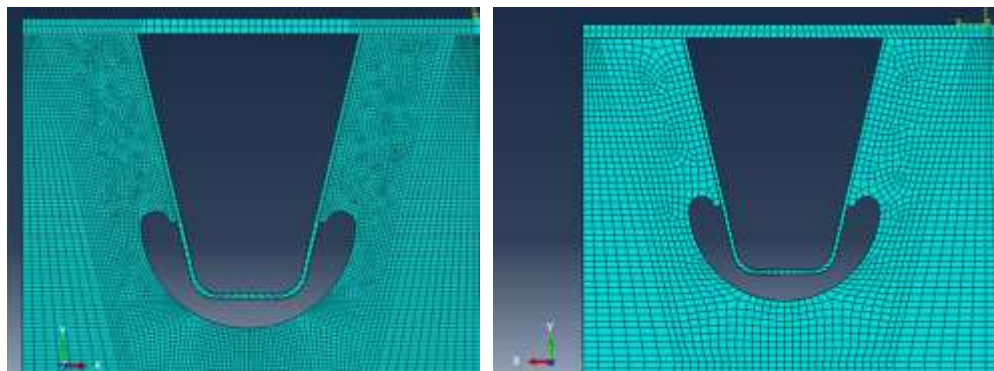


Figure 63. Cross section mesh (left image: 5 mm, right image: 10 mm)

6.4. Validation of Finite Element Model With Measurement Results

6.4.1. Validation of FEM with Strain Gauges & LVDT Measurement at Free Edge Side

The following figure describes the location of the strain gauges and LVDT from the free edge side.

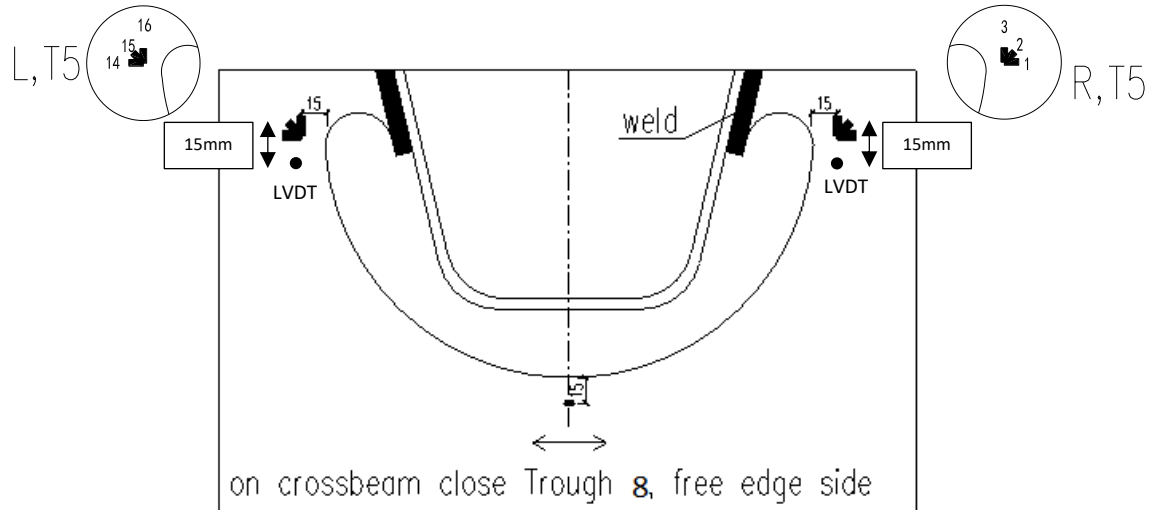


Figure 66. Location of the strain gauges from free edge side

Table 13. Detail of the strain gauge on the crossbeam I

Position of the Strain Gauges Relative from Outer Side of Crossbeam	Parameter	Code Name
Left	ϵ_{xx}^{left}	Rk014
Left	ϵ_{45}^{left}	Rk015
Left	ϵ_{yy}^{left}	Rk016
Right	ϵ_{xx}^{right}	Rk001
Right	ϵ_{45}^{right}	Rk002
Right	ϵ_{yy}^{right}	Rk003

Figure below depicts the strain distribution from ABAQUS software for ϵ_{xx}^{left} & ϵ_{xx}^{right}

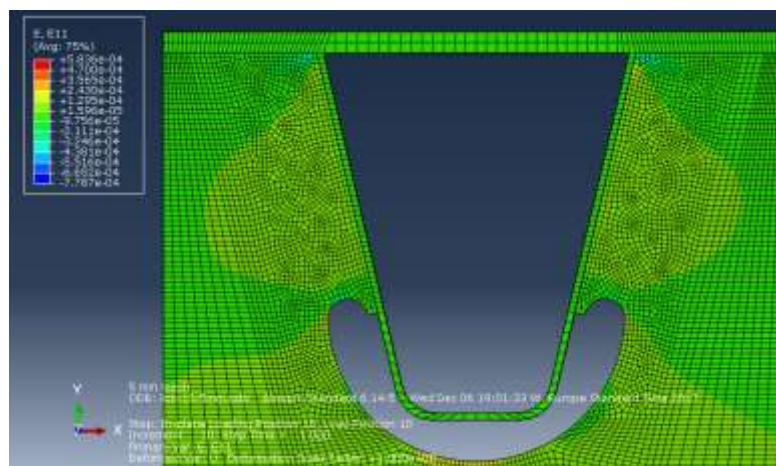


Figure 67. Strain distribution ϵ_{xx} from the free edge side

Followed by figure below shows the strain distribution for ϵ_{yy}^{left} & ϵ_{yy}^{right}

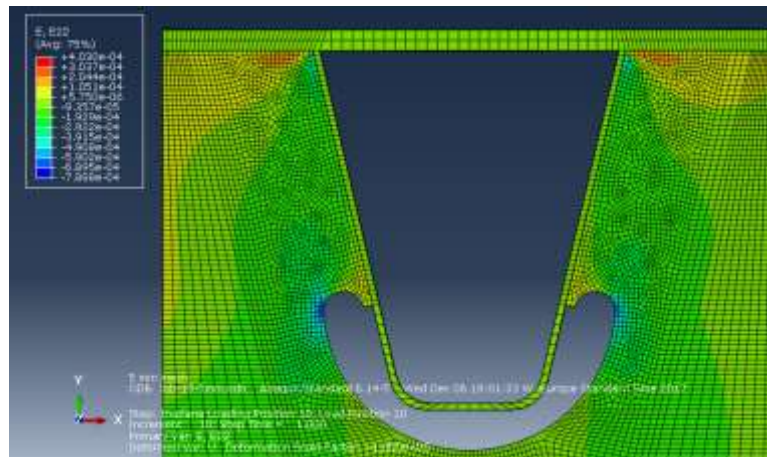


Figure 68. Strain distribution ϵ_{yy} from the free edge side

Table 14. Strain measurement results from strain gauges and FEM for in-plane quasi-static loading

Step	Loading Value (kN)	Strain Gauges (μ strain)				FEM Result (μ strain)				Deviation Strain Relative to Strain Gauge			
		Rk001 (μ strain)	Rk003 (μ strain)	Rk014 (μ strain)	Rk016 (μ strain)	Right Strain xx	Right Strain yy	Left Strain xx	Left Strain yy	Right		Left Side	
										x	y	x	y
0	-2	0	0	0	0	0	0	0	0	0	0	0	0
1	-25	-3.10	-38.00	-0.23	-29.38	-3.32	-29.32	-3.52	-33.67	7%	-23%	1429%	15%
2	-50	-6.01	-77.31	-2.87	-70.13	-6.63	-58.64	-7.05	-67.34	10%	-24%	146%	-4%
3	-75	-9.29	-117.36	-5.17	-112.24	-9.95	-87.96	-10.57	-67.34	7%	-25%	104%	-40%
4	-100	-12.86	-153.44	-8.71	-153.68	-13.27	-117.27	-14.10	-134.67	3%	-24%	62%	-12%
5	-125	-16.82	-186.89	-12.22	-194.78	-16.59	-146.59	-17.62	-134.67	-1%	-22%	44%	-31%
6	-150	-21.25	-220.18	-15.56	-235.23	-19.90	-175.91	-21.14	-202.01	-6%	-20%	36%	-14%
7	-175	-25.42	-254.12	-19.65	-277.67	-23.22	-205.23	-24.67	-235.68	-9%	-19%	26%	-15%
8	-200	-29.58	-288.22	-23.30	-320.50	-26.54	-234.55	-28.19	-269.35	-10%	-19%	21%	-16%
9	-225	-33.59	-322.51	-26.92	-364.40	-29.86	-263.87	-31.72	-303.01	-11%	-18%	18%	-17%
10	-250	-37.66	-356.80	-30.42	-408.98	-33.17	-293.19	-35.24	-336.68	-12%	-18%	16%	-18%

From the table above, it can be seen that the strain measurement results in x and y-axis from finite element model has a similar trend with the results from the strain gauges measurements. Both of the results (FEM and strain gauge) gives slightly greater ϵ_{yy}^{left} values than ϵ_{yy}^{right} . Although for ϵ_{xx}^{left} , the results are off from measurement trend at the beginning of the loading, yet it converges when the load approaches its maximum. For the 15 mm at the left edge of the cope hole, the FEM gives 16 % deviation for ϵ_{xx}^{left} and 18% deviation for the ϵ_{yy}^{left} at the maximum load 250 kN. For the 15 mm at the right edge of the cope hole, the FEM gives 12% deviation for ϵ_{xx}^{right} and 18% deviation for ϵ_{yy}^{right} at the maximum load 250 kN. The difference between the FEM model and the real measurement can be explained by multiple reasons such as mesh quality, element size, and non-uniform material. Having said that, it can be inferred that the difference between FEM and

experiment is in the acceptable range. Therefore, it can be concluded that the finite element model with solid element and 5 mm fine mesh at the region of interest, can be established and used for modeling the strain distribution at the 15 mm next to the edge of the cope hole.

For Out-of-plane deformation at 15 mm below the strain gauges, the results from the measurement and the FEM can be seen from the table and figure below.

Table 15. Out-of-plane deformation results from FEM and LVDT for in-plane quasi-static loading

Step	Loading Value (kN)	LVDT Measurement		FEM Results		Deviation	
		Left Side	Right Side	Left Side	Right Side	Left Side	Right Side
0	-2	0.000	0.000	0.0000	0.0000	0%	0%
1	-25	0.077	0.085	-0.0009	0.0003	-101%	-100%
2	-50	0.076	0.080	-0.0018	0.0005	-102%	-99%
3	-75	0.050	0.051	-0.0026	0.0008	-105%	-98%
4	-100	0.019	0.015	-0.0035	0.0010	-118%	-93%
5	-125	-0.018	-0.025	-0.0044	0.0013	-76%	-105%
6	-150	-0.052	-0.061	-0.0053	0.0016	-90%	-103%
7	-175	-0.069	-0.080	-0.0061	0.0018	-91%	-102%
8	-200	-0.081	-0.093	-0.0070	0.0021	-91%	-102%
9	-225	-0.091	-0.105	-0.0079	0.0023	-91%	-102%
10	-250	-0.099	-0.117	-0.0088	0.0026	-91%	-102%

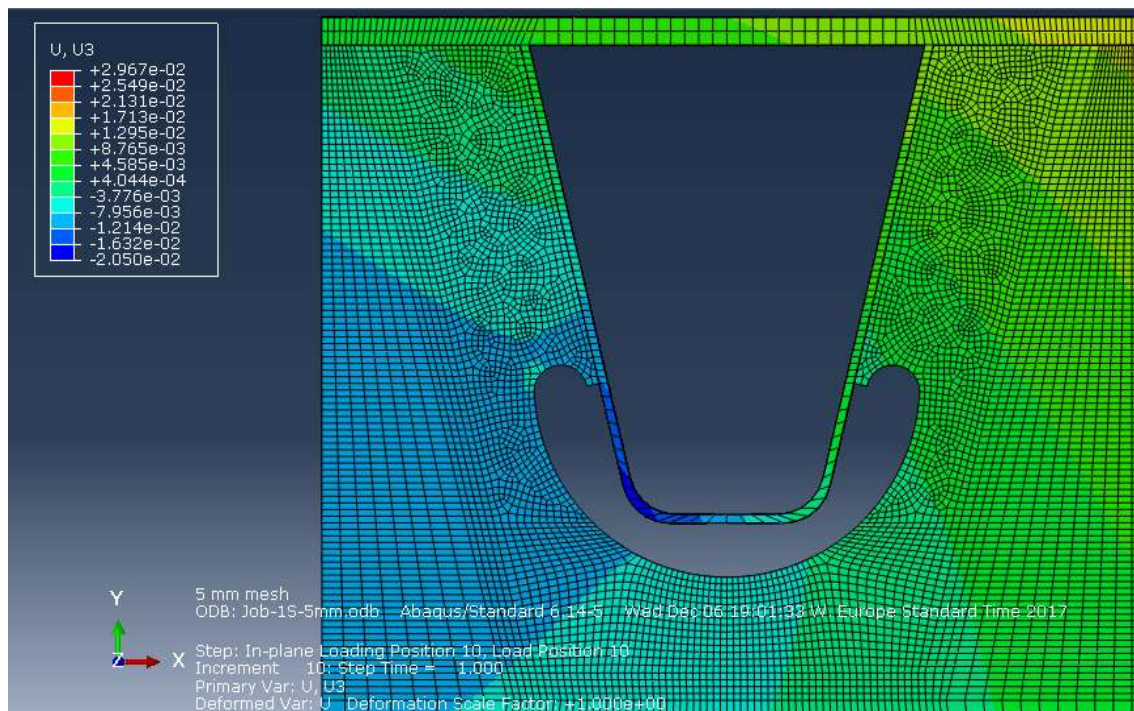


Figure 69. Out-of-plane distribution at the crossbeam I

The results from finite element do not show a good agreement with the results from LVDT measurements. It can be seen that for experimental results, the out-of-plane deformation for both sides of the cope hole moves in the same direction for every time step. It moves from positive z-direction to negative z-direction along the process. For the FEM results, the direction of the displacement is consistent for each side of the crossbeam. At the left side of the crossbeam, the displacement is constantly at the negative sign, or it moves toward the negative z-direction. While on the right side of the cope hole, the crossbeam moves toward the positive z-direction. Several factors can explain this phenomenon:

- There is an initial bending imperfection on the crossbeam. In finite element model, the specimen is modelled in perfect straight shape, while in reality, the shape of the crossbeam might be not straight.
- The second reason is due to the eccentricity of the crossbeam relative to the loading position. In FEM the loading position is located exactly at the top of the crossbeam and deck. However, in reality, the position of the crossbeam might not have been straight, thus creating eccentricity towards the loading position.

Based on that, the current finite element model for Out-of-plane deformation approach results is not reliable to use. Sensitivity study of this problem is recommended to be performed using finite element analysis in the further study.

6.4.2. Validation of FEM with DIC Measurement

In this section, the results from the inner side of the crossbeam one will be evaluated. Location of the monitored area is depicted in the figure 70 below. The position of the measurement will be represented by “A” location and “B” location



Figure 70. Location of the DIC measurement

FEM results for both strain measurements and Out-of-plane deformations will be compared and analysed relative to the DIC measurement. The table below gives both the calculation FEM results and DIC measurement results for strain distribution and strain measurement.

Table 16. Strain Measurement Results from FEM & DIC

Step	Loading Value (kN)	DIC Measurement (μ strain)				FEM Result (μ strain)				Deviation Strain Relative to Strain Gauge			
		A Strain xx	A Strain yy	B Strain xx	B Strain yy	A Strain xx	A Strain yy	B Strain xx	B Strain yy	A		B	
										x	y	x	y
0	-2	0	0	0	0	0	0	0	0	0	0	0	0
1	-25	-40	-40	-10	-40	-3.32	-29.32	-3.52	-33.67	-92%	-27%	-65%	-16%
2	-50	-115	-80	-35	-50	-6.63	-58.64	-7.05	-67.34	-94%	-27%	-80%	35%
3	-75	-50	-40	-30	-20	-9.95	-87.96	-10.57	-67.34	-80%	120%	-65%	237%
4	-100	-100	-120	-35	-100	-13.27	-117.27	-14.10	-134.67	-87%	-2%	-60%	35%
5	-125	-20	-130	-85	-140	-16.59	-146.59	-17.62	-134.67	-17%	13%	-79%	-4%
6	-150	-20	-170	-50	-160	-19.90	-175.91	-21.14	-202.01	0%	3%	-58%	26%
7	-175	-30	-200	-75	-200	-23.22	-205.23	-24.67	-235.68	-23%	3%	-67%	18%
8	-200	-40	-220	-125	-250	-26.54	-234.55	-28.19	-269.35	-34%	7%	-77%	8%
9	-225	-110	-250	-100	-300	-29.86	-263.87	-31.72	-303.01	-73%	6%	-68%	1%
10	-250	-110	-340	-118	-330	-33.17	-293.19	-35.24	-336.68	-70%	-14%	-70%	2%

According to the table, the strain in x-direction gives significant discrepancy between the FEM calculation and DIC measurements. As it is already mentioned in chapter 5, due to the low strain limit of the equipment (100 μ strain), the comparison results of strain in x-direction is unreliable thus it can be completely neglected. For the strain in y-direction results, the deviation gives relatively small error. At the maximum load (-250 kN), the strain y in location A shows the difference of 14% while at the location B the strain error is 2%. This significant discrepancies between FEM and DIC measurement below 100 μ strain occurred owing to the low strain limit of DIC equipment. One important note to highlighted, for FEM estimation the strain-yy in location A gives lower results than location B. While DIC results and trends show otherwise.

The table below describes the comparison results of Out-of-plane deformation at the chosen location along with its error calculation.

Step	Loading Value (kN)	LVDT Measurement		FEM Results		Deviation	
		Location B	Location A	Location B	Location A	Location B	Location A
0	-2	0.000	0.000	0.0000	0.0000	0%	0%
1	-25	-0.077	-0.085	-0.0009	0.0003	-99%	-100%
2	-50	-0.076	-0.080	-0.0018	0.0005	-98%	-101%
3	-75	-0.050	-0.051	-0.0026	0.0008	-95%	-102%
4	-100	-0.019	-0.015	-0.0035	0.0010	-82%	-107%
5	-125	0.018	0.025	-0.0044	0.0013	-124%	-95%
6	-150	0.052	0.061	-0.0053	0.0016	-110%	-97%
7	-175	0.069	0.080	-0.0061	0.0018	-109%	-98%
8	-200	0.081	0.093	-0.0070	0.0021	-109%	-98%
9	-225	0.091	0.105	-0.0079	0.0023	-109%	-98%

10	-250	0.099	0.117	-0.0088	0.0026	-109%	-98%
----	------	-------	-------	---------	--------	-------	------

The DIC measurement has an identical result with LVDT measurement. So the significant discrepancies between the FEM and DIC measurement can be explained by the same reason that has been explained in the section 6.4.1.

6.5. Sensitivity Analysis on Mesh Refinement

As it is stated in the section 6.3.3, finer mesh at strain gauges area is expected. Therefore the sensitivity analysis is necessary to estimate the required size of element to obtain a reliable FEA result. The left side of the cope hole from the free edge side is chosen as the reference of the study. The strain distribution from the tip of the cope hole until 25 mm line horizontal will be compared for a varied element size. Element size of 2mm, 5 mm, 10 mm, and 15 mm are compared through graph below.

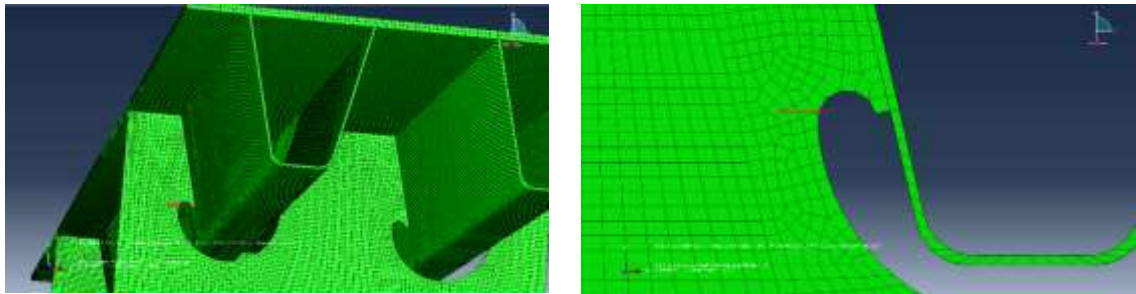


Figure 72. Location of the mesh study

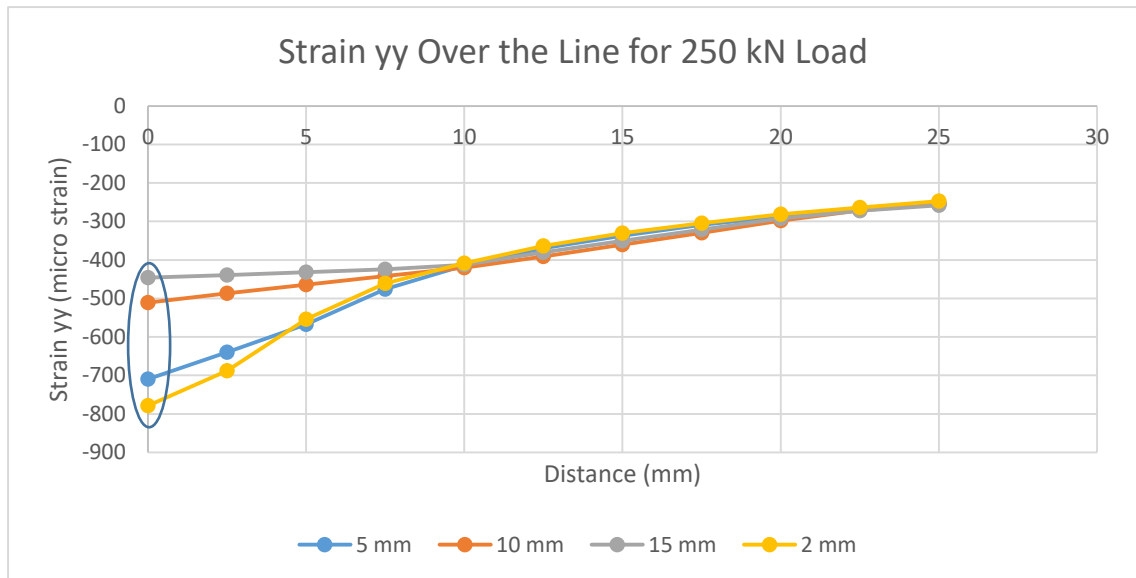


Figure 71. Strain-yy distribution along the 25 mm horizontal line path

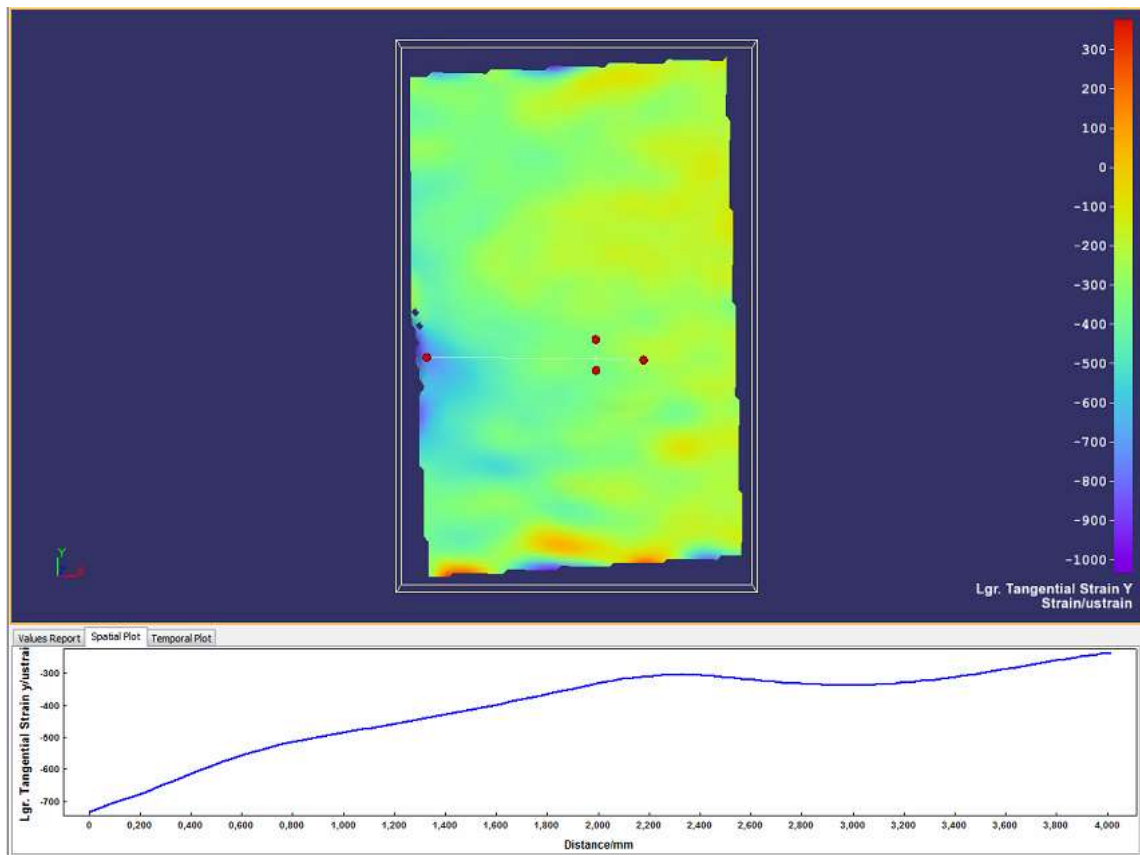


Figure 73. DIC result for strain yy distribution along the 25 mm horizontal line path

The figure 71 above shows the of strain-yy distribution for a different number of element size. The results can be compared with the result with figure 73 from DIC measurement of strain yy distribution. At 15 mm from the edge of the cope hole, the strain estimation for each element size gives a close match with a difference $<30 \mu\text{strain}$ between the largest and the smallest strain result. However, at the edge of the cope hole, 10 mm and 15 mm of element size gives a low strain estimation ($-510 \mu\text{strain}$ and $-445 \mu\text{strain}$) relatively compare to 2 mm and 5 mm element size (-770 and $-710 \mu\text{strain}$). Strain estimation results for element size 10 mm and 15 mm gives quite unreliable data compare the results from the measurement data. As it can be seen from figure 73, the strain value is around $-720 \mu\text{strain}$ for the particular location. For 2 mm element size, it gives slightly higher strain result ($-770 \mu\text{strain}$) compare to 5 mm ($-710 \mu\text{strain}$) with a difference $<10\%$. However, the computational time to calculate 2 mm element size is longer than 5 mm element size. Considering the small deviation strain measurement between 2 mm and 5 element size and the computing time efficiency, the 5 mm element size is chosen for the study.

6.6. Conclusion on Finite Element Method

Based on all measurement data and analysis from the previous section, here are some conclusion from Finite Element Model analysis:

- The current finite element model gives adequate results regarding strain distribution calculation. It is shown from the comparison with real scale experiment, all of the strain measurement (in x & y-direction) gives deviation below 20%. The difference between the numerical method and the experimental results can be explained by several factors:
 - Finite element method is using perfect model. The numerical effect is accountable for the discrepancies. While in reality, the specimen must have some certain degree of imperfection, which can be: global imperfection such as bending of the crossbeam, local imperfection such as dimples on the surface of the specimen.
 - Inaccuracy results from the measurements. Multiple reasons can explain this: human error (testing process and measurement installation), temperature influence on the strain gauges, lack of light system on the DIC measurement, vibration in the laboratory during the experiment can affect the LVDT measurement.
- For out-of-plane deformation, current finite element model can be considered as unreliable. For the difference between the results are more than 100%, and inconsistency of the direction movement between the FEM computation and measurement leads to the conclusion that sensitivity analysis is necessary to be performed. Global & local imperfection of the crossbeam can be applied to the new model.

7 DISCUSSION OF RESULTS AND ANSWERS TO RESEARCH QUESTIONS

Having all the results, analysis, and discussion of the research results in the previous chapters, the answers to the research questions are addressed in this chapter.

1. *Is it reliable to use Digital Image Correlation (DIC) system to measure the behaviour of the crossbeam with 'haibach' cope hole due to the in-plane quasi-static loading?*

Yes, it is to some extent. It is proven by the results on the crossbeam around the cope hole area for strain measurement in the y-direction and out-of-plane deformation. The table below shows the deviation of DIC measurement relative to other measurement techniques such as strain gauges and LVDT. In general, for this particular research, the deviation below 20% is considered as in acceptable range.

Table 17. Deviation of DIC measurement relative to other measurement technique for strain and out-of-plane deformation

	Deviation Strain Relative to Strain Gauge				Deviation Out-of-plane Deformation Relative to LVDT	
	Strain xx		Strain yy		Location A	Location B
	Location A	Location B	Location A	Location B		
Deviation at The Last Step of Loading (-250 kN)	192%	288%	5%	19%	12%	23%
Average Deviation of All Loading Step	462%	342%	21%	26%	12%	20%

Some of the results show difference more than 20% and even more than 100%. That can be explained by following reasons:

- Due to low strain limit of the DIC equipment (100 μ strain), the accuracy of measurement at the lower level of strain is difficult to achieve. In this particular research, benchmark study shows even greater low strain limit number, with 150 μ strain. From the strain gauges reading, measured strain in x-direction shows that the results fall below 100 μ strain. Considering the limitations of the DIC equipment, all the strain data in x-direction can be completely neglected. Therefore, it is unreliable.
- One of the main challenges in this research is the inhospitality of the environment. The crossbeam is located under the deck bridge, meaning the natural light intensity is very low. It might affect the DIC measurement results since the accuracy of the DIC heavily depends on the quality of the captured image.
- Strain gauges and LVDT are positioned at the opposite side of the DIC equipment. It is possible that the measured strain on each side of the crossbeam does not produce the same result, due to a different location of the monitoring, and imperfection of the crossbeam.

- Human error during the process of testing, strain gauges instalment, can affect the accuracy of the measurement

Therefore, it can be concluded that it is reliable to use 3D Digital Image Correlation (DIC) system to measure the behaviour of the crossbeam with 'haibach' cope hole due to the in-plane quasi-static loading. It will be valid as long as the monitored parameters do not exceed the DIC low limit threshold.

Where this research question was sub-divided into:

a. *What is the best method to apply Digital Image Correlation System in Orthotropic Bridge Deck to measure the behaviour of the crossbeam?*

The best method to apply the DIC system in orthotropic deck steel is by using 3D DIC measurement. This study proves that due to the in-plane quasi-static loading, the crossbeam experience out-of-plane behaviour (0.1mm out-of-plane deformation). The speckle pattern which is applied by the airbrush system is also proved to be sufficient, with average speckle size 0.2 mm.

b. *What is the optimum number of pixels for one particular dot of speckle pattern and field of view of the measurement to get the optimum measurement results, given by the circumstances of the experiment and limitation of the equipment specification?*

Benchmark testing shows that with 50 mm and 75 mm field of view or equal to an average 45 pixel² and 36 pixel² for one particular dot, gives adequate results of measurement. The actual test on orthotropic deck gives an average 38 pixel² for a particular area, also produces satisfying results of measurements. It can be concluded that for the level of expected strain and deformation, number of pixel² between 36 and 45 can lead to reliable 3D measurement.

2. *What is the reliability of the Finite Element Model that has been developed in this research, to estimate the behaviour of the crossbeam with the 'haibach' cope hole?*

- The finite element model with the solid element (C3D8R) and 5 mm element size around the cope hole has proven to be a reliable model for strain estimation. It gives deviation less than 20% relative to DIC strain gauges measurement. However, for out-of-plane deformation, the model can be considered as invalid. The error is almost 100%, with the inconsistent sign of motion comparison. The possible explanation for the difference in FEM model estimation with measurement techniques:
 - The finite element model assumed a perfect shape of the specimen. While in reality the imperfection always occurs. In this particular case, there might be an initial imperfection shape of the crossbeam, which creates inconsistent motion of the crossbeam.
 - The material of the specimen is given by default. However, in reality, the nonuniform material properties might occur. It can lead to different stiffness of the crossbeam or monitored area which later can affect the strain distribution and also out-of-plane deformation results.

8 CONCLUSION & RECOMMENDATION

The conclusion of the research can be stated as:

- 3D DIC measurements on the orthotropic deck steel give close match for strain below $<-150 \mu\text{strain}$. With an average deviation 21% and 26% for location A & B respectively relative to strain gauges measurement (Rk003 & Rk016). For the final step of loading (-250kN) the measurement gives even closer results with deviation 5% and 19% for location A & B respectively.
- All the strain in x-direction measurement data gives deviation more than 100% compared to strain gauges (Rk001 & Rk014). Due to the strain limit of the camera $\pm 100 \mu\text{strain}$, all the strain xx DIC measurement data can be considered as invalid (the smallest strain in the x-direction is around $40 \mu\text{strain}$ according to the strain gauges).
- Out-of-plane deformation measurement using DIC gives a close match with LVDT measurement. The average deviation for every step is 12 % and 20 % for location A & B respectively.
- Finite element model gives a close match of strain estimation in x and y-direction relative to both measurement technique DIC & strain gauges. The deviation is less than 20% for all strain estimation except for strain in x-direction comparison with DIC measurement (the data of DIC is invalid)
- The out-of-plane deformation of finite element model estimation does not show a good agreement with DIC or LVDT measurement. The error is around 100%, and the estimation of the deformation sign is also invalid.
- Both strain gauges and finite element model estimates a slightly bigger strain value at the left side of the cope hole (location B) relative to the right side of the cope hole (location A). The possible explanation is:
 - Due to the different boundary condition of the monitored area. The left side of the cope hole (location B) has a free edge boundary condition, while the right side of cope hole(location A) has fixed boundary condition on both sides. It produces different stiffness therefore different strain and stress distribution trajectory between this 2 location

The recommendation for further research:

- Light intensity plays a significant role in DIC measurement, especially for a very low-level strain and deformation measurement. Therefore it is fundamental to set a proper environment with sufficient lighting system before conduct an experiment with DIC.
- From the test on the orthotropic steel deck, it is proven that the DIC can measure strain distribution over a certain area. DIC is more beneficial relative to the strain gauges since it can only measure strain at one single point. However, DIC works best to measure strain which values are greater than 100 microstrains.

REFERENCES

- [1] Leendertz, Johan Sebastiaan. *Fatigue Behaviour of Closed Stiffener to Crossbeam Connections in Orthotropic Steel Bridge Decks*. Netherlands. 2008.
- [2] Kolstein, M.H. *Fatigue Classification of Welded Joints in Orthotropic Steel Bridge Decks*, Ph.D Thesis. Department of Design and Construction, Delft University of Technology, The Netherlands. 2007.
- [3] Lehrke, H-P. *Messung und Interpretation von Dynamischen Lasten an Stahlbrücken – Phase III: Schwingungsverhalten von orthotropen Platten in Stahlstrassenbrücken*, Final report ECSC research 7210-KD/1119, Dramstadt, Germany.1989
- [4] B. Pan, H. Xie, Z. Wang, K. Qian, and Z. Wang. *Study on subset size selection in digital image correlation for speckle patterns*. Opt. Express 16, 7037-7048 (2008).
- [5] University of South Carolina, Correlated Solutions, Inc. *Digital Image Correlation: Overview of Principles and Software*. SEM Workshop.2009.
- [6] Lydon, Myra & Robinson, D & Taylor, Su & Amato, Giuseppina & OBrien, Eugene & Uddin, Nasim. (2017). Improved axle detection for bridge weigh-in-motion systems using fiber optic sensors. Journal of Civil Structural Health Monitoring. 7. . 10.1007/s13349-017-0229-4.
- [7] CSI Application Note AN-525. *Speckle Pattern Fundamental*.
- [8] US Department of Transportation (2012): Manual for Design, Construction, and Maintenance of Orthotropic Steel Deck Bridge. US Department of Transportation, Federal Highway Administration, Publication no. FHWA-IF-12-027. USA February 2012.
- [9] Kolstein, M.H., Leendertz, J.S., Wardenier, J. (1995c) *Fatigue performance of the trough to crossbeam connection in orthotropic steel bridge decks*, Proceedings Nordic Steel Conference, Malmö, Sweden
- [10] Weijian Wu, Henk Kolstein, Milan Veljkovic, Richard Pijpers, Jos Vorstenbosch-Krabbe. *Fatigue behaviour of the closed rib to deck and crossbeam joint in a newly designed orthotropic bridge deck*. EUROSTEEL 2017, Copenhagen Denmark.2017
- [11] http://web.mit.edu/calculix_v2.7/CalculiX/ccx_2.7/doc/ccx/node27.html. Access date: 11/20/2017
- [12] Corneliu Cofaru, Wilfried Philips, and Wim Van Paepegem, "Pixel-level robust digital image correlation," Opt. Express 21, 29979-29999 (2013).
- [13] Y. F. Sun and H. J. Pang, "Study of optimal subset size in digital image correlation of speckle pattern images," Opt. Lasers Eng. 45, 967-974 (2007).

ANNEX A – 2D BENCHMARK TESTING

INTRODUCTION

The previous test has been conducted on orthotropic deck bridges and simple test using DIC equipment. The results are not satisfactory compared to the results from strain gauges (for strain measurement) and LVDT (for out-of-plane deformation). Therefore, it is necessary to do a benchmark test to investigate the cause of the problem. The purpose of this test is to observe the accuracy of the DIC system on measuring strain in elastic zone steel material and also to see whether the captured area and also the distance between the camera and the specimen affecting the accuracy of the test. The test is conducted in 2D measurement, particularly in the tensile test with a uniformly distributed load. In the end, the strain result from theory calculation will be compared with the result from the DIC measurement.

DIMENSION & PROPERTIES OF THE SPECIMEN

The dimension of the specimen is shown by the picture below.

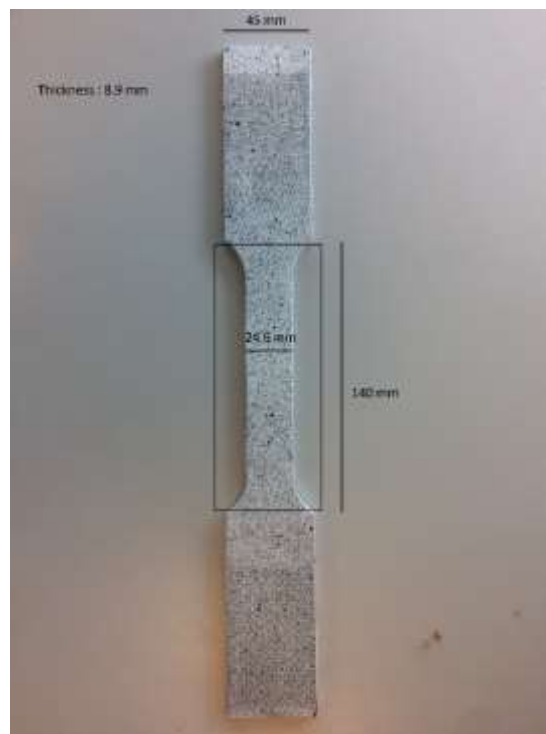


Figure 1. Dimension of Specimen

Height	8.9	mm
Width	24.6	mm
Area of the specimen	218.94	mm ²
Modulus of Elasticity	210000	Mpa
F_yyield	355	Mpa

The properties of the material are not known for sure, so the modulus of elasticity and also the yield strength of the specimen is assumed to be 210000 MPa and 355 MPa respectively.

The speckle pattern is different from the previous test. This time, an airbrush is used instead of the spray. The pattern now is denser, and the size is more uniform compared to the pattern that was produced by the spray. The figure below shows the comparison between the pattern from the first test and now.

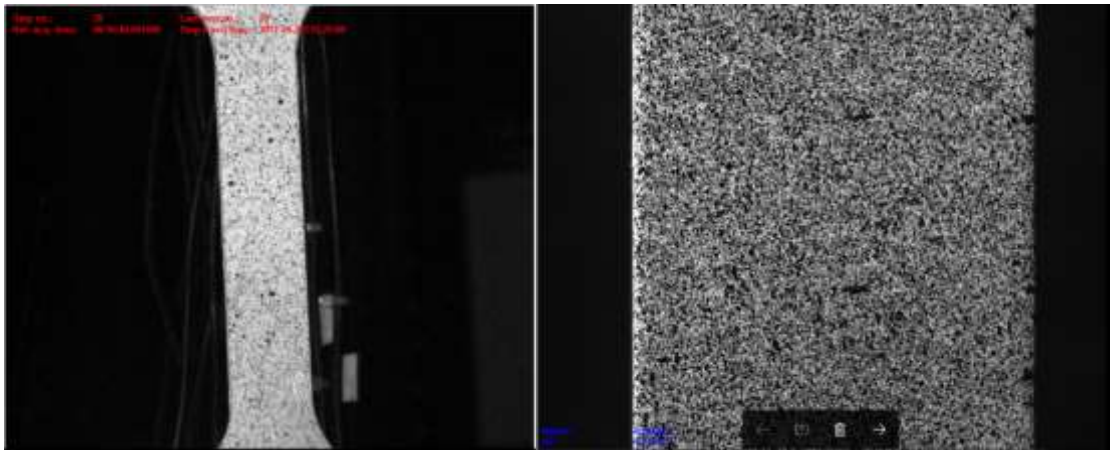


Figure 2. Speckle Pattern from Spray (Left) and Speckle Pattern from Airbrush (Right)

TESTING PROCESS

To investigate the accuracy of the DIC measurement for the strain in the elastic zone of steel material, tensile tests with uniformly distributed loads are chosen. The loading is applied in one direction (Y global) without any out-of-plane deformation.



Figure 3. Tensile Test on The Steel Specimen

The test is based on force control. The given load is calculated by using the constitutive equation below :

$$F = \varepsilon * E * A$$

- ε = strain or elongation of the specimen due to the tensile loading
- E = Modulus elasticity of the specimen (210000 MPa)
- A = Area of the monitored specimen (218.94 mm²)

Number of Steps	Approx Loading (kN)	Load Increment (kN)	Strain (*10 ⁻⁶)	Strain Increment (*10 ⁻⁶)	Approx Stress (Mpa)
0	0.00	0	0	0	0
1	0.00	0.00	0	0	0
2	11.49	11.49	250	250	52.50
3	20.69	9.20	450	200	94.50
4	29.89	9.20	650	200	136.50
5	34.48	4.60	750	100	157.50
6	39.08	4.60	850	100	178.50
7	41.38	2.30	900	50	189.00
8	43.68	2.30	950	50	199.50
9	45.98	2.30	1000	50	210.00
10	48.28	2.30	1050	50	220.50
11	49.66	1.38	1080	30	226.80
12	51.03	1.38	1110	30	233.10
13	52.41	1.38	1140	30	239.40
14	53.33	0.92	1160	20	243.60
15	54.25	0.92	1180	20	247.80
16	55.17	0.92	1200	20	252.00
17	55.63	0.46	1210	10	254.10
18	56.09	0.46	1220	10	256.20
19	56.55	0.46	1230	10	258.30
20	56.78	0.23	1235	5	259.35
21	57.01	0.23	1240	5	260.40
22	57.24	0.23	1245	5	261.45

Since the properties of the material are not known for sure, there will be two parameters that will be checked during the test, first is the strain relative to step 0, and second is the increment of the strain relative to one step before.

The tests are conducted five times, with the different captured area :

- 10 mm x 13.33 mm area
- 20 mm x 26.67 mm area
- 30 mm x 45 mm area
- 50 mm x 66.67 mm area
- 100 mm x 133.33 mm area

For the field of view 10, 20, 30 mm it is used the 1 mm calibration plate for one square. While for the 50 mm field of view, 5 mm calibration board is used and for 100 mm field of view, 10 mm calibration board is used. Lens extension is also used in this test. It is necessary to use the extension due to the limitation focus of the camera

Field of View	Length of Lense Extension
10 mm	40 mm
20 mm	20 mm
30 mm	10 mm
50 mm	-
100 mm	-

TEST RESULT

Field of View 10 mm x 13.33 mm

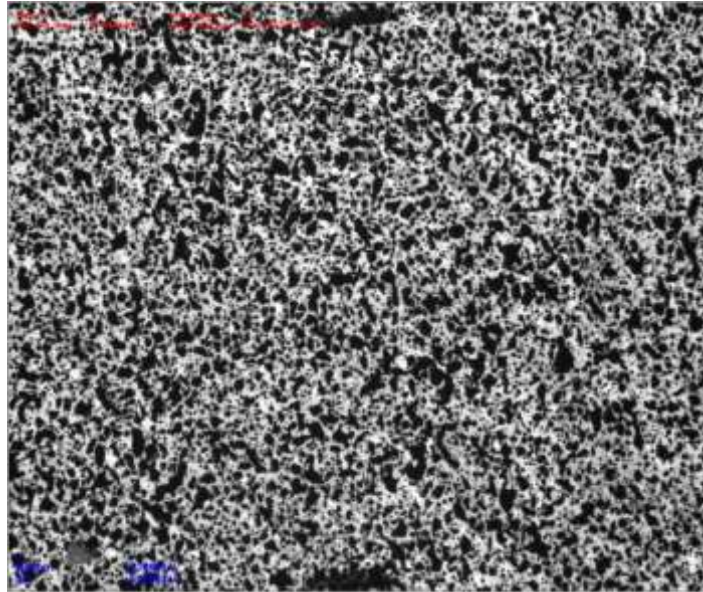


Figure 4. Capture Area 10 mm x 13.33 mm

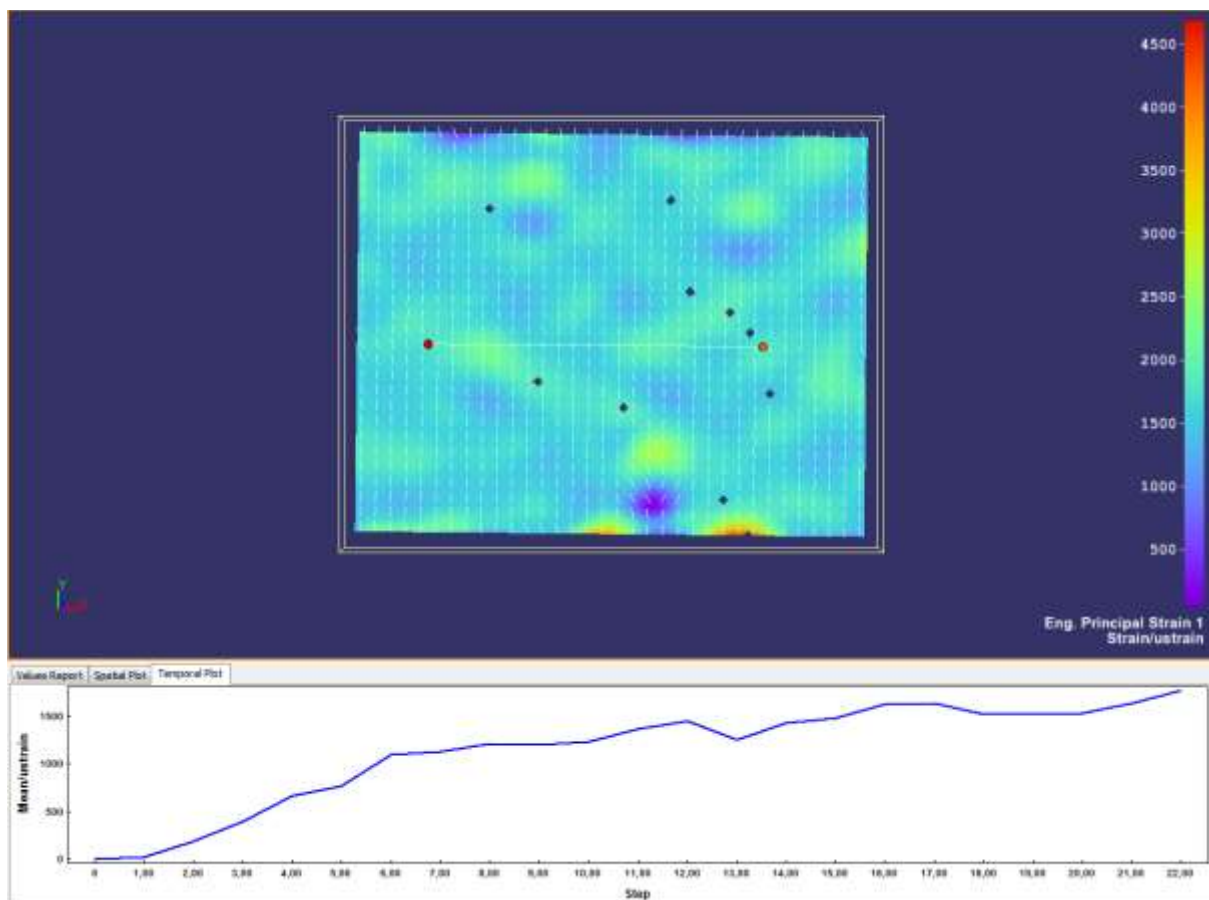


Figure 5. Strain in Y Direction on For Every Step

Number of Steps	Approx Loading (kN)	Load Increment (kN)	Theory Strain (*10 ⁻⁶)	DIC Strain (*10 ⁻⁶)	Strain Difference	Theory Strain Increment (*10 ⁻⁶)	DIC Strain Increment (*10 ⁻⁶)	Strain Increment Difference
0	0.00	0.00	0	0	-	0	0	-
1	0.00	0.00	0	10	-	0	10	-
2	11.49	11.49	250	310	24%	250	300	20%
3	20.69	9.20	450	440	-2%	200	130	-35%
4	29.89	9.20	650	565	-13%	200	125	-38%
5	34.48	4.60	750	930	24%	100	365	265%
6	39.08	4.60	850	1130	33%	100	200	100%
7	41.38	2.30	900	1070	19%	50	-60	-220%
8	43.68	2.30	950	1170	23%	50	100	100%
9	45.98	2.30	1000	1182	18%	50	12	-76%
10	48.28	2.30	1050	1333	27%	50	151	202%
11	49.66	1.38	1080	1349	25%	30	16	-47%
12	51.03	1.38	1110	1430	29%	30	81	170%
13	52.41	1.38	1140	1291	13%	30	-139	-563%
14	53.33	0.92	1160	1460	26%	20	169	745%
15	54.25	0.92	1180	1479	25%	20	19	-5%
16	55.17	0.92	1200	1570	31%	20	91	355%
17	55.63	0.46	1210	1510	25%	10	-60	-700%
18	56.09	0.46	1220	1650	35%	10	140	1300%
19	56.55	0.46	1230	1492	21%	10	-158	-1680%
20	56.78	0.23	1235	1537	24%	5	45	800%
21	57.01	0.23	1240	1670	35%	5	133	2560%
22	57.24	0.23	1245	1705	37%	5	35	600%

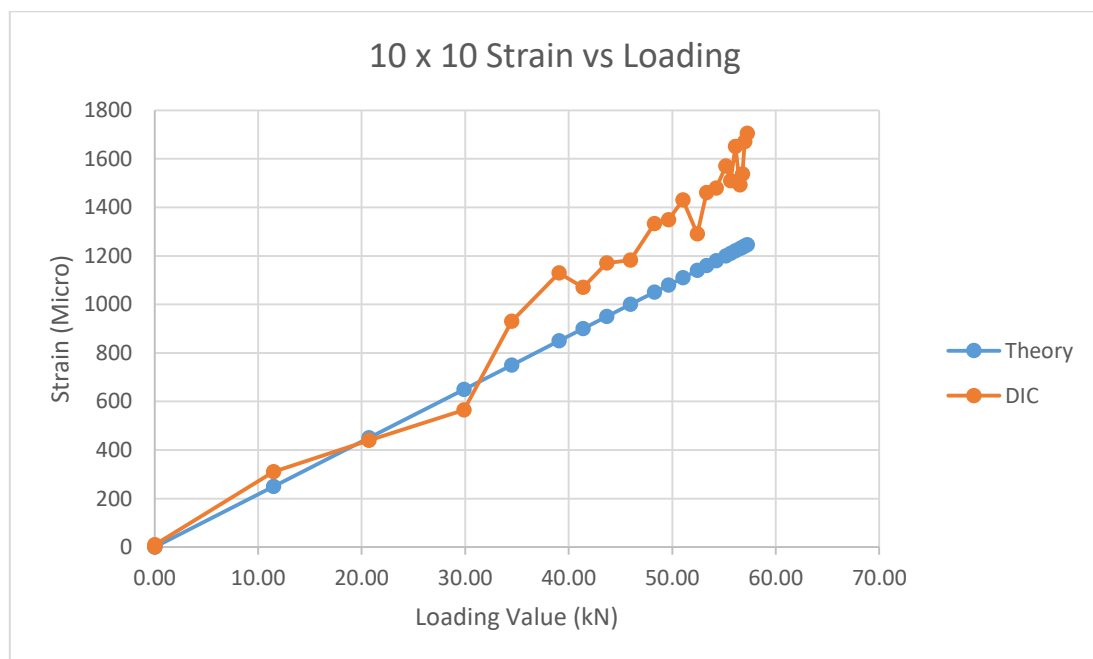


Figure 6. Graph of Strain vs Loading For DIC and Calculation

Field of View 20 mm x 26.67 mm

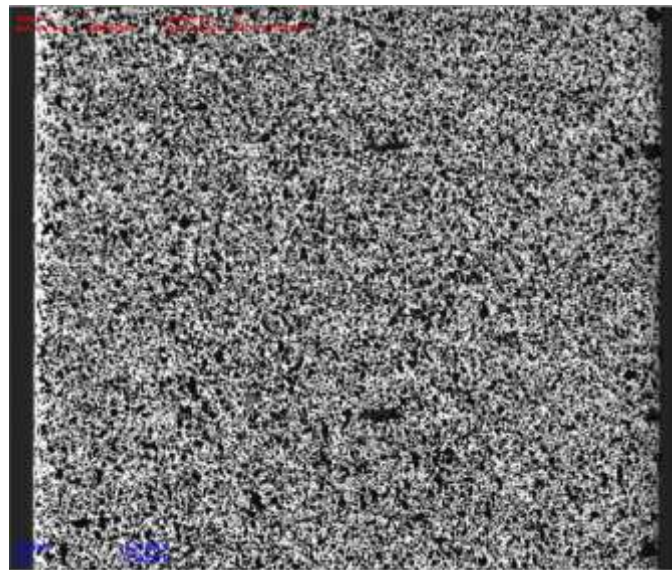


Figure 7. Captured Area of 20 mm x 26.67 mm

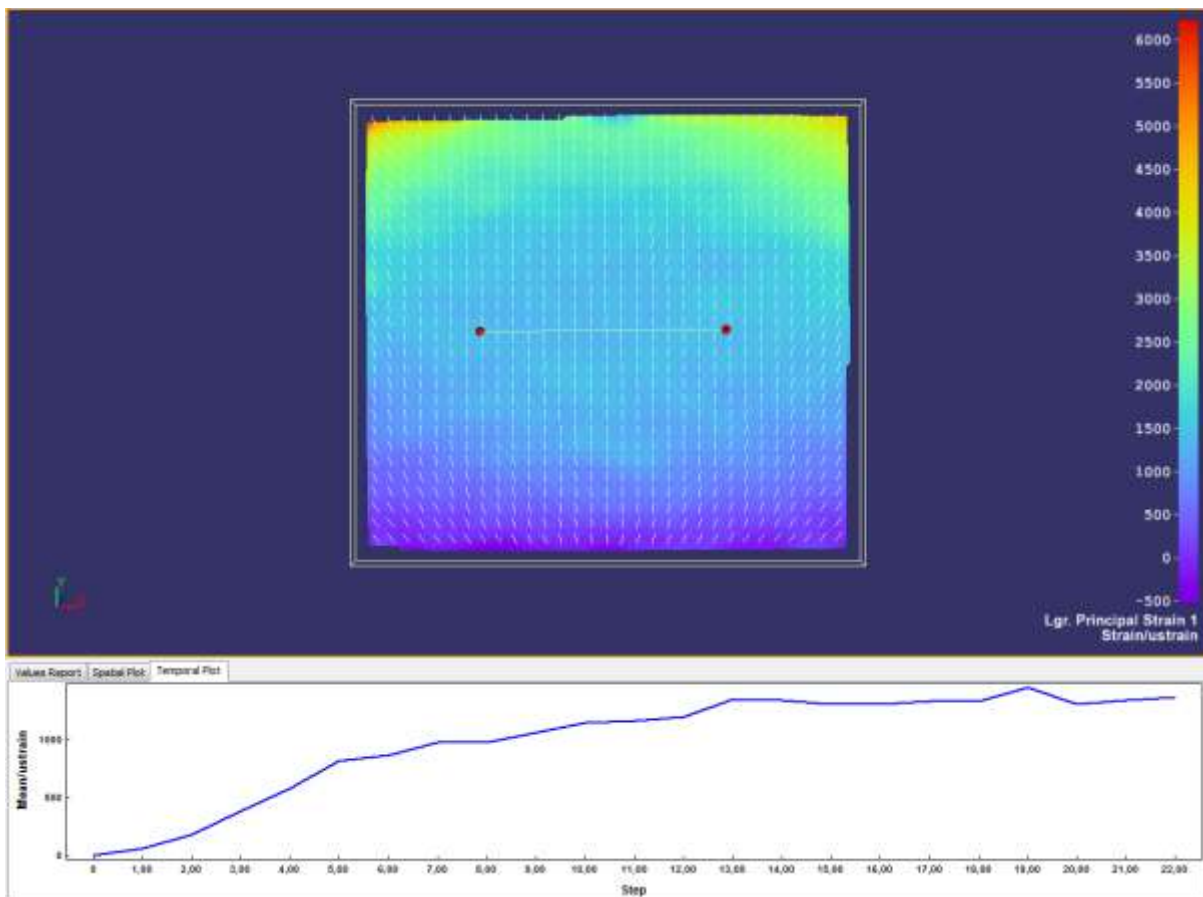


Figure 8. Strain in Y Direction For Every Number of Step

Number of Steps	Approx Loading (kN)	Load Increment (kN)	Theory Strain (*10 ⁻⁶)	DIC Strain (*10 ⁻⁶)	Strain Difference	Theory Strain Increment (*10 ⁻⁶)	DIC Strain Increment (*10 ⁻⁶)	Strain Increment Difference
0	0.00	0.00	0	0	-	0	0	-
1	0.00	0.00	0	53	-	0	53	-
2	11.49	11.49	250	204	-18%	250	151	-40%
3	20.69	9.20	450	409	-9%	200	205	3%
4	29.89	9.20	650	597	-8%	200	188	-6%
5	34.48	4.60	750	792	6%	100	195	95%
6	39.08	4.60	850	875	3%	100	83	-17%
7	41.38	2.30	900	991	10%	50	116	132%
8	43.68	2.30	950	958	1%	50	-33	-166%
9	45.98	2.30	1000	1077	8%	50	119	138%
10	48.28	2.30	1050	1164	11%	50	87	74%
11	49.66	1.38	1080	1157	7%	30	-7	-123%
12	51.03	1.38	1110	1233	11%	30	76	153%
13	52.41	1.38	1140	1362	19%	30	129	330%
14	53.33	0.92	1160	1344	16%	20	-18	-190%
15	54.25	0.92	1180	1299	10%	20	-45	-325%
16	55.17	0.92	1200	1331	11%	20	32	60%
17	55.63	0.46	1210	1337	10%	10	6	-40%
18	56.09	0.46	1220	1335	9%	10	-2	-120%
19	56.55	0.46	1230	1448	18%	10	113	1030%
20	56.78	0.23	1235	1323	7%	5	-125	-2600%
21	57.01	0.23	1240	1349	9%	5	26	420%
22	57.24	0.23	1245	1395	12%	5	46	820%

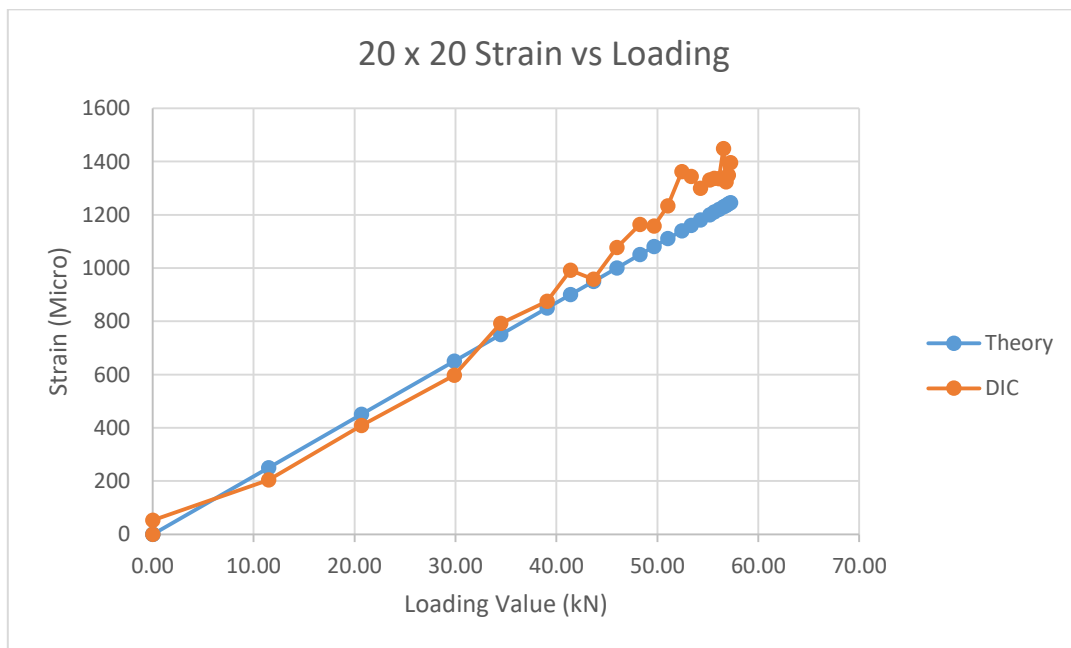


Figure 9. Figure 6. Graph of Strain vs Loading For DIC and Calculation

Field of View 30 mm x 45 mm

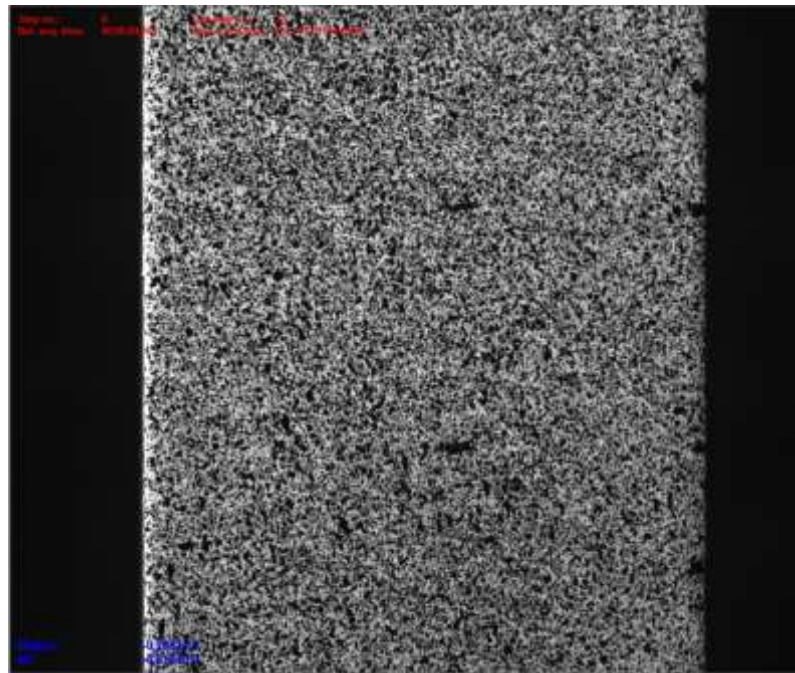


Figure 10. Captured Area of 30 mm x 45 mm

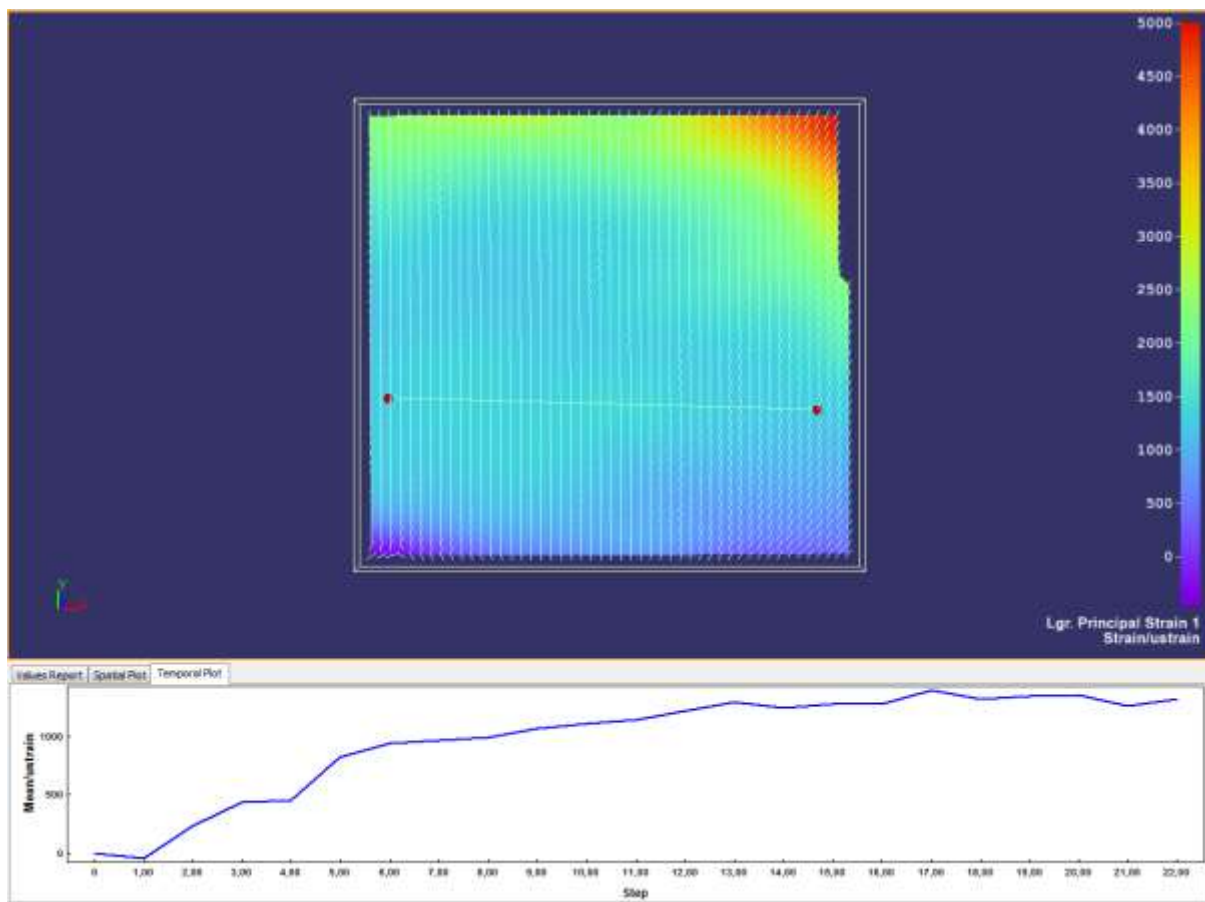


Figure 11. Strain in Y Direction For Every Number of Step

Number of Steps	Approx Loading (kN)	Load Increment (kN)	Theory Strain (*10 ⁻⁶)	DIC Strain (*10 ⁻⁶)	Strain Difference	Theory Strain Increment (*10 ⁻⁶)	DIC Strain Increment (*10 ⁻⁶)	Strain Increment Difference
0	0.00	0.00	0	0	-	0	0	-
1	0.00	0.00	0	-40	-	0	-40	-
2	11.49	11.49	250	230	-8%	250	270	8%
3	20.69	9.20	450	430	-4%	200	200	0%
4	29.89	9.20	650	450	-31%	200	20	-90%
5	34.48	4.60	750	820	9%	100	370	270%
6	39.08	4.60	850	940	11%	100	120	20%
7	41.38	2.30	900	960	7%	50	20	-60%
8	43.68	2.30	950	990	4%	50	30	-40%
9	45.98	2.30	1000	1060	6%	50	70	40%
10	48.28	2.30	1050	1110	6%	50	50	0%
11	49.66	1.38	1080	1150	6%	30	40	33%
12	51.03	1.38	1110	1210	9%	30	60	100%
13	52.41	1.38	1140	1290	13%	30	80	167%
14	53.33	0.92	1160	1240	7%	20	-50	-350%
15	54.25	0.92	1180	1270	8%	20	30	50%
16	55.17	0.92	1200	1280	7%	20	10	-50%
17	55.63	0.46	1210	1390	15%	10	110	1000%
18	56.09	0.46	1220	1320	8%	10	-70	-800%
19	56.55	0.46	1230	1340	9%	10	20	100%
20	56.78	0.23	1235	1360	10%	5	20	300%
21	57.01	0.23	1240	1260	2%	5	-100	-2100%
22	57.24	0.23	1245	1310	5%	5	50	900%

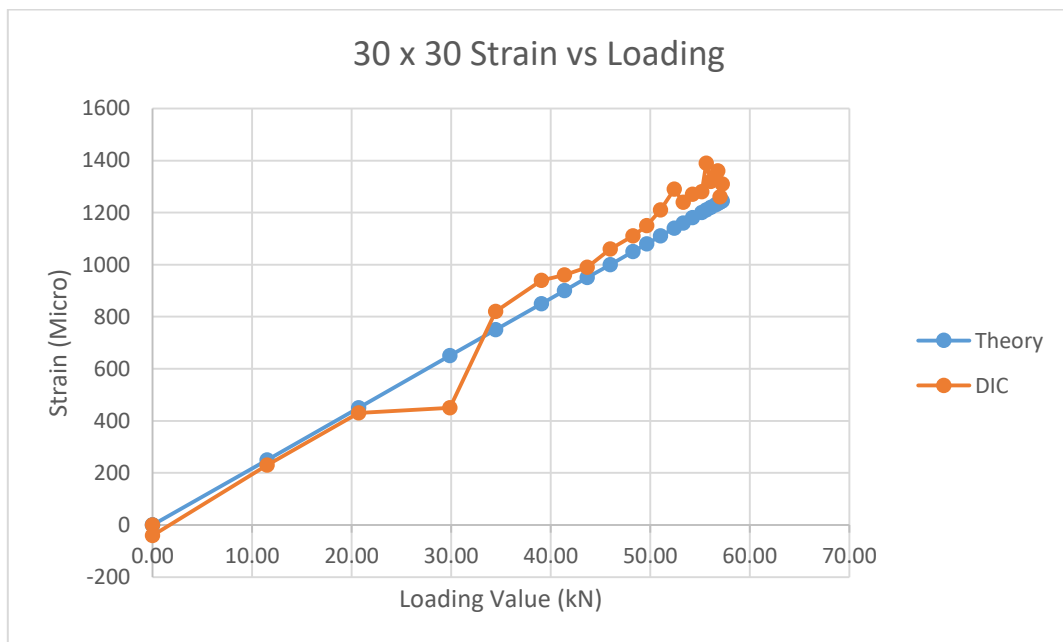


Figure 12. Graph of Strain vs Loading For DIC and Calculation

Field of View 50 mm x 66.67 mm

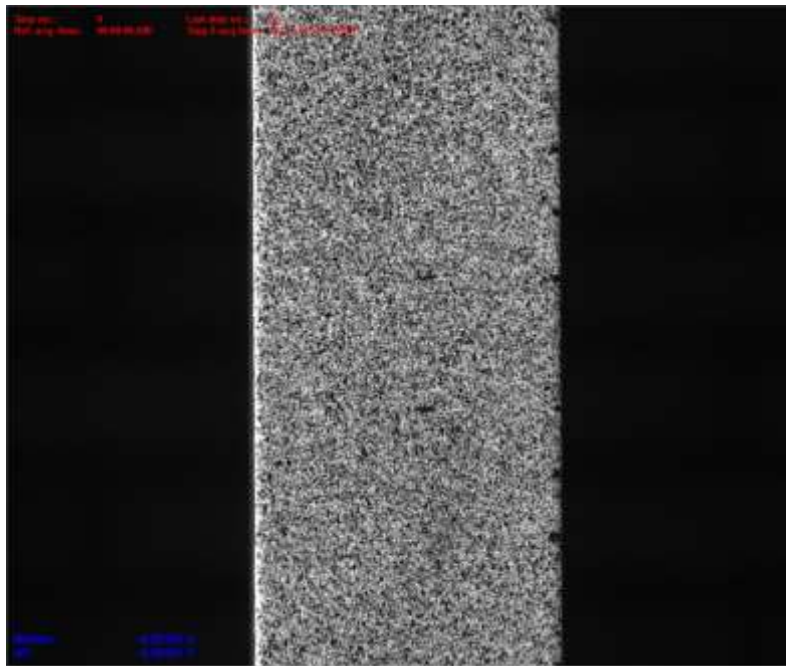


Figure 13. Captured Area of 50 mm x 66.67 mm

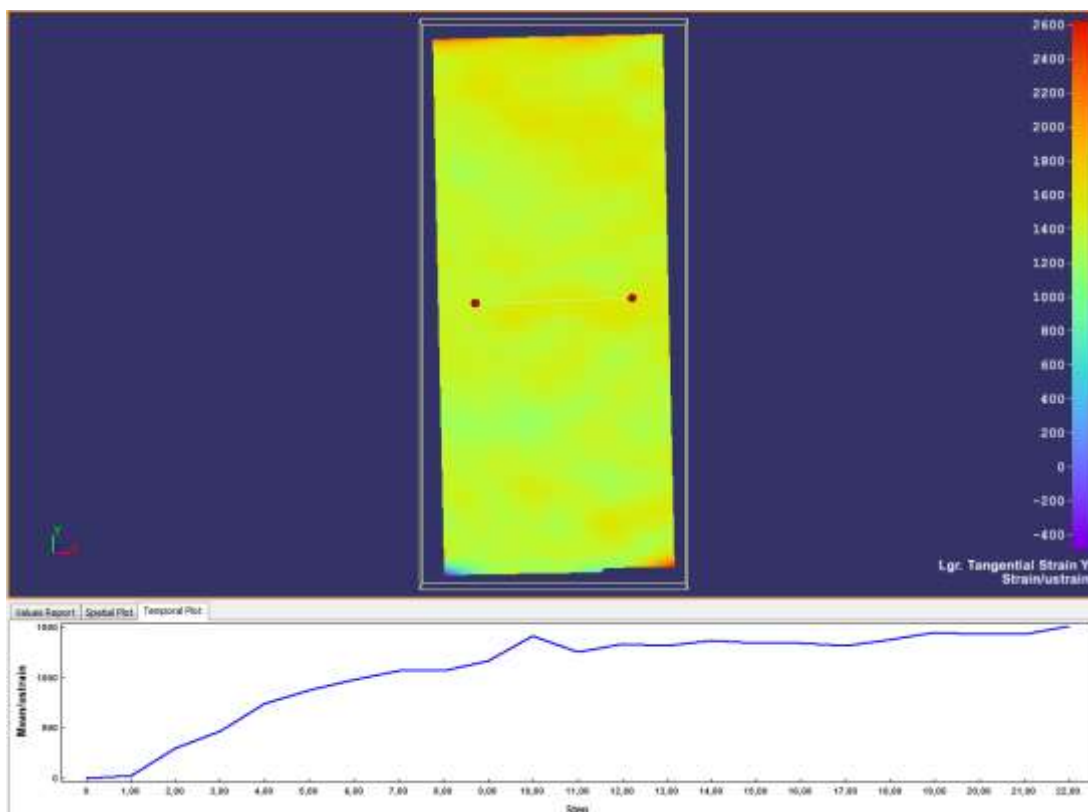


Figure 14. Strain in Y Direction For Every Number of Step

Number of Steps	Approx Loading (kN)	Load Increment (kN)	Theory Strain (*10 ⁻⁶)	DIC Strain (*10 ⁻⁶)	Strain Difference	Theory Strain Increment (*10 ⁻⁶)	DIC Strain Increment (*10 ⁻⁶)	Strain Increment Difference
0	0.00	0.00	0	0	-	0	0	-
1	0.00	0.00	0	40	-	0	40	-
2	11.49	11.49	250	280	12%	250	240	-4%
3	20.69	9.20	450	410	-9%	200	130	-35%
4	29.89	9.20	650	720	11%	200	310	55%
5	34.48	4.60	750	820	9%	100	100	0%
6	39.08	4.60	850	960	13%	100	140	40%
7	41.38	2.30	900	980	9%	50	20	-60%
8	43.68	2.30	950	1030	8%	50	50	0%
9	45.98	2.30	1000	1110	11%	50	80	60%
10	48.28	2.30	1050	1410	34%	50	300	500%
11	49.66	1.38	1080	1270	18%	30	-140	-567%
12	51.03	1.38	1110	1260	14%	30	-10	-133%
13	52.41	1.38	1140	1260	11%	30	0	-100%
14	53.33	0.92	1160	1340	16%	20	80	300%
15	54.25	0.92	1180	1320	12%	20	-20	-200%
16	55.17	0.92	1200	1360	13%	20	40	100%
17	55.63	0.46	1210	1360	12%	10	0	-100%
18	56.09	0.46	1220	1320	8%	10	-40	-500%
19	56.55	0.46	1230	1420	15%	10	100	900%
20	56.78	0.23	1235	1460	18%	5	40	700%
21	57.01	0.23	1240	1400	13%	5	-60	-1300%
22	57.24	0.23	1245	1430	15%	5	30	500%

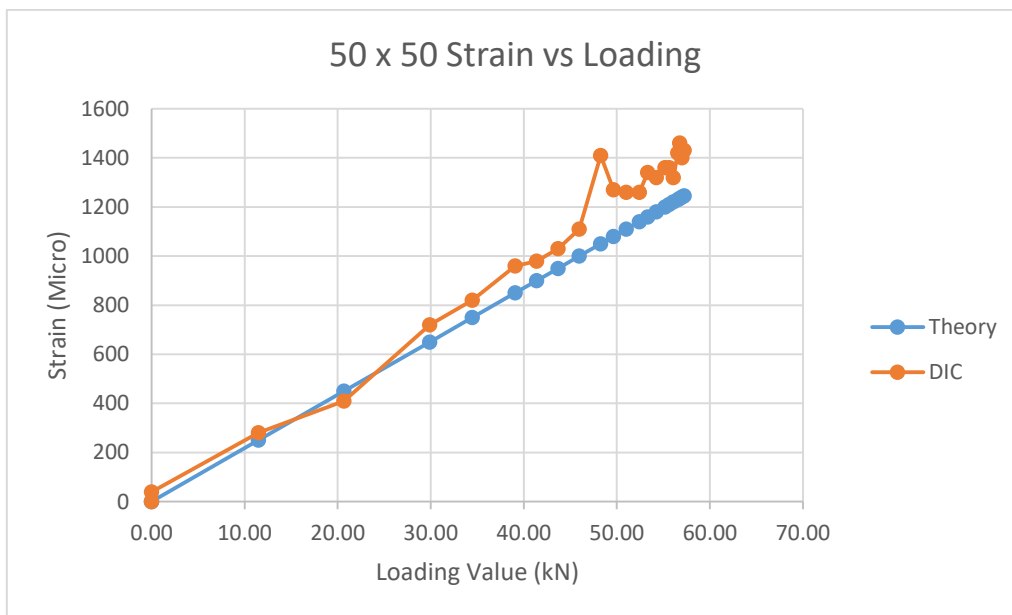


Figure 15. Graph of Strain vs Loading For DIC and Calculation

Field of View 100 mm x 133.33 mm

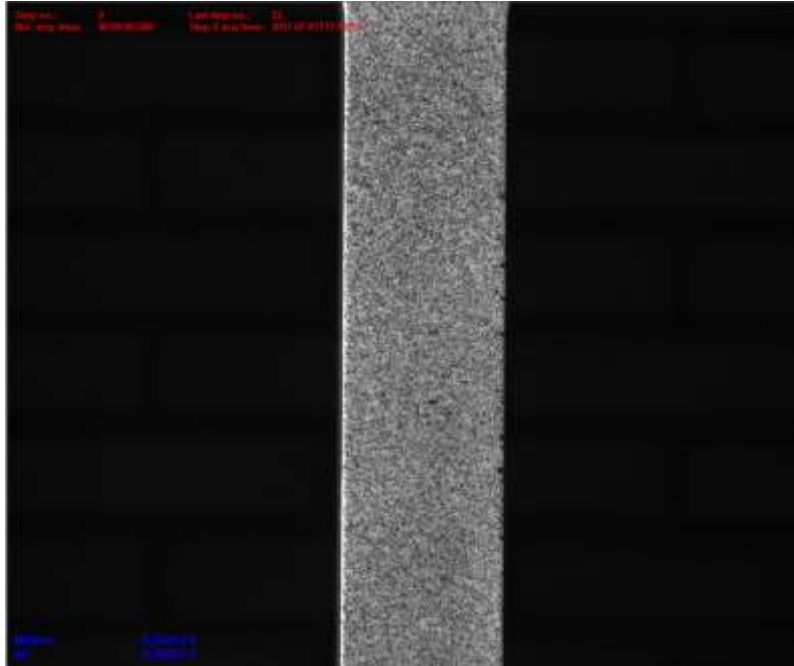


Figure 16. Captured Area of 100 mm x 133.33 mm

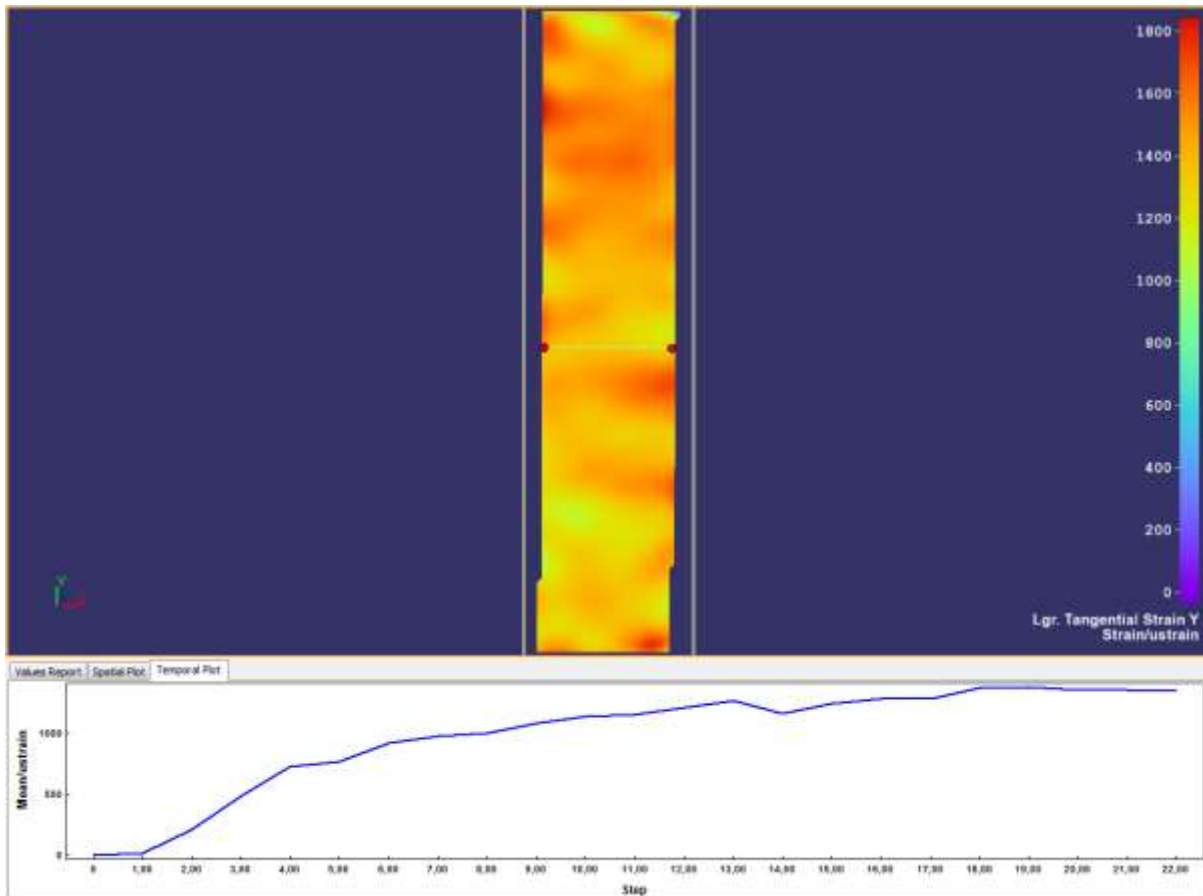


Figure 17. Strain in Y Direction For Every Number of Step

Number of Steps	Approx Loading (kN)	Load Increment (kN)	Theory Strain (*10 ⁻⁶)	DIC Strain (*10 ⁻⁶)	Strain Difference	Theory Strain Increment (*10 ⁻⁶)	DIC Strain Increment (*10 ⁻⁶)	Strain Increment Difference
0	0.00	0.00	0	0	-	0	0	-
1	0.00	0.00	0	40	-	0	40	-
2	11.49	11.49	250	230	-8%	250	190	-24%
3	20.69	9.20	450	450	0%	200	220	10%
4	29.89	9.20	650	720	11%	200	270	35%
5	34.48	4.60	750	730	-3%	100	10	-90%
6	39.08	4.60	850	950	12%	100	220	120%
7	41.38	2.30	900	970	8%	50	20	-60%
8	43.68	2.30	950	960	1%	50	-10	-120%
9	45.98	2.30	1000	1080	8%	50	120	140%
10	48.28	2.30	1050	1230	17%	50	150	200%
11	49.66	1.38	1080	1180	9%	30	-50	-267%
12	51.03	1.38	1110	1190	7%	30	10	-67%
13	52.41	1.38	1140	1210	6%	30	20	-33%
14	53.33	0.92	1160	1140	-2%	20	-70	-450%
15	54.25	0.92	1180	1220	3%	20	80	300%
16	55.17	0.92	1200	1260	5%	20	40	100%
17	55.63	0.46	1210	1280	6%	10	20	100%
18	56.09	0.46	1220	1370	12%	10	90	800%
19	56.55	0.46	1230	1390	13%	10	20	100%
20	56.78	0.23	1235	1350	9%	5	-40	-900%
21	57.01	0.23	1240	1390	12%	5	40	700%
22	57.24	0.23	1245	1400	12%	5	10	100%

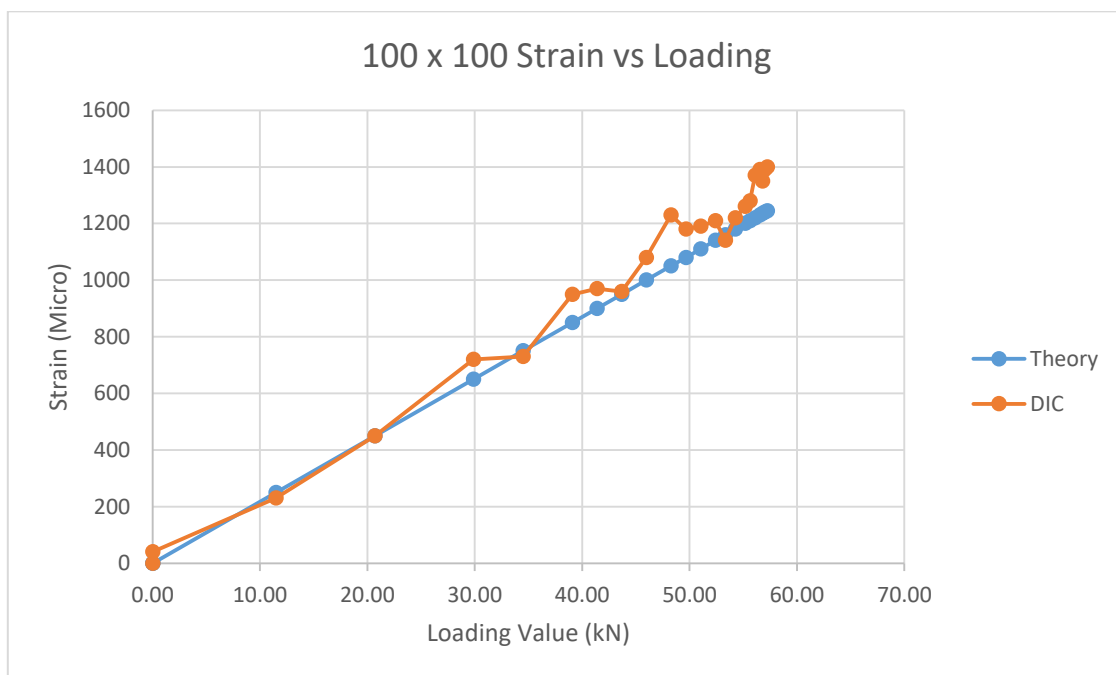


Figure 18. Graph of Strain vs Loading For DIC and Calculation

ANALYSIS

Difference between Theory Calculation and DIC Measurement for Every Field of View

Field of View	Average Strain Error	Average Increment Strain Error
10 mm	24%	504%
20 mm	10%	328%
30 mm	9%	308%
50 mm	13%	293%
100 mm	8%	225%

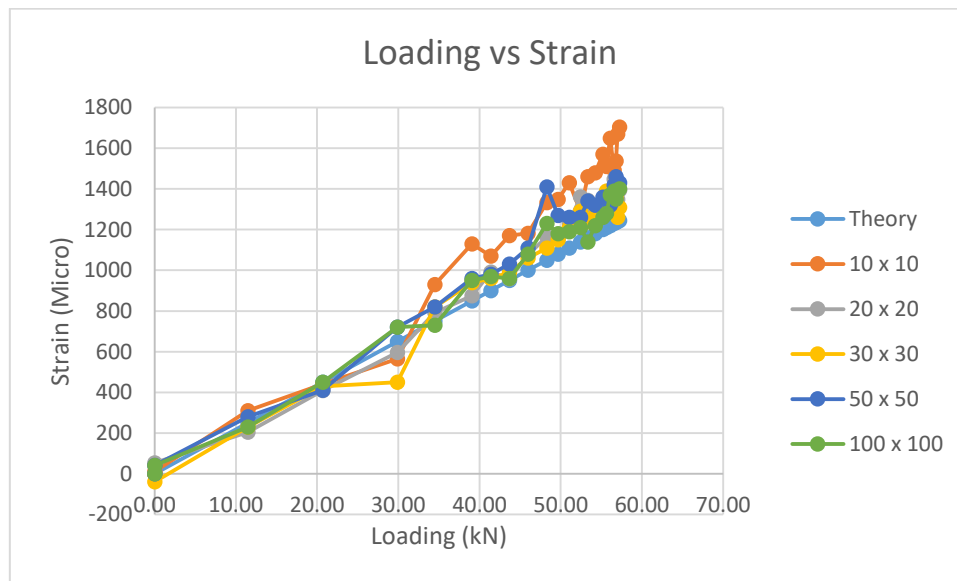


Figure 19. Strain Comparison For Every Field of View

In general, the results that are provided from the tests are quite satisfactory. As it can be seen from the average of the error, all the average value of error are below 15% except for the 10 mm field of view. The result from 10 mm x 13.33 mm field have the most undesirable results, which be explained due to the distance between the camera and the specimen. Close distance between them creating problem to set the focus for calibration board. The calibration board has some certain thickness which is creating different focus length between the actual specimen and the camera. On the other hand, the strain increment error result is quite bad. It can be seen all the data shows value more than 200 % difference. There are several steps of load/strain increment that is applied to the specimen. It can be seen that the most severe error happens after the load increment decrease below 100 microstrain. The explanation for this phenomena is due to the strain limit of the DIC equipment. It is known that 100 microstrain is the lower limit strain measurement of the equipment.

Having said them, it is safe to say that distance between the camera and the specimen, as well as the field of view of the specimen, is not affecting the results for the field of view between 10 mm until 100 mm.

DISCUSSION ON THE BENCHMARK TESTING RESULT

Based on the benchmark tensile, it can be concluded that:

- The result for field of view 20 mm, 30 mm, 50 mm, and 100 mm are satisfactory with error less than 15 %

Field of View	Average Strain Error	Average Increment Strain Error
10 mm	24%	504%
20 mm	10%	328%
30 mm	9%	308%
50 mm	13%	293%
100 mm	8%	225%

- Due to the strain low limit of the equipment, the strain measurement or strain increment below 100 microstrain can be considered as an unreliable measurement.
- For this particular test, the field of view between 10 mm until 100 mm are not affecting the final result of the measurement.

ANNEX B – 2D & 3D BENCHMARK TESTING UNDER THE ORTHOTROPIC BRIDGE DECK

INTRODUCTION

Series of tests using DIC measurement are conducted between periods of 10 November 2017- 13 November 2017. The tests are classified into these purposes:

- Study the effect of different field of view and number of pixels for 3D out-of-plane deformation with given rigid body movement
- Study the effect of given rigid body movement for 3D strain measurement with no internal forces present
- Study the effect of out-of-plane deformation on 2D strain measurement with no internal forces present

All the tests above are performed under the orthotropic deck bridge. The purpose is to see whether due to the same inhospitality of the environment, proper results can be achieved. Finally, the results and recommendation of these study can be further applied to the actual test for the orthotropic bridge deck.

PROPERTIES AND SCENE OF THE TEST

Properties

The material/specimen that is used for the following tests are made of steel with texture and properties are depicted in figure 1 and table 1 below respectively.



Figure 1. Dimension of the Steel Specimen

Table1. Details on the Materials

Height	8.9	mm
Width	24.6	mm
Area of the specimen	218.94	mm ²
Modulus of Elasticity	210000	Mpa
F_{yield}	355	Mpa

Scene of the Test

As it is mentioned in the previous section, the scene for this test is below the orthotropic bridge deck specimen in Stevinweg laboratory. While the purpose of the study for each case is different, but the principal is to check the reliability of using DIC Measurement under this circumstances. Further, in the results and analysis, these purposes will be divided into several sub-objectives. Figure below shows the position of the camera, the specimen and the calibration machine that are used for this test.

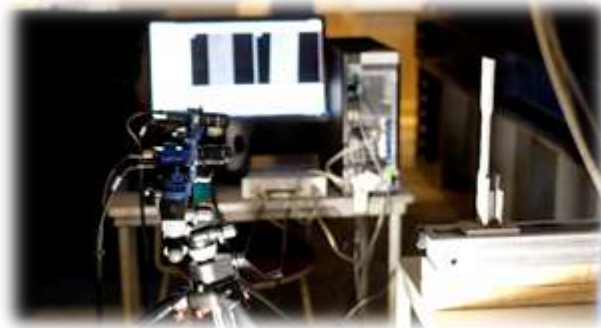


Figure 2. Location of the Camera, Calibration Machine, and Steel Specimen



Figure 3. Calibration Machine and The Steel Specimen

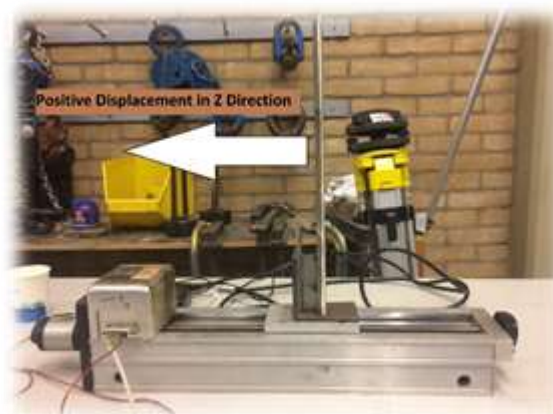


Figure 4. Positive Direction of Given Displacement

For all of the cases, the value of the given displacement is the same as it is described in the table 2 below. For some of the tests, the displacement is given in positive direction and negative direction.

Table 2. Given Out-of-plane deformation

Step	Given Displacement			
	Increment		Total Displacement	
0	0	mm	0	mm
1	0	mm	0	mm
2	0.05	mm	0.05	mm
3	0.05	mm	0.1	mm
4	0.1	mm	0.2	mm
5	0.1	mm	0.3	mm
6	0.1	mm	0.4	mm
7	0.2	mm	0.6	mm
8	0.2	mm	0.8	mm
9	0.5	mm	1.3	mm

The measurement system that is used in these tests is product Q400 LIMESS DIC system for both 2D and 3D measurement.

RESULTS OF THE TEST

3D Out-of-plane Deformation

It is the purpose of the test, to observe the influence of different field of view and triangulation angle between optical axis of two cameras on monitoring 3D deformation.

For this type of test, three fields of view is used: 50 mm field of view, 75 fields of view, and 150 mm field of view. Figure 5 below depicts the captured image for initial step (step 0) for each field of view.

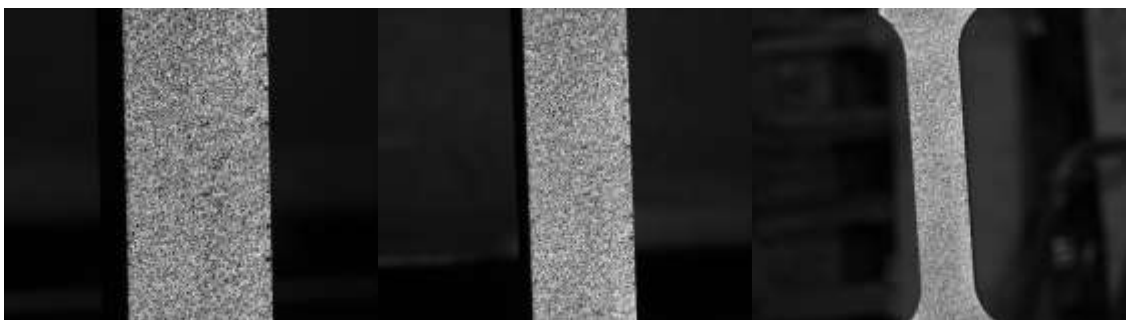


Figure 5. 50 mm Field of View (Left Image), 75mm Field of View (Middle Image), and 150 mm Field of View (Right Image). All Images Are Taken at Initial Step (Step 0) and From Camera 1

Beside a field of view, another variable that is changed during the test is triangulation angle between optical axis of the two cameras. The angle is defined by the symbol alpha, shown in figure 6 below.

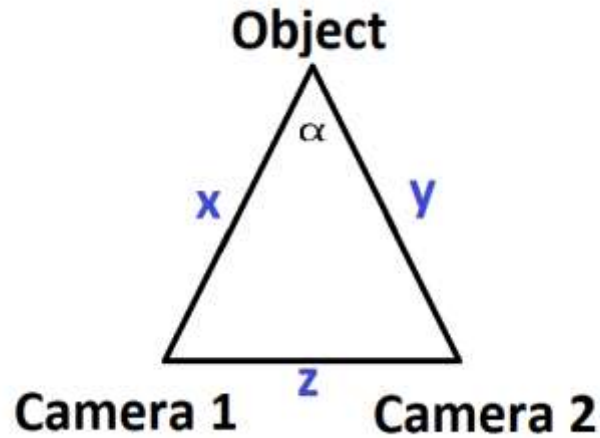


Figure 6. Triangulation angle of Optical Axis Between 2 Camera

Where x and y symbol is the working distance between the camera to the object, and z is the distance between the camera. In this test, 50 mm field of view is chosen as the fixed variable. While z distance between the camera is changed.



Figure 7. Distance Between Camera 1 and Camera 2 for the Same Field of View 50 mm. Left Image Shows for z = 44 cm and Right Image Shows for z = 14 cm

Table 3. Different Applied Triangulation Angle

	50 mm Field of View	
	Wide	Narrow
x (mm)	520	520
y (mm)	520	520
z (mm)	440	140
Alpha (degree)	50.06	15.47

For the test with the field of view 50 and 75 mm, the calibration plate with 5 mm square is used. While for the tests with the field of view 150 mm, the calibration plate with 10 mm square is used. This means the reading from the LIMESS DIC system needs to be multiplied by its calibration value.

To read the results from Q400 DIC System LIMESS, a particular line is put on the middle of the captured image. The average value of the line is then taken and compared with the results from the calibration machine. Besides the average value of the line, there

are also other values from the certain area of the monitored specimen. The maximum and minimum value of this results are important to be taken to see how big the deviation of the displacement from the chosen average value. Figure 8 below depicts the position of the line, while figure 9 shows the deviation value of the displacement over the area.

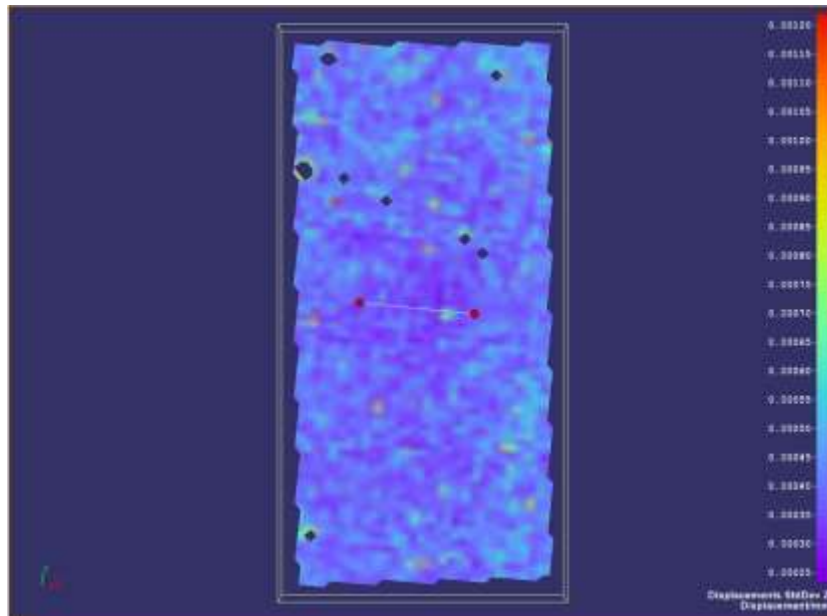


Figure 8. Location of Straight Line for 75 Field of View

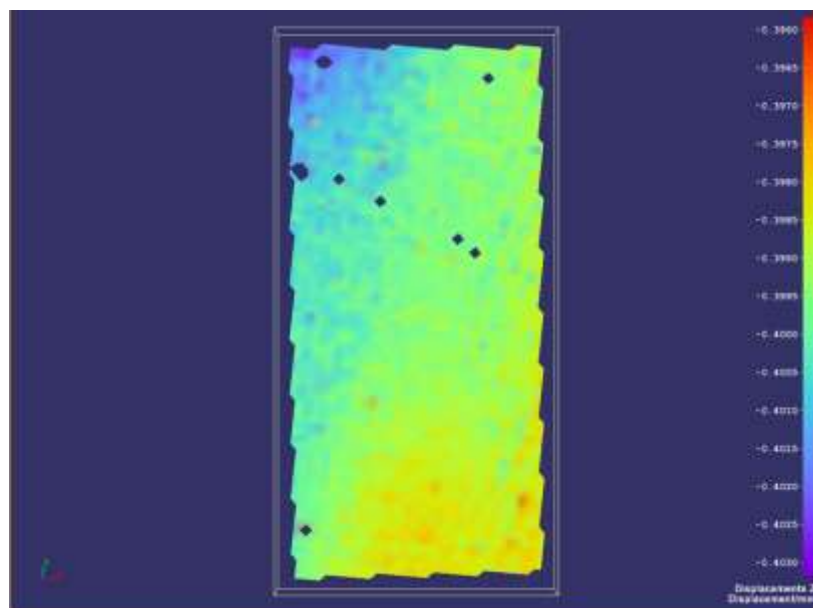


Figure 9. Displacement Distribution Over the Region of Interest

In this report, two deviation value is computed. First is the deviation of DIC reading relative to calibration machine reading, and second is the deviation of maximum and minimum value displacement relative to the average value of the line. The formula for the second deviation is given below:

$$\sigma = \pm \frac{S_1 - S_2}{S_1 + S_2}$$

Where S1 is the maximum value, and S2 is the minimum value. The positive and negative sign shows the value of the deviation relative to the maximum and minimum value respectively.

Table 4. 50 mm Field of View Wide Angle Out-of-plane Deformation Result

Step	Given Displacement				Dantec Reading						Deviation Relative to	
	Increment		Total Displacement		Average Value		Minimum Value		Maximum Value		Calibration Machine	Average Value (±)
0	0	mm	0	mm	0.00	mm	0.00	mm	0.00	mm	0%	0%
1	0	mm	0	mm	0.00	mm	0.00	mm	0.00	mm	0%	0%
2	0.05	mm	0.05	mm	0.04	mm	0.05	mm	0.05	mm	11%	0%
3	0.05	mm	0.1	mm	0.09	mm	0.09	mm	0.09	mm	10%	1%
4	0.1	mm	0.2	mm	0.20	mm	0.20	mm	0.20	mm	1%	1%
5	0.1	mm	0.3	mm	0.29	mm	0.29	mm	0.30	mm	2%	0%
6	0.1	mm	0.4	mm	0.40	mm	0.40	mm	0.40	mm	1%	0%
7	0.2	mm	0.6	mm	0.58	mm	0.58	mm	0.59	mm	3%	0%
8	0.2	mm	0.8	mm	0.79	mm	0.78	mm	0.79	mm	2%	0%
9	0.5	mm	1.3	mm	1.30	mm	1.29	mm	1.30	mm	0%	0%

Table 5. 50 mm Field of View Narrow Angle Out-of-plane Deformation Result

Step	Given Displacement				Dantec Reading						Deviation Relative to	
	Increment		Total Displacement		Average Value		Minimum Value		Maximum Value		Calibration Machine	Average Value (±)
0	0	mm	0	mm	0.00	mm	0.00	mm	0.00	mm	0%	0%
1	0	mm	0	mm	0.00	mm	-0.01	mm	0.01	mm	0%	0%
2	0.05	mm	0.05	mm	0.05	mm	0.05	mm	0.05	mm	6%	0%
3	0.05	mm	0.1	mm	0.10	mm	0.09	mm	0.11	mm	0%	7%
4	0.1	mm	0.2	mm	0.21	mm	0.20	mm	0.21	mm	4%	4%
5	0.1	mm	0.3	mm	0.30	mm	0.28	mm	0.31	mm	1%	4%
6	0.1	mm	0.4	mm	0.40	mm	0.39	mm	0.41	mm	1%	2%
7	0.2	mm	0.6	mm	0.59	mm	0.58	mm	0.60	mm	2%	1%
8	0.2	mm	0.8	mm	0.79	mm	0.78	mm	0.80	mm	1%	1%
9	0.5	mm	1.3	mm	1.30	mm	1.28	mm	1.30	mm	0%	1%

Table 6. 75 mm Field of View Out-of-plane Deformation Result

Step	Given Displacement				Dantec Reading						Deviation Relative to	
	Increment		Total Displacement		Average Value		Minimum Value		Maximum Value		Calibration Machine	Average Value (±)
0	0	mm	0	mm	0.00	mm	0.00	mm	0.00	mm	0%	0%
1	0	mm	0	mm	-0.02	mm	-0.03	mm	-0.01	mm	0%	0%
2	0.05	mm	0.05	mm	0.06	mm	0.06	mm	0.06	mm	21%	0%
3	0.05	mm	0.1	mm	0.10	mm	0.10	mm	0.11	mm	4%	4%
4	0.1	mm	0.2	mm	0.20	mm	0.20	mm	0.20	mm	0%	1%
5	0.1	mm	0.3	mm	0.30	mm	0.29	mm	0.30	mm	1%	1%
6	0.1	mm	0.4	mm	0.40	mm	0.40	mm	0.40	mm	0%	1%
7	0.2	mm	0.6	mm	0.60	mm	0.59	mm	0.60	mm	1%	1%
8	0.2	mm	0.8	mm	0.80	mm	0.80	mm	0.81	mm	0%	0%
9	0.5	mm	1.3	mm	1.30	mm	1.29	mm	1.30	mm	0%	0%

Table 7. 150 mm Field of View Out-of-plane Deformation Result

Step	Given Displacement				Dantec Reading						Deviation Relative to	
	Increment		Total Displacement		Average Value		Minimum Value		Maximum Value		Calibration Machine	Average Value
0	0.00	mm	0.00	mm	0.00	mm	0.00	mm	0.00	mm	0%	0%
1	0.00	mm	0.00	mm	0.00	mm	0.00	mm	0.00	mm	0%	0%
2	0.05	mm	0.05	mm	0.03	mm	0.00	mm	0.01	mm	32%	76%
3	0.05	mm	0.10	mm	0.05	mm	0.00	mm	0.01	mm	49%	71%
4	0.10	mm	0.20	mm	0.28	mm	0.02	mm	0.03	mm	39%	15%
5	0.10	mm	0.30	mm	0.33	mm	0.03	mm	0.04	mm	8%	17%
6	0.10	mm	0.40	mm	0.42	mm	0.04	mm	0.05	mm	4%	11%
7	0.20	mm	0.60	mm	0.65	mm	0.06	mm	0.07	mm	9%	13%
8	0.20	mm	0.80	mm	0.95	mm	0.08	mm	0.10	mm	19%	12%
9	0.50	mm	1.30	mm	1.48	mm	0.13	mm	0.16	mm	14%	11%

3D Strain Benchmark Test

In this test, the same procedure is applied as the 3D Out-of-plane Deformation. With no internal forces present, only rigid body motion is given to the specimen. The information that is provided by the Q400 LIMESS DIC System is that the low strain threshold of the equipment to monitor strain is between 10 μ strain – 100 μ strain. So if the results show the strain measurement in between these values for only rigid body movement is given, then it is a good indication that satisfying 3D strain results might be achieved in the further test.

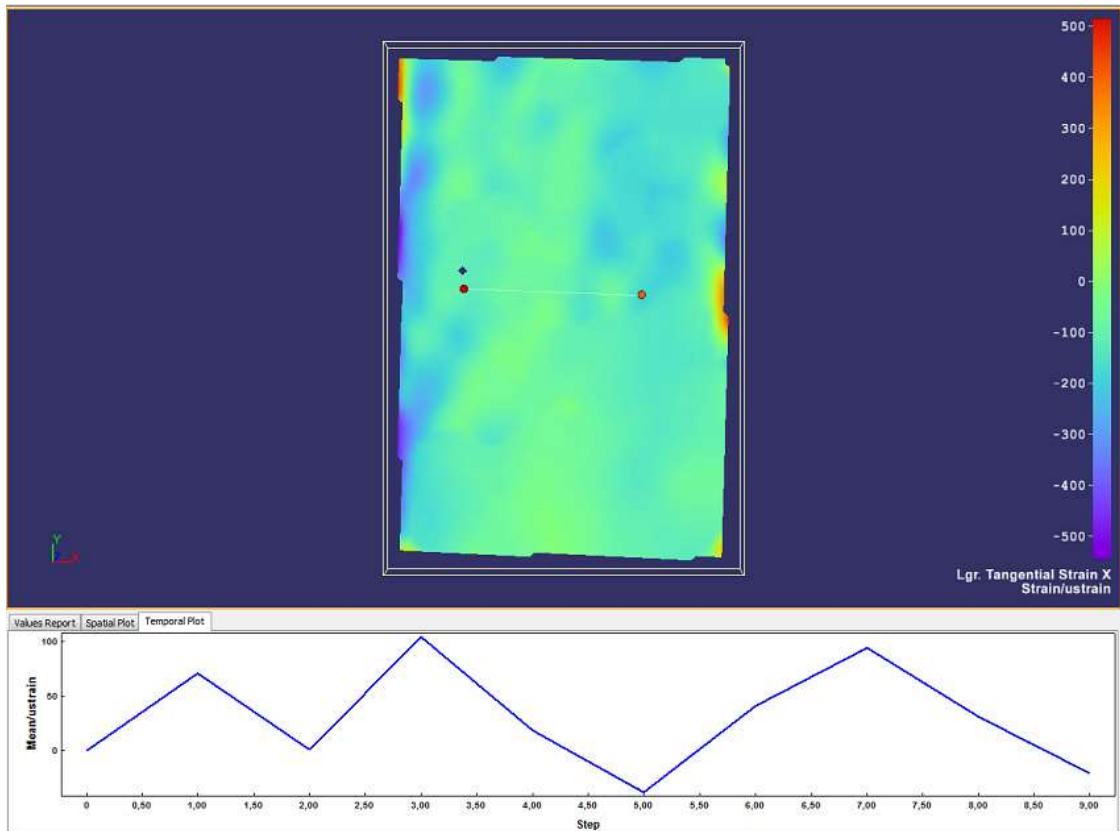


Figure 10. 50 mm Field of View Wide Angle Principal Strain Plot Over The Step

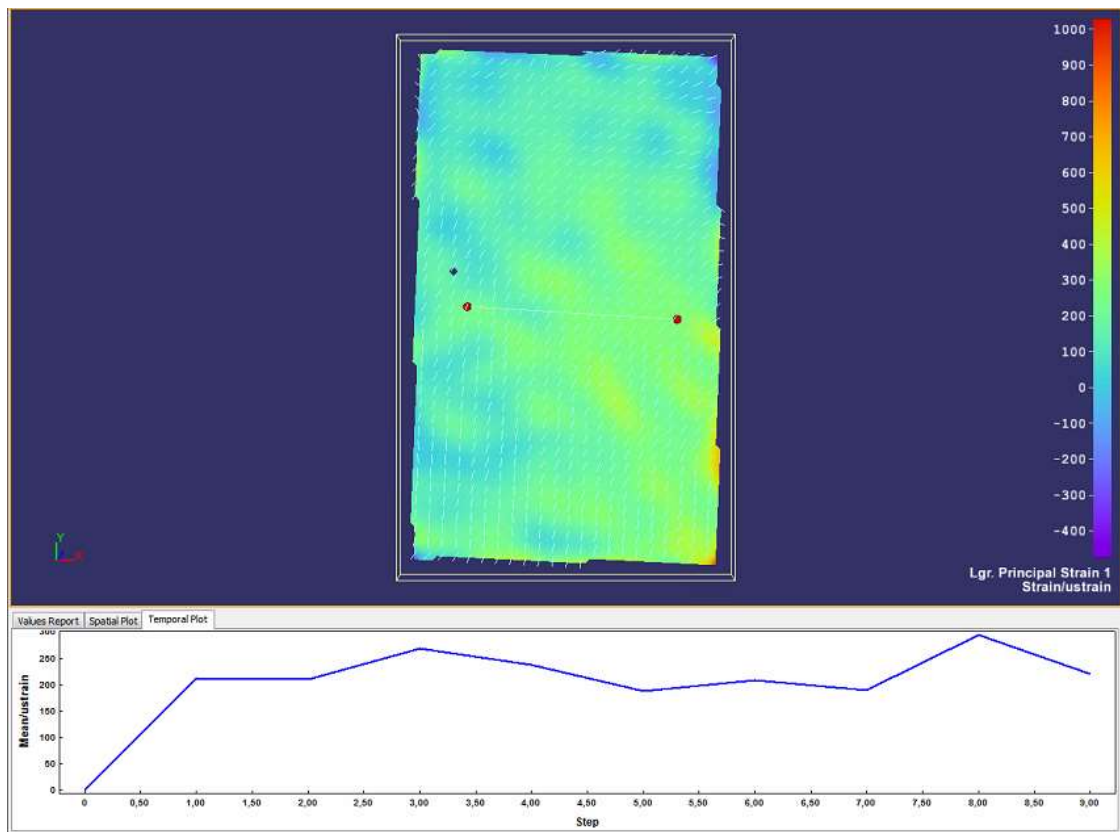


Figure 11. 50 mm Field of View Narrow Angle Principal Strain Plot Over The Step

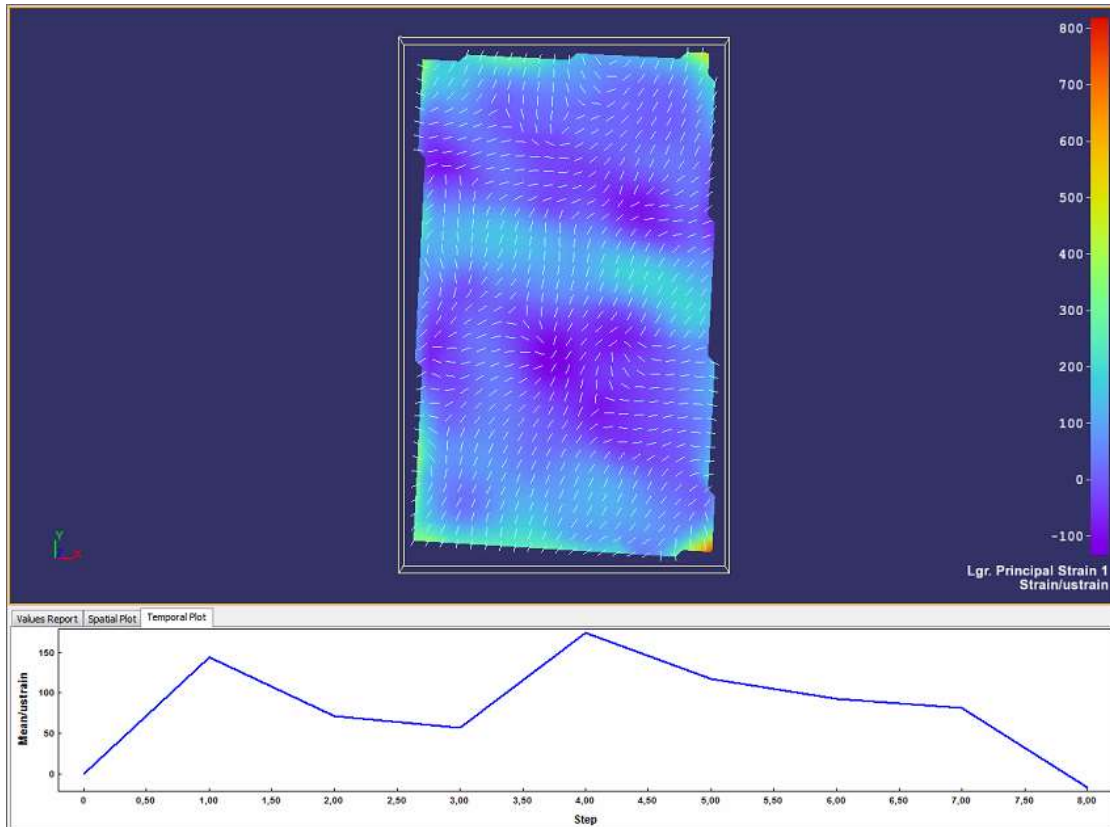


Figure 12. 75 mm Field of View Principal Strain Plot Over The Step

As it can be seen from the table, for 50 mm wide angle field of view, the strain oscillate between 0 – 100 microstrain. For 50 mm narrow-angle field of view, the strain value varies between 0 – 250 microstrain. Moreover, for 75 mm field of view, the strain value varies between 0 – 200 microstrain.

2D Strain Benchmark Test

From the information that provided from the company, the strain error for the 2D system is proportional to distance change/working distance. 1 mm distance change at 100 mm working distance causes $1/100 = 0.01 = 1\%$ strain error. Any out of plane movement of an object will cause a systematic strain error. When the object moves towards the camera it gets larger in the image and "tension" is measured. The purpose of this test is to prove these information. Two field of view is chosen in this test: 10 mm and 50 mm.

Table 8. 2D Benchmark Strain Test For 10 mm Field of View

10 mm Field of View

Working Distance 250.9338 mm

Step	Given Displacement		2D Dantec Reading in Positive Z		2D Dantec Reading in Negative Z		Theoretical Error Strain (\pm)		Deviation Positive	Deviation Negative
				μ strain		μ strain		μ strain		
0	0	mm	0	μ strain	0	μ strain	0.00	μ strain	-	-
1	0	mm	-15	μ strain	50	μ strain	0.00	μ strain	-	-
2	0.05	mm	-82	μ strain	270	μ strain	199.26	μ strain	59%	-36%
3	0.1	mm	-251	μ strain	444	μ strain	398.51	μ strain	37%	-11%
4	0.2	mm	-704	μ strain	835	μ strain	797.02	μ strain	12%	-5%
5	0.3	mm	-905	μ strain	1134	μ strain	1195.53	μ strain	24%	5%
6	0.4	mm	-1220	μ strain	1966	μ strain	1594.05	μ strain	23%	-23%
7	0.6	mm	-2040	μ strain	2404	μ strain	2391.07	μ strain	15%	-1%
Average Error									29%	15%

As it can be seen from table 8 above, the 2D strain benchmark test with no internal forces present and only out-of-plane motion are given, shows good agreement with the theoretical strain calculation. Although there is some value which shows big differences, the possible explanation is due to the tolerance or low strain threshold that the system has. It is known that the low strain limit of the equipment is between 10 μ strain – 100 μ strain. So in this test, it is assumed, that only strain due to displacement above 0.1 mm that can be assumed as reliable data.

Table 9. 2D Benchmark Strain Test for 50 mm Field of View

50 mm Field of View

Working Distance 587.36 mm

Step	Given Displacement		2D Dantec Reading in Positive Z		2D Dantec Reading in Negative Z		Theoretical Error Strain (\pm)		Deviation Positive	Deviation Negative
				μ strain		μ strain		μ strain		
0	0	mm	0	μ strain	0	μ strain	0.00	μ strain	-	-
1	0	mm	70	μ strain	50	μ strain	0.00	μ strain	-	-
2	0.05	mm	30	μ strain	120	μ strain	85.13	μ strain	65%	-41%
3	0.1	mm	-50	μ strain	150	μ strain	170.25	μ strain	71%	12%
4	0.2	mm	-160	μ strain	280	μ strain	340.50	μ strain	53%	18%
5	0.3	mm	-430	μ strain	540	μ strain	510.76	μ strain	16%	-6%
6	0.4	mm	-500	μ strain	930	μ strain	681.01	μ strain	27%	-37%
7	0.6	mm	-900	μ strain	1040	μ strain	1021.51	μ strain	12%	-2%
8	0.8	mm	-1160	μ strain	1340	μ strain	1362.02	μ strain	15%	2%
9	1.3	mm	-1910	μ strain	2200	μ strain	2213.28	μ strain	14%	1%
Average Error									28%	13%

Table 9 above also shows the good agreement between the theoretical strain error calculation and the benchmark test. It is mentioned before that due to the tolerance of the system and low strain threshold, some of the results gives big differences. In this particular case, it is assumed, that the data from above 0.1 mm can be assumed as a reliable data. Related to the orthotropic bridge deck test with quasi static in-plane load, this data is a proof to use 3D DIC measurement instead of 2D measurement.

ANALYSIS AND COMPARISON

Q400 DIC System LIMESS Reading Compare to Calibration Reading

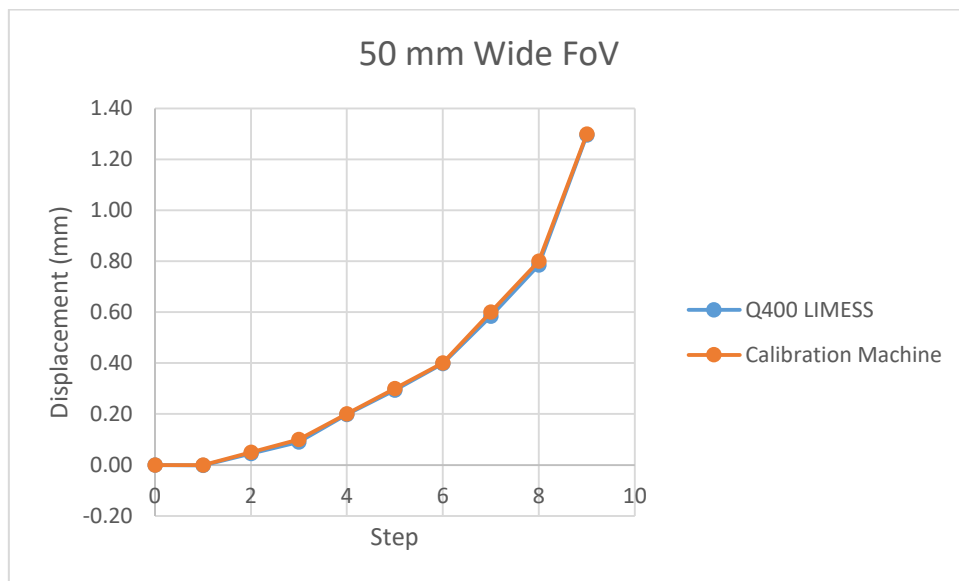


Figure 13. LIMESS Measurement vs Calibration Machine 50 mm Wide Field of View

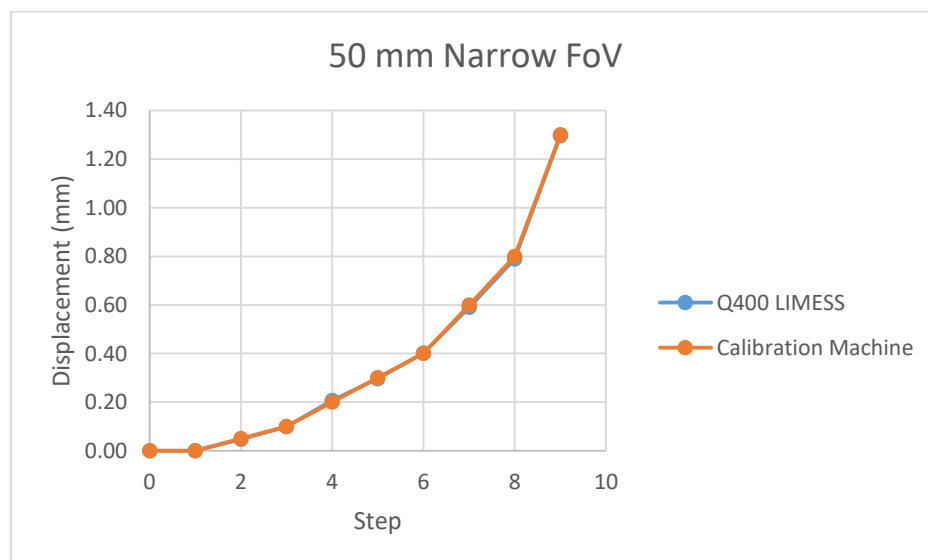


Figure 14. LIMESS Measurement vs Calibration Machine 50 mm Narrow Field of View

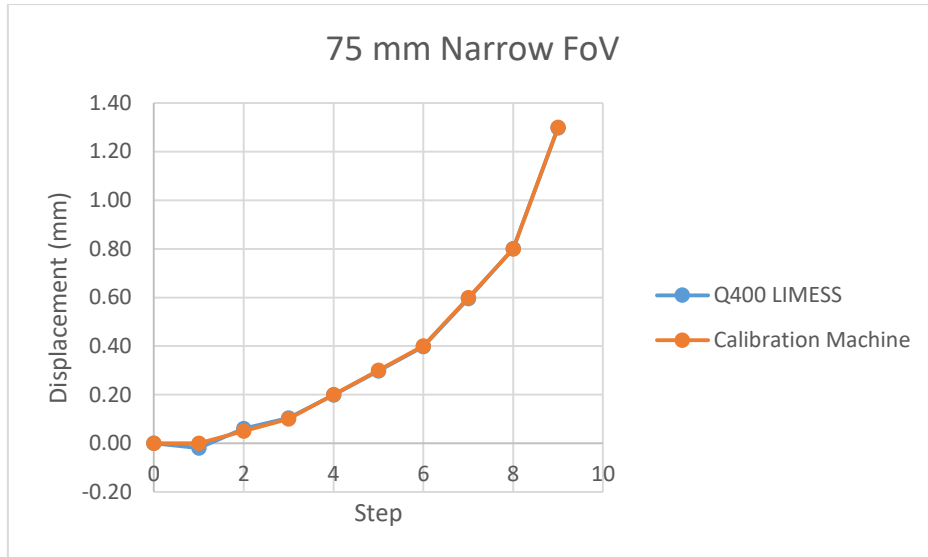


Figure 15. LIMESS VS Calibration Machine 75 mm Field of View

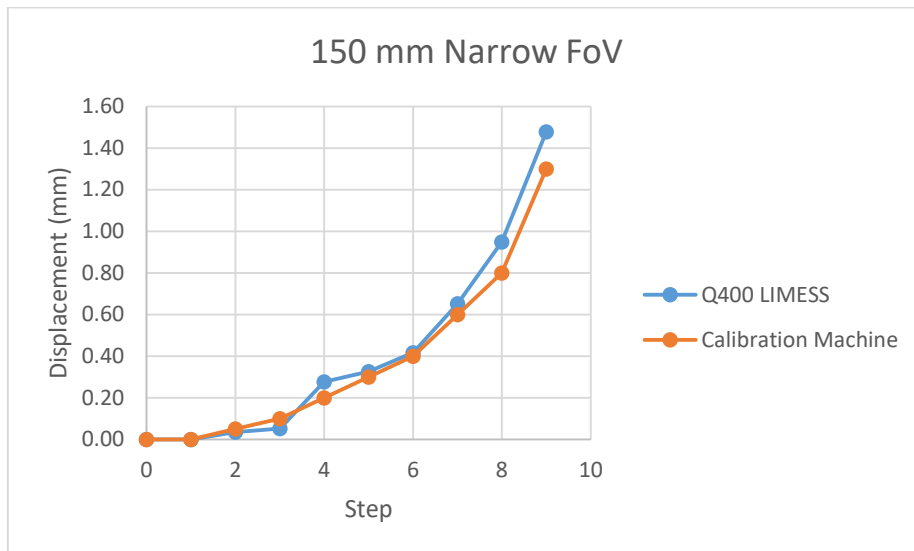


Figure 16. LIMESS vs Calibration Machine 150 mm Field of View

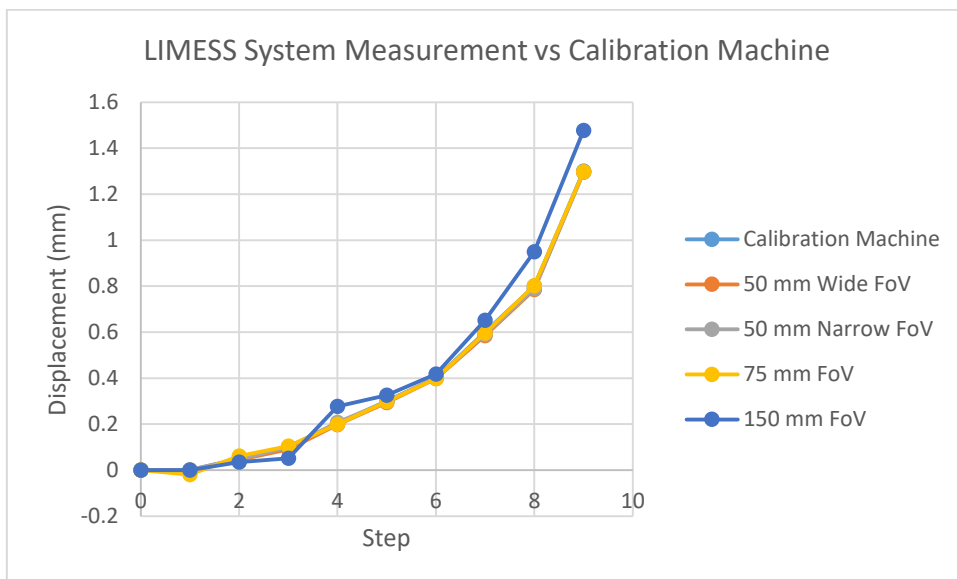


Figure 17. LIMESS System Measurement vs Calibration System for All Field of View

Table 10. Deviation Average for Every Measurement

Step	Given Displacement (mm)	Deviation to Calibration Machine				Deviation to The Average Value			
		50 mm Wide FoV	50 mm Narrow FoV	75 mm FoV	150 mm FoV	50 mm Wide FoV	50 mm Narrow FoV	75 mm FoV	150 mm FoV
0	0	0%	0%	0%	0%	0%	0%	0%	0%
1	0	0%	0%	0%	0%	0%	0%	0%	0%
2	0.05	11%	6%	21%	32%	7%	44%	11%	76%
3	0.1	10%	0%	4%	49%	1%	7%	4%	71%
4	0.2	1%	4%	0%	39%	1%	4%	1%	15%
5	0.3	2%	1%	1%	8%	0%	4%	1%	17%
6	0.4	1%	1%	0%	4%	0%	2%	1%	11%
7	0.6	3%	2%	1%	9%	0%	1%	1%	13%
8	0.8	2%	1%	0%	19%	0%	1%	0%	12%
9	1.3	0%	0%	0%	14%	0%	1%	0%	11%
Average Deviation		4%	2%	3%	22%				

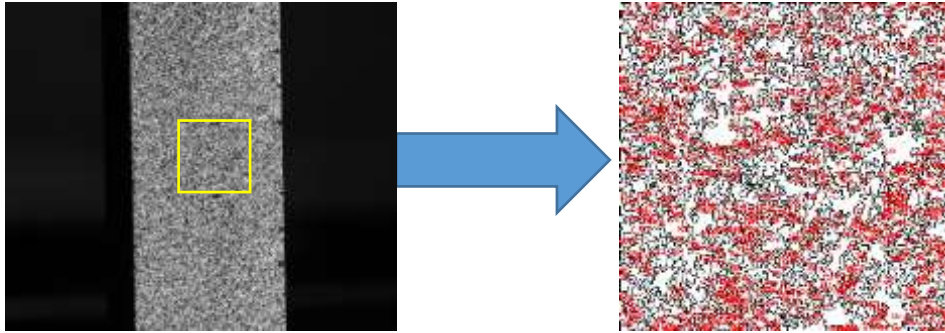
In general, almost all the test results show good agreement with the given calibration which is read by the calibration machine. It is a good indication that the chosen field of view is sufficient to get the proper results under the orthotropic deck bridge environment. One results with the field of view 150 mm can be categorised as unreliable. The possible explanation is that, due to the limitation of the camera specification, there is some working distance from objective to the camera that cannot be exceeded. In this case, the field of view 50 mm, 75 mm and 150 mm are used. If we transform it into the working distance between the camera and the object, the result will be shown in table 11 below.

Table 11. Working Distance For Each Field of View

Field of view (mm)	50.00	75	150
Focal length (mm)	85.00	75	75
Working distance (mm)	587.36	739.9	1404.8

Influence Number of Pixels for One Particular Dot in Speckle Pattern

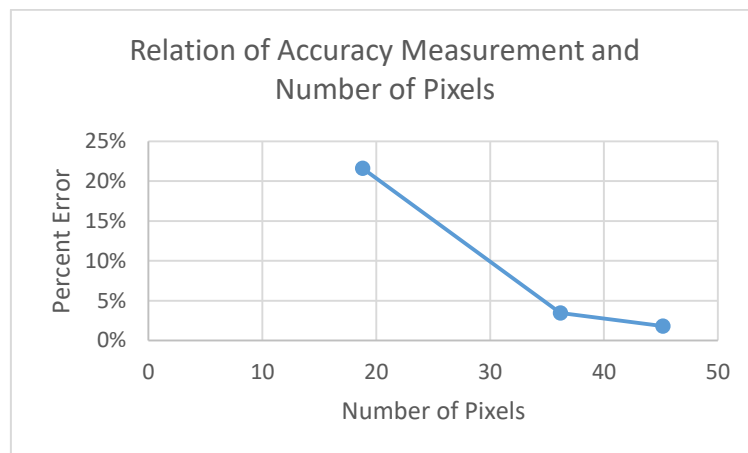
Quality of the image is a vital factor that can affect the accuracy of the measurement. Theoretically, the closer distance between object and camera will yield a better quality of the image. In this section, the influence number of pixels in one particular dot will be examined more thoroughly. Figure below depict the field of view 50 mm. The area with the yellow square sign will be the location to be compared with each of field of view.



To represent the dot size calculation, an image is taken with 440 x 440-pixel size (or equal to 10 x 10 mm) to represent other speckle pattern size. Using software imageJ, it can be computed there are 2009 number of dots inside 440 x 440-pixel size with the size of the dot varies between 1 pixel² to 473 pixel². To represent the size of all the dot, the average value of the dot size is then computed. It is known that for 50 mm field of view, the dot size is averaging 45.15 pixel². For the other field of view, the table below provides the information.

	Field of View		
	50 mm	75 mm	150 mm
Number of Dot Counted	2009	1073	463
Smallest Dot Size	1	1	1
Biggest Dot Size	473	286	91.882
Average Dot Size	45.15	36.159	18.8

It can be seen that the number of computed dot in each field of view is decreased along with the growth of the field of view for the same region of interest (440 x 440 pixels). The average dot size is also decreased from 45.15 to 18.8 for the field of view 50 mm and 150 mm. The graph below depicts the relation of the accuracy of the measurement with the dot size.



For some pixels 45.15 and 36.1 over one dot, it gives an error below 5 percent, while for a number of pixel 18.8, it gives an error over than 20%. It can be summarised that

for the given level of displacement, 50 mm and 75 mm field of view are more reliable to use than using 150 mm field of view.

Influence of the Angle to the Displacement and Strain Measurement

In this study, it is also investigated whether angle plays an important role in the displacement and strain measurement. For out-of-plane deformation measurement, we can see from the table below, that there is almost no difference in terms of results between the field of view 50 mm with the triangulation angle of 50 degrees compare to the same field of view but with a different angle which is 15 degree. So it can be concluded that for this level of out-of-plane deformation, and only out-of-plane in one direction is applied, the triangulation angle between optical axis of the camera is not playing an important role.

Step	Given Displacement (mm)	Deviation to Calibration Machine	
		50 mm Wide FoV	50 mm Narrow FoV
0	0	0%	0%
1	0	0%	0%
2	0.05	11%	6%
3	0.1	10%	0%
4	0.2	1%	4%
5	0.3	2%	1%
6	0.4	1%	1%
7	0.6	3%	2%
8	0.8	2%	1%
9	1.3	0%	0%
Average Deviation		4%	2%

However, in benchmark testing for 3D strain measurement, the results show the opposite results of displacement test. It can be seen that for bigger triangulation angle, the smaller low strain threshold can be achieved. Although further study needs to be done because the strain measurement really depends on the calibration procedure. Where for 3D calibration procedure cannot be done at the same method for each test. So The results below, the lowest strain threshold might be due to perfect calibration procedure.

Field of View	Triangulation Angle	Strain Range for Given Displacement
50 mm (Wide)	50.06	0 -100
75 mm	34.60	0 - 200
50 mm (Narrow)	15.47	0 -250

DISCUSSION OF MAIN FINDING IN BENCHMARK TESTING RESULTS

Here is some conclusion that can be drawn from series of tests of benchmark testing which has been done by Q400 DIC LIMESS system :

- With given environment (under the orthotropic bridge deck) the series test of 3D out-of-plane deformation with the field of view of 50 mm and 75 mm shows a good agreement between the DIC measurement and calibration machine with an average of deviation below 5%. One results 150 mm field of view has a bigger deviation (more than 20% difference). The study shows, with the given specification of Q400 DIC LIMESS System, 50 mm and 75 mm gives an adequate resolution of the images, while 150 mm field of view gives lack of resolution, therefore bad results.
- Given the circumstances of the experiment, and the level of the expected displacement, one particular dot size equal to 36 and 45 pixels are proved as an optimum speckle pattern to give adequate measurement results.
- For 3D strain benchmark testing without internal force present and only out-of-plane deformation given in z-direction, the results show that for 50 mm with 50-degree triangulation angle of optical axis camera gives the lowest strain threshold (100 microstrains). Assuming the measurement has an adequate of resolution, along with the growth of triangulation angle, the threshold of 3D strain measurement is increased.
- It is shown in the study that triangulation angle is not affecting the out-of-plane deformation in one direction only.
- The 2D strain benchmark testing shows the good agreement between theoretical of strain error calculation and the test, therefore the 3D DIC measurement on orthotropic deck with quasi static in-plane load is necessary to be performed instead of 2D measurement.

After reaching some of the conclusion, here are some recommendation for further study:

- For the test on orthotropic deck bridge with an in-plane loading, it is recommended to use 50 mm field of view with some pixel for one particular dot around 36 pixels, and also the triangulation angle of 50 degrees. It is shown that for the given level of displacement, the low strain threshold can be achieved at 100 microstrains.
- The benchmark testing which has been done, only motion in one direction (z-axis). Further study might be required to reach the same purpose of the study, but also the effect of given motion in 3 directions.

